

# An Oceanographic Characterization of the Olympic Coast National Marine Sanctuary and Pacific Northwest

*Interpretive Summary of Ocean Climate and Regional Processes  
through Satellite Remote Sensing*

Douglas Pirhalla

NOAA National Centers for Coastal Ocean Science

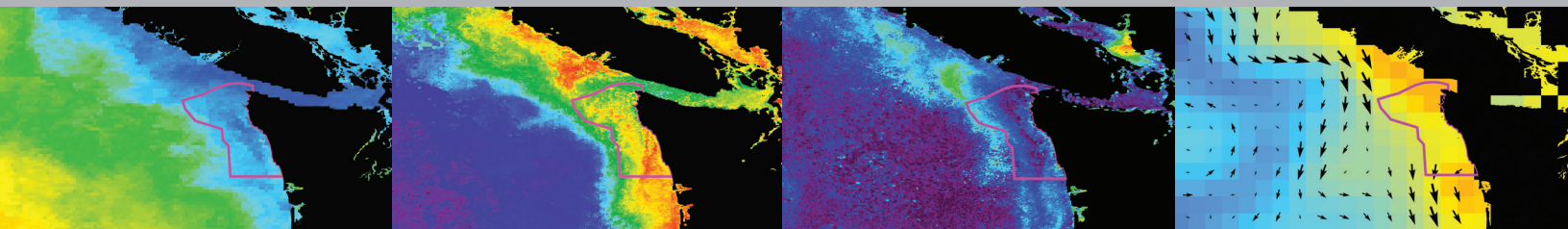
Varis Ransibrahmanakul

NOAA National Centers for Coastal Ocean Science

Randy Clark

NOAA National Centers for Coastal Ocean Science

April 2009



NOAA TECHNICAL MEMORANDUM NOS NCCOS 90



## **CITATION:**

Pirhalla D.E., V. Ransibrahmanakul, R. Clark, A. Desch, T. Wynne, and M. Edwards. 2009. An Oceanographic Characterization of the Olympic Coast National Marine Sanctuary and Pacific Northwest: Interpretive Summary of Ocean Climate and Regional Processes Through Satellite Remote Sensing. NOAA Technical Memorandum NOS NCCOS 90. Prepared by NCCOS's Coastal Oceanographic Assessments, Status and Trends Division in cooperation with the National Marine Sanctuary Program. Silver Spring, MD. 53 pp.

## **FOR MORE INFORMATION**

For more information or to download this report, please contact the NCCOS Coastal and Oceanographic Assessment, Status & Trends (COAST) at 301-713-3028, visit: <http://ccmaserver.nos.noaa.gov/about/coast/welcome.html> or contact [doug.pirhalla@noaa.gov](mailto:doug.pirhalla@noaa.gov)

## **COVER**

The covers were designed and created by Gini Kennedy (NOAA). Front cover: Medium Resolution Imaging Spectrometer (MERIS) true color image from July 17, 2003 provided by Fisheries and Oceans Canada. Back cover: Graphic provided by Nancy Wright from the Olympic Coast National Marine Sanctuary.

Mention of trade names or commercial products does not constitute endorsement or recommendation for their use by the United States Government.

# **An Oceanographic Characterization of the Olympic Coast National Marine Sanctuary and Pacific Northwest:**

*Interpretive Summary of Ocean Climate and  
Regional Processes through Satellite Remote Sensing*

Center for Coastal Monitoring and Assessment (CCMA)  
NOAA/NOS/NCCOS  
1305 East West Highway (SSMC-IV, N/SCI-1)  
Silver Spring, MD 20910-3281

NOAA Technical Memorandum NOS NCCOS 90

April 2009



---

United States Department of  
Commerce

Gary Locke  
Secretary

National Oceanic and  
Atmospheric Administration

Jane Lubchenco  
Under Secretary

National Ocean Service

John H. Dunnigan  
Assistant Administrator

---



## ABOUT THIS DOCUMENT

This summary represents the continuation of an ongoing collaboration with the Office of National Marine Sanctuaries (ONMS), Olympic Coast National Marine Sanctuary (OCNMS), and the National Centers for Coastal Ocean Science (NCCOS) Center for Coastal Monitoring and Assessment (CCMA), through a comprehensive regional oceanographic data synthesis and integration effort for the U.S. Pacific Northwest (PNW). Multiple long-term satellite oceanographic datasets made available through NASA, NOAA and other world-wide operational data centers were evaluated and summarized to provide scientific information and insights on system variability and processes affecting the PNW and, in particular, the OCNMS. The synoptic-scale viewpoint provided by satellite data made it possible to combine multiple observations on physical, biological, and sediment characteristics to fill existing data gaps, and document oceanic events for the entire region. The result is a unique representation of PNW ocean climate and behavior, an oceanographic baseline from which multiple ecosystem-based assessments can be built. Intended audiences of the assessment include the National and Regional Sanctuary Management Offices, IOOS Associations, NOAA Ecosystems Program, and other Federal and State agencies, universities, and tribal staff.

The characterization consists of three complementary components: a text report; a suite of quantitative spatial and statistical analyses that characterize oceanographic and physical patterns of the PNW and OCNMS region; and an extensive geodatabase of all spatial, temporal, derived, and primary remote sensing datasets acquired, assimilated, and analyzed to conduct the characterization. This particular work builds on and advances data synthesis and analytical techniques developed for other National Marine Sanctuaries, including the Channel Islands, Cordell Bank, Gulf of the Farallones, Monterey Bay, Gray's Reef, and Stellwagen Bank (NCCOS, 2003, 2006, 2007).

For questions or comments, please contact:

John D. Christensen, Branch Chief  
NOAA/NCCOS/CCMA  
Coastal and Oceanographic Assessment, Status & Trends  
1305 East West Highway, N/SCI1  
Silver Spring, MD 20910  
Phone: 301-713-3028 x 153  
Email: [john.christensen@noaa.gov](mailto:john.christensen@noaa.gov)

or

Douglas E. Pirhalla, Project Manager  
NOAA/NCCOS/CCMA  
Coastal and Oceanographic Assessment, Status & Trends  
1305 East West Highway, N/SCI1  
Silver Spring, MD 20910  
Phone: 301-713-3028 x 167  
Email: [doug.pirhalla@noaa.gov](mailto:doug.pirhalla@noaa.gov)

## PROJECT TEAM

### NOAA NCCOS Center for Coastal Monitoring and Assessment

Douglas Pirhalla

Varis Ransibrahmanakul

Randy Clark

Arthur Desch

Timothy Wynne

Michael Edwards

### NOAA Olympic Coast National Marine Sanctuary

Ed Bowlby

Barbara Blackie

George Galasso

Nancy Wright

John Barimo

## EXECUTIVE SUMMARY

This report presents the results of a two-year investigation and summary of oceanographic satellite data obtained from multiple operational data providers and sources, spanning years of operational data collection. Long-term summaries of Sea Surface Temperature (SST) and SST fronts, Sea Surface Height Anomalies (SSHA), surface currents, ocean color chlorophyll and turbidity, and winds are provided.

### Overall Conclusions

Merged satellite oceanographic data revealed information on: (1) seasonal cycles and timing of transition periods; (2) linkages between seasonal effects (warming and cooling), upwelling processes and transport; and (3) nutrient/sediment sources, sinks, and physical limiting factors controlling surface response for Olympic Coast marine environments. These data and information can be used for building relevant hind cast models, ecological forecasts, and regional environmental indices (e.g. upwelling, climate, “hot spot”) on biological distribution and/or response in the PNW.

### Key Findings

*(1) Patterns of SST and SSHA reveal linkages between seasonal heating effects and dominant physical processes affecting the sanctuary including upwelling, downwelling, and transport.*

- SST patterns reveal seasonal maximums in August and minimums in January, with spring and fall transitions in May and November. Juan de Fuca Strait outflow results in suppressed SST during summer. Upwelling influences on SST are more dramatic inside the sanctuary versus points south of the sanctuary.
- SSHA patterns reflect vertical changes from mean sea level and reveal seasonal maximums in January and minimums in July, coincident with the peak of the downwelling and upwelling seasons, respectively. Maximum transition periods occur in March and November. Heights respond to coastal wind forcing, upwelling-induced (salinity and temperature driven) effects and freshwater influence inside the sanctuary.
- Altimetry-derived radar estimates of SSHA could be used in combination with thermal infrared SST to isolate upwelling activity and biological response for PNW marine environments.

*(2) Patterns of ocean color chlorophyll and turbidity reveal insights on nutrient/sediment sources, timing of bloom response, and wind-driven processes affecting the sanctuary.*

- Chlorophyll patterns show spatially distinct pulses during the spring bloom period (April-June) just north of and inside the sanctuary, followed by strong upwelling-induced pulses inside the sanctuary from July through mid-October.
- Turbidity maximums occur during the fall-winter period inside the sanctuary; minimums occur in association with the Juan de Fuca Strait outflow in summer.
- Columbia River plume influence on ocean color is most evident in southern portions of the study area, with seasonal precipitation significantly correlated with ocean color turbidity inside the sanctuary.

*(3) Co-variability of surface water properties reveals subseasonal processes and modes of influence that limit chlorophyll production during the downwelling/upwelling cycles.*

- Correlation patterns among precipitation, discharge, and ocean color in January suggest a strong coastal influence on surface sediment response characteristics inside the sanctuary.
- Correlation patterns among SST, SSHA, and ocean color in May suggest that increased regional heating, physical circulation and mixing processes limit chlorophyll production most dramatically.
- Correlation patterns among SST, SSHA, and ocean color in July suggest that increased light and temperature, along with upwelling, drive production inside the sanctuary.
- Correlation patterns in September suggest that coastal processes (Juan de Fuca outflow and Ekman transport) lead to fall chlorophyll maximums inside the sanctuary.

*(4) Climatological anomalies of surface water properties reveal varied levels of response to environmental perturbations.*

- Broad-scale climate patterns such as El Niño Southern Oscillation (ENSO) promote varying levels of surface anomalies inside the sanctuary, including extreme positive and negative SST, SSHA, chlorophyll, and turbidity.
- Regional and local OCNMS SST and SSHA anomalies trend positive with ENSO warm phases and negative with cool phases.
- Regional and local OCNMS chlorophyll and turbidity anomalies vary in both strength and direction with documented ENSO and non-ENSO (neutral) periods.

# TABLE OF CONTENTS

<b>1.0 INTRODUCTION AND BACKGROUND</b> .....	1
1.1 Regional Setting and Study Area .....	2
1.2 Regional Oceanographic Summary.....	2
1.3 Seasonal Cycles.....	3
1.4 Interannual Cycles.....	4
<b>2. DATA AND METHODS</b> .....	5
2.1 Data Synthesis.....	5
<i>Sea Surface Temperature (SST)</i> .....	5
<i>SST Fronts</i> .....	5
<i>Sea Surface Height Anomalies (SSHA)</i> .....	6
<i>Geostrophic Currents</i> .....	7
<i>Ocean Color</i> .....	7
<i>Winds</i> .....	7
<i>Land Precipitation and PNW drainage boundaries</i> .....	7
<i>Climatological Summaries</i> .....	7
2.2 Visual Representation Of Data .....	8
2.3 Quantitative Representation Of Data .....	8
<i>Data Disclaimer</i> .....	9
<b>3. RESULTS</b> .....	11
3.1 Seasonal Patterns of SST, SSHA, and Currents .....	11
<i>East-West summary</i> .....	13
<i>Cross-shelf summary</i> .....	13
<i>Alongshore summary</i> .....	14
<i>Summary of processes influencing SST and SSHA</i> .....	15
3.2 Seasonal Patterns of Chlorophyll, Turbidity and Winds .....	17
<i>East-West summary</i> .....	19
<i>Cross-shelf summary</i> .....	20
<i>Alongshore summary</i> .....	20
<i>Summary of ocean color response characteristics</i> .....	22
3.3 OCNMS Seasonal Cycles and Transition Periods .....	23
<i>Winter</i> .....	23
<i>Spring transition</i> .....	23
<i>Spring/early summer bloom period</i> .....	23
<i>Late summer/early fall transport and upwelling period</i> .....	23
<i>Fall transition</i> .....	23
3.4 Seasonal Patterns of Oceanic Fronts, Gradients, and Ocean Color Variability.....	25
<i>Juan de Fuca Eddy</i> .....	27
<i>Summary of SST fronts and chlorophyll variability</i> .....	27
3.5 Ocean Climate Data Summary.....	29
<i>East-West summary</i> .....	29
<i>Cross-shelf summary</i> .....	30
<i>Alongshore summary</i> .....	31
3.6 Surface Property Relationships and Processes Affecting the OCNMS.....	32
<i>SST and SSHA co-variability</i> .....	32
<i>SST, SSHA, and chlorophyll co-variability</i> .....	32
<i>Nutrient/sediment sources and ocean color co-variability</i> .....	34
<i>Summary of intraseasonal (within season) processes influencing surface layer relationships</i> .....	36

<b>3.7</b>	<b>Interannual Patterns of Surface Properties as Indicators to</b>	
	<b>Environmental Perturbations.....</b>	<b>39</b>
	<i>Interannual patterns of SST and SSHA .....</i>	<b>39</b>
	<i>Interannual patterns of chlorophyll and turbidity .....</i>	<b>42</b>
	<i>Summary of surface anomalies for the OCNMS.....</i>	<b>45</b>
<b>4.</b>	<b>CONCLUSIONS AND RECOMMENDATIONS .....</b>	<b>47</b>
	<b>REFERENCES .....</b>	<b>49</b>
	<b>ACKNOWLEDGMENTS .....</b>	<b>53</b>

## LIST OF TABLES

Table 1.	Remote sensing data products and source specifications for the Olympic Coast National Marine Sanctuary Oceanographic Characterization.....	6
Table 2.	Levels of association between remote sensing parameters, Columbia River discharge and land-based precipitation inside and outside OCNMS boundaries .....	36
Table 3.	Relative level of contribution of physical limiting factors on surface layer response inside OCNMS boundaries. Determination of contribution level based on analysis of expected conditions and intra-seasonal correlation patterns .....	38
Table 4.	Comparison of ENSO index values and remotely sensed variable anomalies from extracted data averaged for the Olympic Coast National Marine Sanctuary .....	45

## LIST OF FIGURES

Figure 1.	Physiographic features off Washington coast and within the Olympic Coast NMS .....	2
Figure 2.	General schematic of the California Current System and North Pacific Gyre .....	3
Figure 3.	Generalized surface flow of the California Current System in the PNW during typical (a) summer and (b) winter conditions.....	4
Figure 4.	Transects used for seasonal satellite oceanographic data extractions .....	8
Figure 5.	Example plot showing long-term weekly averaged (expected) SST conditions along a North-South transect line for Olympic Coast shelf waters (red line) and Washington Coast shelf waters (blue line), and SSHA-derived surface currents depicting magnitude and direction along the southern portion of the transect .....	9
Figure 6.	Example time series plot (Hovmöller) of weekly gap-filled CoRTAD SST (C°) revealing SST along a North-South transect line for Olympic Coast shelf waters (red line) and Washington Coast shelf waters (blue line).....	9
Figure 7.	CoRTAD SST monthly climatologies (1985-2005) showing typical SST distribution during winter (December-February), spring (March-May), summer (June-September) and fall (October- November) periods .....	11
Figure 8.	AVISO SSHA monthly climatologies (1992-2006) showing typical SSHA distribution during the winter (December-February), spring (March-May), summer (June-September) and fall (October-November) periods .....	12
Figure 9.	Climatological summary of weekly averaged (expected) conditions of SST and SSHA during a typical annual cycle along an East-West longitudinal (47°N) transect line for the continental shelf (<200m isobath; red line) and continental slope, open ocean (>200m isobath; blue line). SSHA-derived general surface currents are depicted from extracted data along the shelf break of the study area .....	13
Figure 10.	Climatological summary of weekly averaged (expected) conditions of SST and SSHA during a typical annual cycle along a cross-shelf transect line for the continental shelf (<200m isobath; red line) and continental slope, open ocean (>200m isobath; blue line). SSHA-derived general surface currents are depicted from extracted data along the shelf break of the study area .....	14
Figure 11.	Climatological summary of weekly averaged (expected) conditions of SST and SSHA during a typical annual cycle along a North-South transect line for Olympic Coast shelf waters (red line) and Washington Coast shelf waters (blue line). SSHA-derived general surface currents are depicted from extracted data along the shelf break of the study area .....	15
Figure 12.	Monthly mean SST distribution, SSHA, and SSHA-derived surface current velocities for September 2001 and January 2004, during the height of the upwelling and downwelling periods, respectively .....	16
Figure 13.	SeaWiFS monthly climatologies (1997-2007) showing typical chlorophyll distribution during the winter (December-February), spring (March), early summer (April-September), late summer-early fall (July-September) and fall (October-November) periods.....	17

Figure 14. SeaWiFS monthly climatologies (1997-2007) showing typical Rrs670 value distribution during the winter wet season (December-February), spring (March-April), summer dry season (May-September), and fall (October-November) periods..... 18

Figure 15. Climatological summary of weekly averaged (expected) conditions of SeaWiFS chlorophyll, turbidity and QuikSCAT winds during a typical annual cycle along an East-West longitudinal (47°N) transect line for the continental shelf (<200m isobath, red line) and continental slope, open ocean (>200m isobath, blue line). Winds were extracted along the transect line near the shelf break (box) and vectors plotted to reveal direction in oceanographic convention ..... 19

Figure 16. Climatological summary of weekly averaged (expected) conditions of SeaWiFS chlorophyll, turbidity and QuikSCAT winds during a typical annual cycle along a cross-shelf transect line for the continental shelf (<200m isobath, red line) and continental slope, open ocean (>200m isobath, blue line). Winds were extracted along the transect line off the shelf break (box) and vectors plotted to reveal direction in oceanographic convention..... 20

Figure 17. Climatological summary of weekly averaged (expected) conditions of SeaWiFS chlorophyll, turbidity and QuikSCAT winds during a typical annual cycle along a North-South transect line for Olympic Coast shelf waters (red line) and Washington Coast shelf waters (blue line). Winds were extracted along the transect line along shelf (box) and vectors plotted to reveal direction in oceanographic convention ..... 21

Figure 18. SeaWiFS- derived climatological estimates of Rrs670 20th quantile values during July, revealing decreased turbidity associated with Juan de Fuca outflow inside sanctuary boundaries. Note bifurcation near the mouth of the Strait ..... 22

Figure 19. Monthly mean SeaWiFS chlorophyll and turbidity (Rrs670 values) for May 2002 and September 2006 during the spring bloom period and enhanced fall upwelling periods, respectively..... 22

Figure 20. Diagrams of seasonal breakouts and periods of transition for the Olympic Coast Sanctuary. Average (expected) weekly SeaWiFS median chlorophyll data extracted along a North-South transect line, AVISO geostrophic currents (box), and QuikSCAT winds (circle) depict weekly patterns over the calendar year. .... 24

Figure 21. GOES climatological (2000-2007) SST monthly frontal probabilities showing long-term frontal persistence during the winter (December-February), spring (March-May), summer (June-September), and fall (October-November) periods..... 25

Figure 22. SeaWiFS-derived climatological (1997-2007) estimates of chlorophyll variability during the winter (December-February), spring (March), early summer (April-September), late summer-early fall (July-September) and fall (October-November) periods..... 26

Figure 23. Comparison of climatological chlorophyll variability estimates during (a) late March versus (b) mid April. Note the significant enhancement in variability inside the sanctuary ..... 27

Figure 24. CoRTAD SST climatological (1985-2005) monthly gradients and gradient along-front directions for June and July..... 28

Figure 25. CoRTAD SST climatological (1985-2005) monthly along-front gradient directions and climatological monthly median chlorophyll for June, and July..... 28

Figure 26. Diagrams of averaged (expected) daily-weekly AVISO SSHA, CoRTAD SST, SeaWiFS chlorophyll and turbidity (Rrs670), AVISO geostrophic currents, and QuikSCAT winds along an East-West transect line over the calendar year. .... 29

Figure 27. Diagrams of averaged (expected) daily-weekly AVISO SSHA, CoRTAD SST, SeaWiFS chlorophyll and turbidity (Rrs670), AVISO geostrophic currents and QuikSCAT winds along a cross-shelf transect line of each data series over the calendar year..... 30

Figure 28. Diagrams of averaged (expected) daily-weekly AVISO SSHA, CoRTAD SST, SeaWiFS chlorophyll and turbidity (Rrs670), and AVISO geostrophic currents along a North-South transect line of each data series over the calendar year ..... 31

Figure 29. Monthly SST vs. SSHa Spearman correlation coefficients ( $\rho$ ) showing strength and direction (+/-) of spatio-temporal relationship for the months of (a) July and (b) October .....	32
Figure 30. Spearman correlation coefficients ( $\rho$ ) showing strength and direction (+/-) of spatio-temporal relationship between CoRTAD monthly SST and chlorophyll for May ...	33
Figure 31. Scatterplot displaying the relationship between CoRTAD SST and SeaWiFS chlorophyll during climatological May for waters (a) outside and (b) inside the sanctuary. Values are extracted from boxes shown in Figure 30 .....	33
Figure 32. Scatterplot displaying the relationship between CoRTAD SST and SeaWiFS chlorophyll during climatological July for waters (a) outside and (b) inside the sanctuary. Values are extracted from boxes shown in Figure 33 .....	33
Figure 33. Spearman correlation coefficients ( $\rho$ ) showing strength and direction (+/-) of spatio-temporal relationship between monthly SST and chlorophyll for July .....	34
Figure 34. Spearman correlation coefficients ( $\rho$ ) showing strength and direction (+/-) of spatio-temporal relationship between monthly SST and chlorophyll for September .....	34
Figure 35. Spearman correlation coefficients ( $\rho$ ) showing strength and direction (+/-) of spatio-temporal relationship between SeaWiFS January turbidity and (a) USGS gauged Columbia River January discharge and (b) GPCC January precipitation .....	35
Figure 36. Spearman correlation coefficients ( $\rho$ ) showing strength and direction (+/-) of spatio-temporal relationship between SeaWiFS chlorophyll and GPCC precipitation for (a) September and (b) October. ....	35
Figure 37. Schematic representation of physical factors limiting nutrient availability and chlorophyll production during winter (January), spring (May), mid-summer (July), and early fall (September) periods .....	37
Figure 38. Time-series plot (Hovmöller) along a North-South transect line revealing weekly gap-filled CoRTAD SST and weekly SST anomaly values for the period 1985-2005.....	39
Figure 39. CoRTAD monthly mean SST anomaly image maps during ENSO and non-ENSO periods.....	40
Figure 40. Time series plot (Hovmöller) along a North-South transect line revealing weekly AVISO SSHa and weekly SSHa temporal deviation for the period 1992-2006.....	41
Figure 41. AVISO monthly mean SSHa temporal deviation image maps during ENSO and non-ENSO periods .....	41
Figure 42. Time series plot (Hovmöller) along a North-South transect line revealing filtered SeaWiFS chlorophyll and chlorophyll anomaly values for the period 1997-2007 .....	42
Figure 43. SeaWiFS monthly mean chlorophyll anomaly image maps during ENSO and non-ENSO periods .....	43
Figure 44. Time series plot (Hovmöller) along a North-South transect line revealing filtered SeaWiFS turbidity and turbidity anomaly values for the period 1997-2007.....	44
Figure 45. SeaWiFS monthly mean turbidity anomaly image maps during ENSO and non-ENSO periods .....	44
Figure 46. Schematic describing general uses of remotely sensed parameters (proxies) outlined in this report for ecosystem resource evaluation, problem identification, and management decision support .....	48



## 1. INTRODUCTION AND BACKGROUND

In January 2007, the Center for Coastal Monitoring and Assessment (CCMA), Office of National Marine Sanctuaries (ONMS), and Federal/Regional Integrated Ocean Observation System (IOOS) Associations initiated discussions on the importance of broad-scale use of satellite-based oceanographic data to support the Olympic Coast National Marine Sanctuary (OCNMS). Satellite data requirements were identified to: (1) fill existing gaps in baseline environmental data, (2) enhance the understanding of ecological patterns and processes for the Olympic Coast region, and (3) provide information and insights to support the Olympic Coast Sanctuary Management Plan Review process (<http://olympiccoast.noaa.gov/>). To support these requirements, CCMA conducted a two-year investigation and summary of ocean climate, character, and color for the Pacific Northwest (PNW) region through satellite remote sensing.

This oceanographic summary represents a unique regional synthesis, interpretation, and characterization of multiple long-term satellite observational datasets made available through the National Aeronautics and Space Administration (NASA), National Oceanic and Atmospheric Administration (NOAA), and other worldwide operational data centers (see data products and sources). Observational monitoring emphasizes real-time data collection and archiving, product generation, and distribution of information vital for improved understanding of physical and biological characteristics in a regional context. A key benefit of sustained data collection is the potential to provide a clear synoptic-scale vision of important temporal and spatial oceanic events, useful for developing environmental indicators of perturbation and for identifying long-term trends within U.S. (and its associated territories') marine protected areas, including sanctuaries.

The objectives of the characterization were to:

- (1) Identify, obtain, and perform regional syntheses on pertinent long-term satellite data to characterize the physical and oceanographic conditions within the PNW, and specifically the OCNMS; and
- (2) Summarize surface patterns, features, and underlying processes governing oceanographic variability and climate as depicted through satellite remote sensing for consideration in National Marine Sanctuary biodiversity/conservation evaluations, management plan reviews, ecosystem assessments, and other decision-support initiatives.

Herein, seasonal and interannual variability (and co-variability) of surface water properties and features were characterized with reference to dominant physical processes for the region. Seasonal surface patterns and changes over a typical annual cycle were analyzed and documented. Specific spatial-temporal linkages among water properties were analyzed to provide insights on ocean behavior and timing of seasonal transitions. Ocean temperature fronts and chlorophyll variability measures were used to reveal spatial-temporal aspects of phytoplankton (biological) activity for the region. In addition, oceanographic anomalies of key surface properties were documented as potential indicators of environmental perturbation, and for evaluating future trends for the sanctuary.

This study complements prior oceanographic investigations through the use of temporally and spatially robust remote sensing datasets. A characterization of oceanographic baseline conditions for the OCNMS is among the most important components in management decision support because it sets the context for describing the distribution of biological resources and for defining management alternatives. Ultimately, the goal is to link long-term synoptic imagery with direct observational and interpolated data to improve the understanding of environmental variability and perturbations affecting the sanctuary, and to monitor changes occurring in the sanctuary.

The OCNMS was established in 1994 in recognition of its nationally significant and unique marine environment. The sanctuary resides in a dynamic oceanographic setting with broad scale (> 500 km) variability dominated by seasonal upwelling and downwelling. As a result, the PNW and OCNMS support rich marine mammal and seabird faunas, abundant populations of kelp and intertidal algae, and productive fish and invertebrate communities (ONMS 2008, Sydeman and Elliot 2008). Due to the dynamic nature and harsh

oceanographic conditions along the PNW, collecting physical and biological monitoring data poses a significant challenge when using shipboard *in situ* and/or moored buoy monitoring. The satellite-derived proxies developed as fully georeferenced map layers were used to fill existing data gaps in baseline environmental information, and to provide key insights on local variability for the PNW region.

## 1.1 Regional Setting and Study Area

The study area lies in the northern portion of the Oregonian biogeographic province that extends from Pt. Conception, California, to Cape Flattery, Washington (Airame et al. 2003). The province is characterized by a narrow continental shelf, mountainous shoreline, steep rocky headlands, sandy pocket beaches with sea stack islands, many small and a few large rivers, and small estuaries with barrier islands. The province is also noted as exhibiting the greatest volume of upwelling in North America. The study region resides within the California Current System (CCS) and represents one of North America's most productive marine ecosystems.

The OCNMS, located in the northern portion of the study area off the coast of Washington, encompasses approximately 8,572 km<sup>2</sup> (3,310 mi<sup>2</sup>) of coastal and oceanic waters, or approximately 10% of the study area for this assessment (Figure 1). The sanctuary boundary extends from Koitlah Pt. due north to the U.S.-Canada border seaward to the 100 fm isobath. Following the 100 fm (~183 m) isobath southward, the boundary extends approximately 145 km, cutting across the heads of Nitnat, Juan de Fuca, and Quinault Canyons to a point due west of the Copalis River. The shoreward boundary is the mean lower low water line when adjacent to Indian reservations and state and county lands. When adjacent to federally managed lands, the boundary extends to the mean higher high water line.

## 1.2 Regional Oceanographic Summary

The dominant physical broad-scale processes influencing PNW oceanography have been summarized by Hickey (1979, 1989, 1998), Hickey and Banas (2003), Strub et al. (1987), and Strub and James (1988, 2002). The PNW region is characterized by distinct patterns in oceanographic circulation, winter storms, flow-topography interactions, and land-sea influences. Large-scale processes are the predominant influence on seasonal upwelling-downwelling fluctuations, resulting in a highly dynamic oceanographic environment.

PNW oceanography is dominated by the CCS, a broad, meandering system of currents with strong interannual, seasonal and weekly variability (Hickey 1998). The CCS forms the southerly flowing segment of the greater North Pacific Gyre and extends from British Columbia, Canada to Baja California, Mexico (Figure 2). The dominant scales of circulation over much of the CCS are set up by strong alongshore winds, bottom topography, and shelf influences (Halliwell and Allen 1987). Because of these characteristics, coastal trapped waves are efficiently gener-

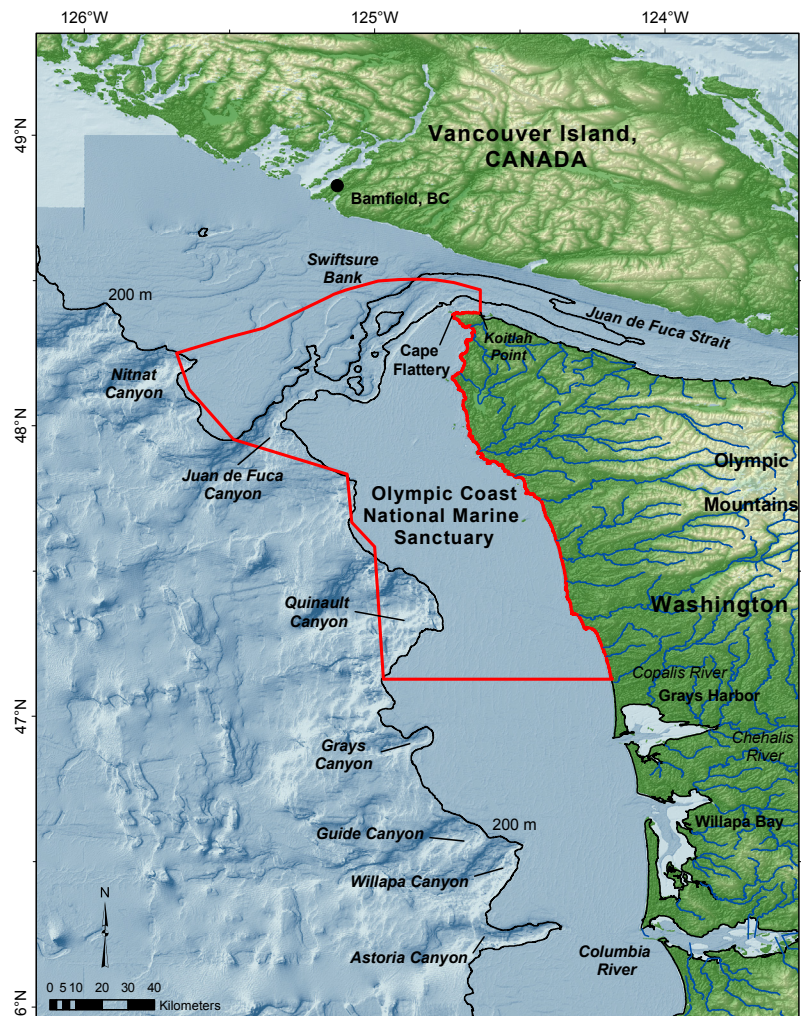


Figure 1. Physiographic features off Washington coast and within the Olympic Coast NMS.

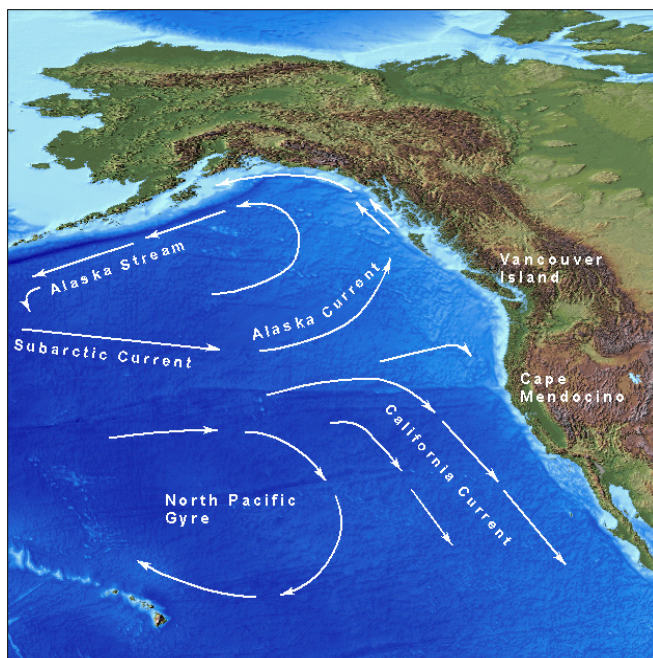


Figure 2. General schematic of the California Current System and North Pacific Gyre. Adapted from NOAA/NCCOS.

ated and propagate long distances along the continental margins of much of western North America (Hickey and Banas 2003).

The CCS includes the slow, southward-moving California Current, the wintertime, northward-flowing Davidson Current, California Undercurrent, and other shelf and slope currents with primarily shorter-than-seasonal time scales. The southward-flowing California Coastal Jet Current and northward Davidson current are commonly observed on the continental shelf during the summer and winter, respectively (Figure 3). The California Current flows southward year round offshore from the shelf break to a distance of 1,000 km from the coast (Hickey 1979, 1998).

Topographic features of the continental shelf interact with and influence flows and circulation in the region. The surface outflow patterns from the Juan de Fuca Strait, and interactions with bottom topography, affect chemical and biological processes, including transport mechanisms for nutrients, larvae, plankton,

and even toxicants (domoic acid) associated with the Juan de Fuca eddy (Trainer et al. 2002, Trainer and Suddleson 2005, Trainer et al. 2009).

The PNW includes one major river plume (the Columbia River), and several smaller estuaries and plumes, particularly evident south of the Juan de Fuca Strait. The Columbia River plume is highly dynamic with variation in direction, depth, and width in response to wind strength and direction (Thomas and Weatherbee, 2006). The plume flows northward over the shelf and slope in the fall and winter. In the spring and summer it flows southward, well offshore of the Oregon shelf.

### 1.3 Seasonal Cycles

Seasonal oceanographic cycles influencing the PNW have been described in detail by Hickey and Banas (2003) and are defined by the dominant circulation patterns in the PNW region. Generally, oceanographic seasons can be characterized as (1) Winter (November-mid-February), (2) Spring (late February-March), (3) Early summer (April-June), (4) Late summer-early fall (July-September), and (5) Fall (October-November), including spring and fall periods of transition.

Coastal upwelling is the dominant process controlling Olympic Coast water property variability over several-day to seasonal time scales. Upwelling along the Olympic Coast typically exemplifies colder, denser, saltier, and nutrient-rich waters that are being forced upward adjacent to the coast, typified by southward winds driving an offshore surface water movement known as Ekman transport. This occurs along the entire U.S. West Coast, but the strength and duration of upwelling increases to the south. With the exception of regions affected by the Columbia plume, stratification in the CCS is remarkably similar at most locations and is largely controlled by seasonal changes in large-scale advection (transport) and upwelling of water masses. Increases in chlorophyll production and biomass are evident during the heightened upwelling season. The region experiences periods of wind relaxation when seas are intermittently calm and winds are variable.

Coastal downwelling generally occurs during the fall and winter, where a marked reversal from the summer pattern is evident along the Olympic Coast. The strong Davidson Current affecting the region is driven not only by the large-scale north-south pressure gradient, but also by strong winds from the south associated with storms entering the region. Wind stress combining with the Coriolis force is especially strong in winter, driving an onshore Ekman transport of water (Thomas, Strub, and Brickley 2003). Downwelled wa-

ter along the coast is typically warmer, less saline, and nutrient reduced. The region can undergo diminishing cross-shelf and alongshore currents, causing a decrease in onshore Ekman transport at times during the winter season (Allen and Newberger, 1996; Austin and Barth, 2002).

For this report, seasonal oceanographic cycles and transition periods will be characterized by surface patterns, and changes in response to the dominant circulation drivers affecting the Olympic Coast region. Seasonal cycles will be documented to better understand expected conditions of each variable and to provide insights on dominant processes influencing variable response. General lags associated with surface characteristics in response to ocean processes also will be documented.

### 1.4 Interannual Cycles

Interannual and decadal-scale variability of the CCS involves complex atmospheric interconnections associated with El Niño Southern Oscillation (ENSO), the Pacific Decadal Oscillation (PDO) and the North Pacific Gyre Oscillation (NPGO) (Halpin et al. 2004, Di Lorenzo et al. 2008). These cycles promote significant long-term variability in the region that can yield extreme oceanographic anomalies on interannual to decadal time scales (Schwing et al. 1996). ENSO conditions are a result of interannual changes in sea level pressure between the eastern and western hemispheres of the tropical Pacific (Conlan and Service 2000). PDO is a long-term climatic pattern that is expressed by altering sea surface temperatures, surface winds, and sea level pressure (Mantua and Hare 2002). PDO shifts generally occur every 20-30 years and have occurred five times in the last century. (Airamé et al. 2003). The PDO can be described as an extensive El Niño-like pattern of Pacific climate variability with warm (positive) and cool (negative) phases. The most recent shifts from warm/cool and cool/warm occurred in 1998 and 2003, (Airamé et al. 2003; Peterson and Schwing 2003). During warm PDO, cold surface water temperature anomalies are observed in the western and central North Pacific Ocean, while the eastern Pacific exhibits above-average temperatures. The opposite patterns occur during cool phases. The NPGO is a climate pattern driven by broad-scale variations in ocean upwelling and transport processes. The NPGO shows strong interannual patterns of association with key physical-biological ocean variables, including salinity, nutrients, and chlorophyll *a* (Di Lorenzo et al. 2008).

For this report, interannual patterns of surface variable response will be presented as climatological anomalies (deviations) to highlight spatial-temporal characteristics of those deviations from expected conditions. Variable response will also be visually compared with documented shifts in ENSO.

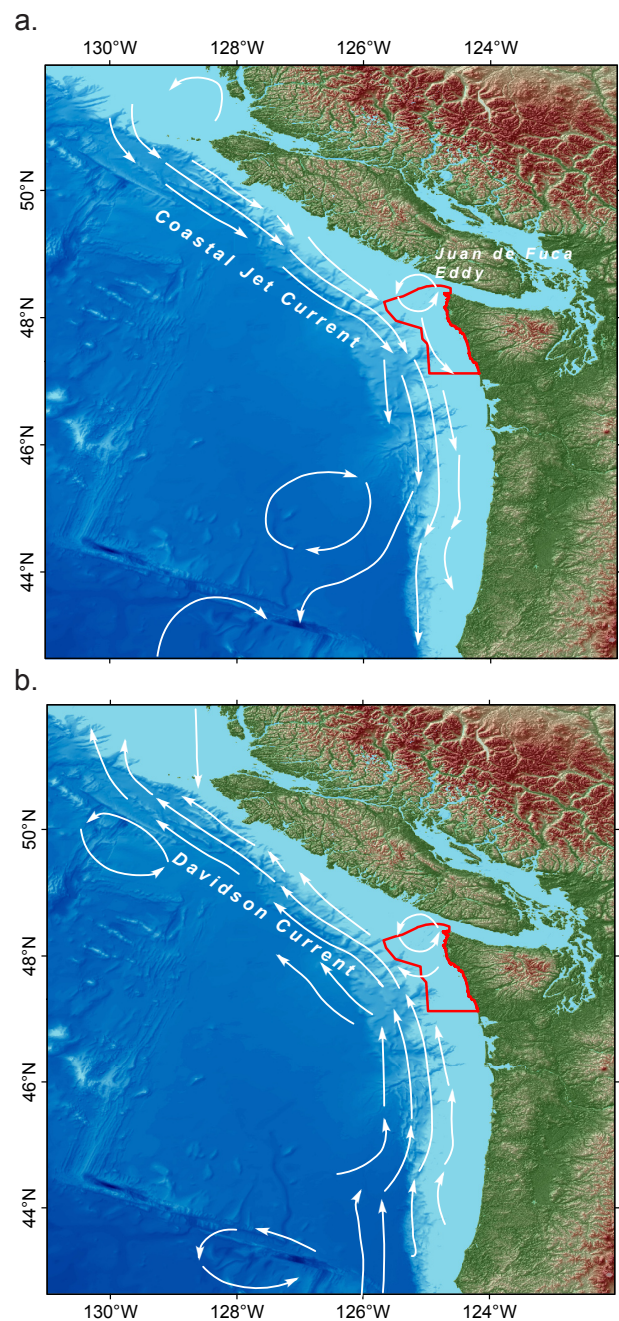


Figure 3. Generalized surface flow of the California Current System in the PNW during typical (a) summer and (b) winter conditions. Source: NOAA.

## 2. DATA AND METHODS

### 2.1 Data Synthesis

Remote sensing data provide key information to understand ocean environments by characterizing the distribution and variability of oceanic surface features. These include ocean fronts, chlorophyll production and transition zones, cold and warm core eddies, convergence zones, and river plumes. Optical observations of physical, biological, and sediment characteristics provide valuable quantitative information on localized transport processes, meso-scale circulation features, and even large-scale water mass characteristics. Radar altimetry estimates of sea surface heights and roughness readily depict ocean surface characteristics including mean sea level, marine currents, winds, and waves. The remote sensing data presented herein were synthesized based on 8+ years of operational coverage, and include weekly to monthly averaged, and climatological anomaly data, for satellite-derived sea surface temperature (SST), sea surface height anomaly (SSHA), geostrophic currents, ocean color products, and winds. In addition to remote sensing data, gridded monthly land precipitation and Columbia River discharge data were used for comparison with remote sensing data, where appropriate. A complete product index for the data used throughout this report can be found in Table 1.

#### *Sea Surface Temperature (SST)*

The Coral Reef Temperature Anomaly Database (CoRTAD) SST estimates were obtained from the NOAA/NASA Advanced Very High Resolution Radiometer (AVHRR) Oceans Pathfinder Version 5.0 Program, developed by the University of Miami's Rosenstiel School of Marine and Atmospheric Science (RSMAS) and the NOAA National Oceanographic Data Center (NODC). The Pathfinder V. 5.0 Program measures global cloud cover, sea surface temperature, and ice, snow, and vegetation cover and characteristics. Weekly (7-day) and monthly averaged data for both the ascending pass (daytime) and descending pass (nighttime) are available on equal-angle grids of 8,192 elements in longitude and 4,096 in latitude (4 km resolution). Gap-filled weekly averaged 4km data were used to achieve the greatest possible spatial coverage over a 7-day cycle. The CoRTAD SST "baseline" temporal resolution encompasses 1,096 weeks for the period January 1985 to December 2005. CoRTAD data were then subset to include the entire West Coast, and weekly data were then binned to monthly averages. CoRTAD SST data series are useful for a range of applications including climatological (1985-2005) baseline and trend determination, ocean frontal boundary delineation, thermal stress detection in coral reefs, and climate indicator development (Halpern et al. 2008, Bruno et al. 2007).

#### *SST Fronts*

SST fronts were detected using CoRTAD data as described above, but also from NOAA/NESDIS/STAR Office holdings of the NOAA Geostationary Operational Environmental Satellites (GOES-10/11) SST and SST fronts data. SST fronts typically occur at the boundaries between various surface water types characterized by different physical, biological and optical properties. Frontal probabilities were calculated from daily-averaged SST fields based on 24-hourly observations. SST fields were processed at NOAA/STAR and CCMA by applying an edge-detection algorithm to identify SST fronts. The probability of detecting fronts (PDF) was calculated based on number of times a particular pixel qualifies as a front divided by the number of clear pixels (following Castelao et al. 2006).

#### *Sea Surface Height Anomaly (SSHA)*

SSHA data from altimetry reflect vertical changes from mean sea level and were obtained from the Archiving, Validation and Interpretation of Satellite Data in Oceanography (AVISO) Program. AVISO delayed time products of sea surface height generated from merged Topex/Poseidon (T/P), Jason-1/2, ERS-1/2 and ENVISAT missions. Delayed time (DT) Reference series products were used to provide accurate, homogeneous measurements across time. Weekly (7-day) and monthly averaged data are available on equal-angle grids of 1080 elements in longitude and 720 in latitude (referred to as 1/4° grid size). In the derivation of SSHA, an estimate of mean sea level (referred to as the mean profile from T/P data for the period January 1993 to December 1999) was applied to develop one merged vertical anomaly map combining measurements from available altimeter missions. SSHA data used in this report encompassed 729 weeks from October 1992 to September 2006. Monthly estimates of vertical sea surface height from mean sea level were

Table 1. Remote sensing data products and source specifications for the Olympic Coast National Marine Sanctuary Oceanographic Characterization.

Product Type	Data Source	Frame	Resolution	Summary	Units
Pathfinder SST and SST Anomaly (CoRTAD)	NOAA/NESDIS/NODC	1985-2005	4km	Weekly/ Monthly	°C
SST gradients (CoRTAD)	NOAA/NESDIS/NODC	1985-2005	4km	Weekly/ Monthly	(°C/12km)
GOES-10/11SST and SST fronts	NESDIS/NODC/STAR	2000-2007	4km	Daily/ Monthly	°C
SeaWiFS Ocean Color Chlorophyll and Anomalies	NASA	1997-2007	1km	Daily/ Monthly	µg L <sup>-1</sup> , Steradian <sup>-1</sup>
SeaWiFS Ocean Color Turbidity; Remote Sensing Reflectance at 670nm)	NASA	1997-2007	1km	Daily/ Monthly	Steradian <sup>-1</sup>
Jason-1, Topex/Poseidon, ERS-1/2ENVISAT Sea Surface Height Anomalies	AVISO, SSALTO/DUACS & CNES	1992-2006	1/4° grids	Weekly/ Monthly	cm
Jason-1, Topex/Poseidon, ERS-1/2ENVISAT Geostrophic Surface Currents	AVISO, SSALTO/DUACS & CNES	1992-2006	1/3° grids	Weekly/ Monthly	cm/s, degrees from north
QuikSCAT Sea Surface Winds	Remote Sensing Systems	1999-2007	25km	Weekly/ Monthly	m/s, degrees from north
Land Precipitation Totals and Anomalies	GPCC	1986-2006	1° grids	Monthly	mm
Columbia River Streamflow Totals	USGS	1986-2006	watershed	Monthly	cfs

obtained following a simple bin averaging technique. Merged SSHA data series provide information on sea level trends, density-driven changes, geostrophic current intensity and direction, and subsurface layers, i.e., mixed and thermocline depths (Strub and James 2002, Wilson and Coles 2004, Gordon and Giulivi 2004).

### Geostrophic Currents

Estimates of geostrophic currents were obtained from merged Jason-1, Topex/Poseidon, ERS-1/2, and ENVISAT missions provided by the AVISO Program. Delayed time Mean Sea Level Anomaly (MSLA) products of geostrophic currents were used. Using oceanographic convention, weekly (7-day) Easterly-toward the East (U) and Northerly-toward the North (V) components, and monthly averaged U-V data, were

made available on a Mercator grid projection with a resolution of  $1/3^\circ$  grid size, encompassing 729 weeks from October 1992 to September 2006. Geostrophic currents result from the balance between Coriolis force and horizontal pressure gradients. Geostrophy implies that the slope of SSHA measured from satellites is directly related to the pressure gradient at the sea surface, and thus, to a geostrophic velocity at the surface.

### *Ocean Color*

The ocean color dataset from Sea-viewing Wide Field-of-View Sensor (SeaWiFS) provided a 10-year (September 1997 to October 2007), near daily set of chlorophyll and light attenuation data, i.e., turbidity, at 1-km spatial resolution. SeaWiFS Ocean Color Level-2 archive products produced and distributed by the NASA Goddard Space Flight Center's Ocean Color Data Processing System (OCDPS) include the geophysical values for chlorophyll *a* using the OC4v5 algorithm. Chlorophyll *a* is the dominant pigment in marine photosynthetic organisms, and is referred to simply as chlorophyll within this report. Light availability, or turbidity, is estimated using the remote sensing reflectance at 670nm  $R_{rs}(670)$  in units of Steradian<sup>-1</sup>, which is a proxy for light scattering due to inorganic sediments in the water. SeaWiFS data are useful for investigating patterns, trends, and episodic events of near-surface ocean phytoplankton variability over a multitude of spatial domains (Sackman et al. 2004, Thomas, Townsend, and Weatherbee 2003).

### *Winds*

QuikSCAT scatterometer wind products derived from Remote Sensing Systems, Inc. (RSS) provided a 7-year (July 1999 to September 2006), weekly set of wind magnitude and direction data at 25km spatial resolution. Winds were calculated using a microwave scatterometer to estimate sea surface roughness and radiometer measurements for rain flagging and sea ice detection. Weekly and monthly averaged data were derived from all data within the calendar month. Wind speeds are scalar averaged and directions are vector averaged.

### *Land Precipitation and PNW Drainage Boundaries*

Regional precipitation data used for spatial comparisons were obtained via the Global Precipitation Climatology Centre (GPCC) real-time precipitation data product based on the complete GPCC monthly rainfall station database in  $1^\circ \times 1^\circ$  resolution (Adler et al. 2003). GPCC land precipitation monitoring data products were processed using area-averaged and time-integrated precipitation fields, based on surface rain gauge measurements collected nationally. The geographic framework (taken from NOAA/NOS/SPO 1999) depicts the boundaries of basins that would include the majority of runoff entering the shelf area of the Olympic Coast, including those from river systems and coastal drainages. Only portions of GPCC grid cells that fell within the coastal drainage basins were used. Monthly precipitation totals were combined as a mean value for the entire coastal basin.

### *Climatological Summaries*

Seasonal to inter-annual shifts in oceanic and atmospheric conditions off the Olympic Coast can significantly influence the persistence, location, and spatial orientation of surface layer features and spatial patterns. The satellite image data series allowed for the extraction of weekly to monthly surface data and for the development of long-term (climatological) weekly to monthly data summaries of average (expected) conditions for each variable presented. In addition, monthly temporal deviation (climatological anomalies) and variability (standard deviation or index) terms were calculated for each variable ( $V$ ). The general formula used in the determination of expected conditions and anomalies follows:

$$V_1'(m, y) = V_1(m, y) - \overline{V_1(m)}$$

where,  $V_1$  represents the monthly average (or median) for month  $m$  of year  $y$ ,  $\overline{V_1}$  is the long-term (grand) mean for month  $m$  of all years, and  $V_1'$  is the climatological anomaly for month  $m$  of year  $y$ . This calculation was performed on all overlapping pixels in the monthly and weekly image databases to create image climatologies for each variable. These climatological images and anomalies will be used to summarize water properties for the upwelling, downwelling, and transition periods, and over interannual cycles.

Assessing variability of surface water properties from satellite provides added spatial and temporal context into the physical processes that limit or enhance phytoplankton production at the surface and at depth.

To address chlorophyll variability, the range (spread) around the monthly and climatological monthly median (50<sup>th</sup> percentile) values were calculated using the difference between the 75<sup>th</sup> and 25<sup>th</sup> quantiles for each overlapping pixel in each month of the calendar year. Quantiling is used to eliminate questionable values in the SeaWiFS dataset. Resulting maps show the spatial distribution of months with the highest variability, revealing chlorophyll “patches” with shape, size, and position occurring at different months of the year.

## 2.2 Visual Representation of Data

The development of consistent daily and weekly time series of multiple image datasets allowed for visual representation and interpretation across variables. Since monthly averaged images are essentially snapshots of expected or average conditions over time, and are not representative of within month variability, extractions of weekly data were performed to help explain temporal patterns of variability important to ocean climate and character within and adjacent to the sanctuary.

Data were extracted along three transect lines in the study area, following a general longitudinal (E-W), cross-shelf, and longshore (N-S) orientation (Figure 4). The longitudinal E-W transect was used to compare patterns of variability inside the sanctuary versus the open ocean environment; the diagonal cross-shelf transect was used to compare shelf patterns influenced by Juan de Fuca Strait outflow and eddy circulation versus shelf slope and open ocean; and the latitudinal N-S transect was used to compare longshore patterns inside the sanctuary versus areas influenced by estuarine and river plumes to the south.

Long-term weekly averaged SST (Figure 5), SSHA, chlorophyll, and turbidity data were extracted along the three transect lines to evaluate spatial-temporal patterns of variability and linkages with complementary satellite datasets. Vector quantities of SSHA-derived geostrophic currents extracted into northerly (toward the north) and easterly (toward the east) components were temporally averaged and plotted as conventional stick plots, depicting magnitude and direction of surface currents (Figure 5, bottom). Weekly (instantaneous) and anomaly data were extracted using time-series color plots (Hovmöller diagrams) and line plots to reveal interannual characteristics of variables (Figure 6). A Hovmöller diagram maps a scalar quantity (e.g., SST in °C) over a span of latitude or longitude through time. The scalar quantities were extracted in the longitudinal, cross-shelf, and longshore directions to depict spatial-temporal variability and episodic (anomalous) events for the period.

## 2.3 Quantitative Representation of Data

Statistical measures of association between remote sensing data types were used to highlight physical and biological coupling, and to infer the nature of oceanographic processes along the Olympic coast. Because these large data sources represent co-located and broad-ranging surfaces (e.g., maps of sea surface temperature, chlorophyll concentration), correlation was used to assess the magnitude and direction (positive/negative) of association among oceanographic variables. Because many of these variables were not normally distributed, Spearman’s nonparametric distribution-free rank correlation was used (Lehmann and D’Abrera 1998). This technique provides a measure of monotone (linear) association, and is often used when the distribution of the data make Pearson’s correlation coefficient undesirable or misleading. Correlation coefficients ( $\rho - \text{rho}$ ) were computed and mapped among monthly mean/median data, and for climatological anomaly data. Correlation matrices describing spatial and temporal associations of all variables, as well as inferred mechanisms influencing variable associations were assessed and documented.

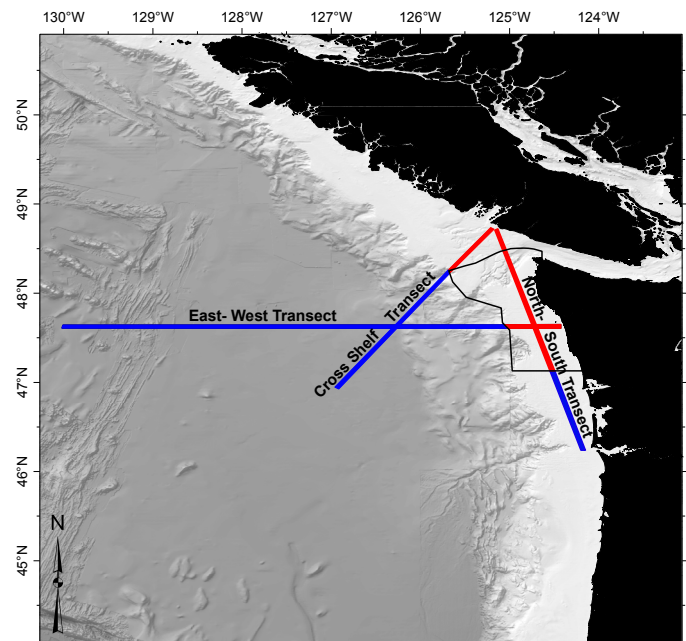


Figure 4. Transects used for seasonal satellite oceanographic data extractions.

**Data Disclaimer**

All remote sensing data, particularly near the coast, should be treated with caution. Near-shore altimetry data that are extrapolated from offshore data typically result in poor sea surface height estimates and subsequently poor geostrophic velocity calculations (Saraceno et al. 2008). Ocean color chlorophyll signals may be biased in some cases due to the presence of color-dissolved organic materials (CDOM) and particulate matter in coastal regions (Gregg and Casey 2004). Turbidity reflectance fields also can be affected by the presence of algal pigments in the water column due to absorption of chlorophyll in the red wavelengths (Dall’Olmo and Gitelson 2005).

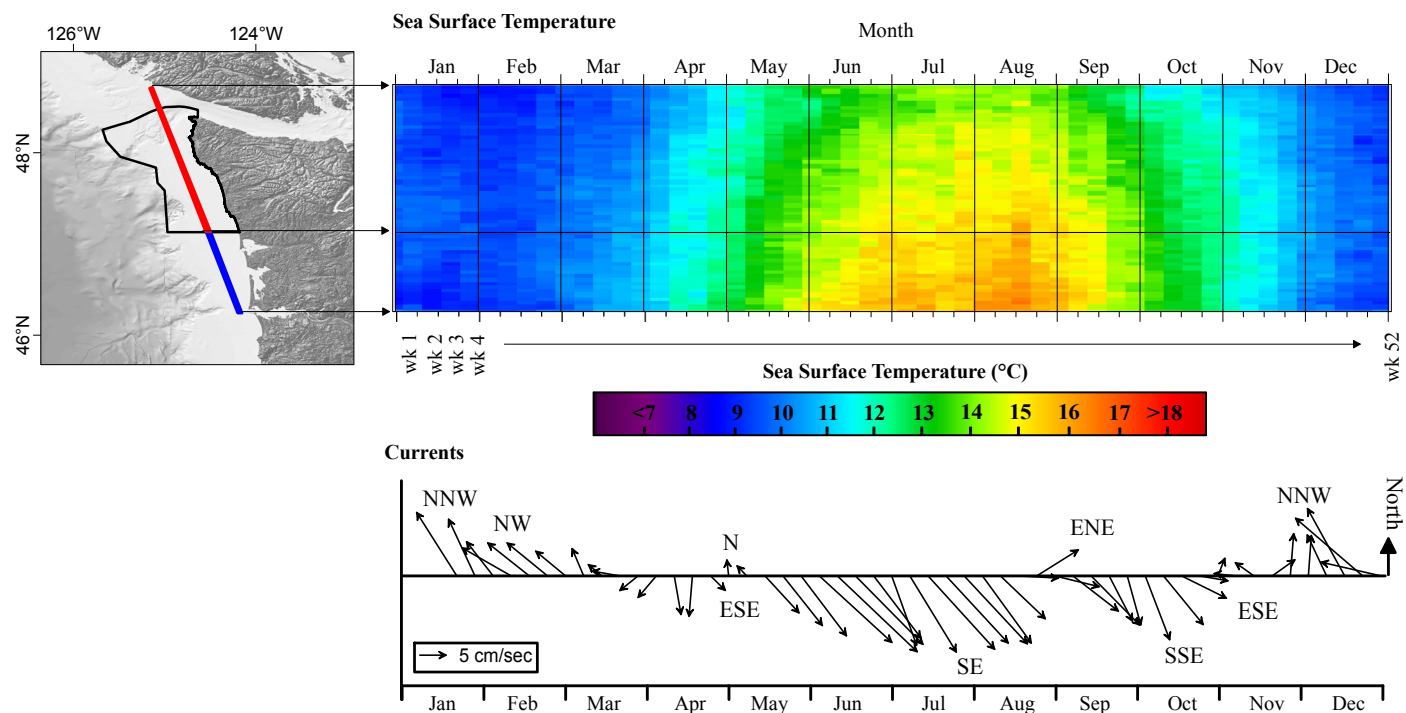


Figure 5. Example plot showing long-term weekly averaged (expected) SST conditions along a North-South transect line for Olympic Coast shelf waters (red line) and Washington Coast shelf waters (blue line), and SSHA-derived surface currents depicting magnitude and direction along the southern portion of the transect. Time period for CoRTAD SST: 1985-2005; AVISO geostrophic currents: 1992-2006.

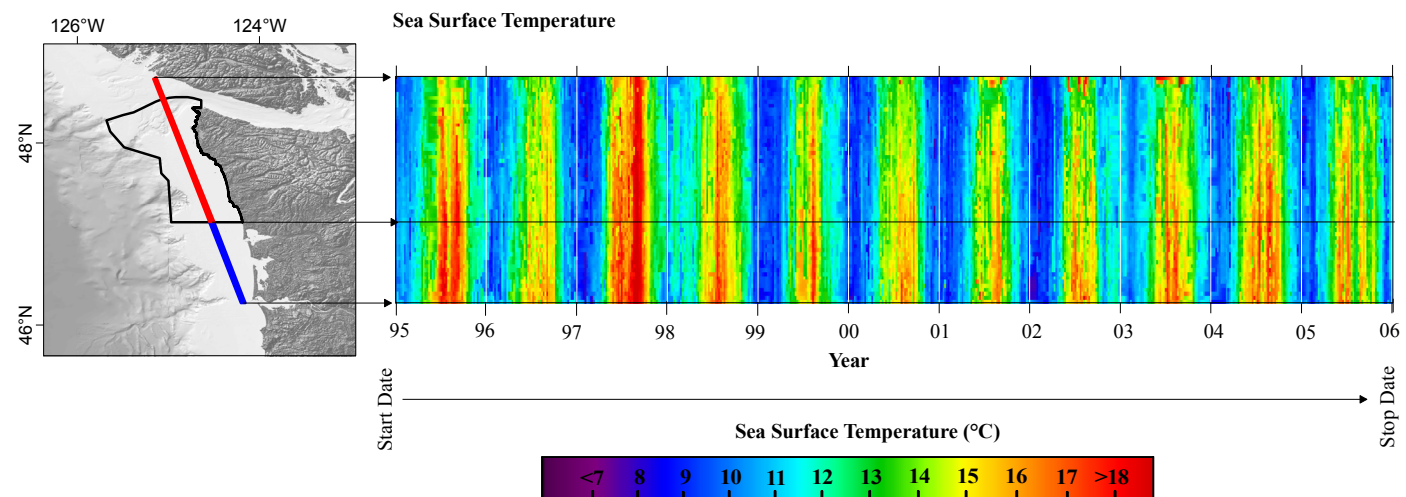


Figure 6. Example time-series plot (Hovmöller) of weekly gap-filled CoRTAD SST (C°) revealing SST along a North-South transect line for Olympic Coast shelf waters (red line) and Washington Coast shelf waters (blue line). Time period: January 1995-December 2005.



### 3. RESULTS

In this section, satellite ocean climate data were summarized to reveal seasonal and interannual variability and transition inside and outside of sanctuary boundaries. Transition is defined as a typical seasonal shift in surface patterns for each variable presented. Highlighted will be the unique spatial and temporal characteristics and differences across variables for the three transects analyzed. Next, the correlation patterns across select remote sensing data types will be evaluated to help identify the scales of influences (local to regional, ephemeral to semi-permanent) on OCNMS water property response. Visual tools including Hovmöller diagrams, correlation ( $\rho$ ) maps, and statistical plots will be presented to illustrate the significance of these relationships. Finally, interrelationships across all data types will be utilized to reveal important limiting factors and modes of influence on surface layer response inside and outside of sanctuary boundaries.

#### 3.1 Seasonal Patterns of SST, SSHA, and Currents

SST data were examined to reveal seasonal characteristics for the PNW region, addressing spatial and temporal variability inside and outside the sanctuary. Seasonal SST patterns (Figure 7) reveal cool wintertime temperatures (purple- blue), indicative of the downwelling season, followed by gradual spring transi-

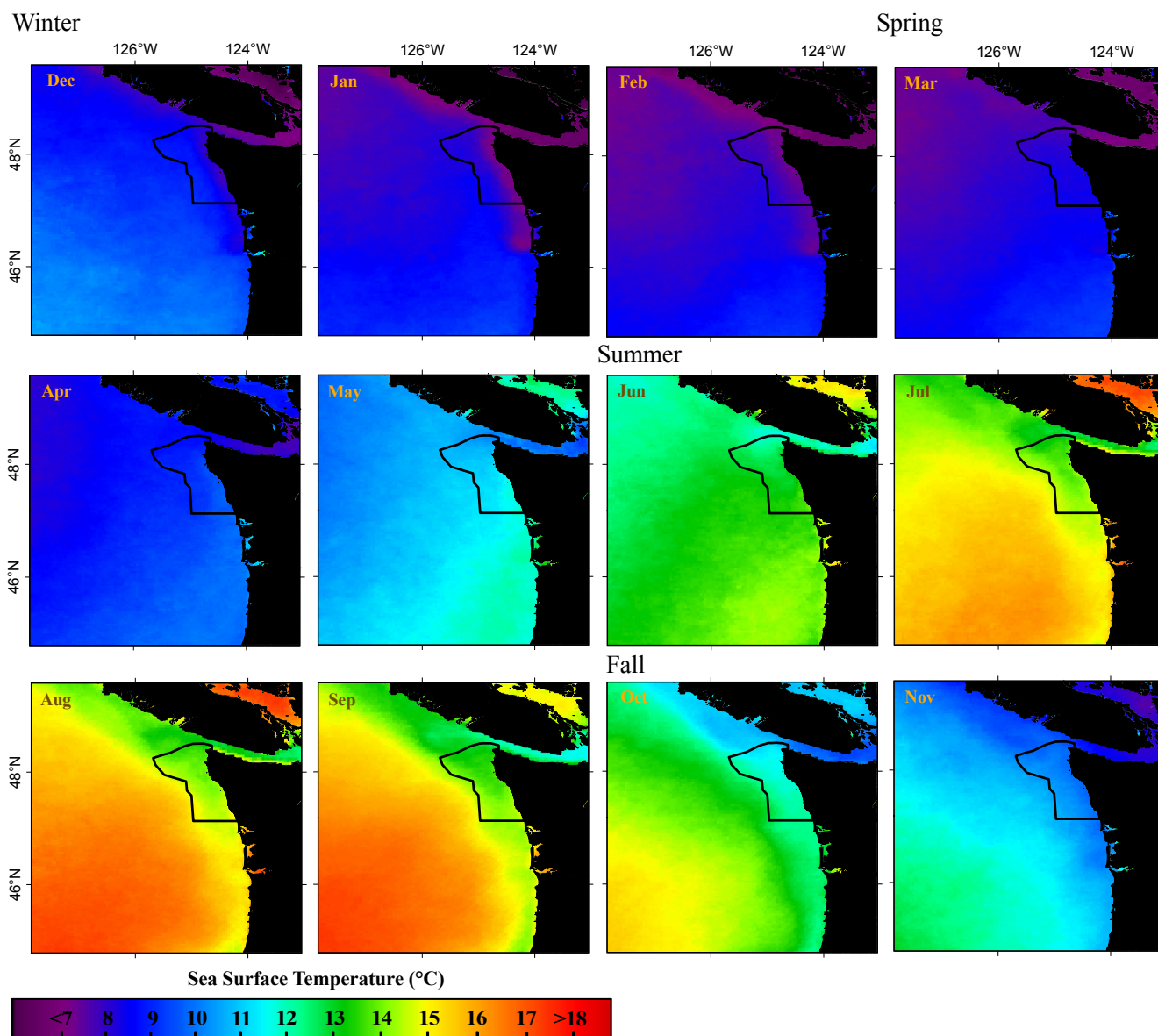


Figure 7. CoRTAD SST monthly climatologies (1985-2005) showing typical SST distribution during winter (December-February), spring (March-May), summer (June-September), and fall (October-November) periods.

tion in March and April. May reveals increased surface heating influence from the south, especially along the coast (cyan-green). Surface heating in summer results in dramatically increased SST mean fields from early June through September, temporally associated with the upwelling season. SST averages range from 8° C to near 16° C in a 4-month interval. A fall transition in SST typically occurs in October and November. Climatological SST maximums occur during August and climatological minimums occur in February (Figure 7).

Seasonal SSHA data were summarized to evaluate coastal perturbations indicative of wind-forcing, density changes from heating/cooling, and salinity (upwelling effects). Because areas surrounding the OCNMS are significantly affected by strong seasonal variation in coastal currents, dynamic month-to-month transitions in SSHA are expected (Figure 8). Seasonal SSHA patterns show positive (orange-red) nearshore heights during the downwelling season, 8-10cm above the vertical mean. Circulation changes during late winter to early spring result in significant SSHA transition from February to April (Figure 8). Spring months are characterized by mainly neutral (cyan) patterns evident in April. During summer upwelling, a sign reversal (+ to -) from winter occurs inside the sanctuary, where heights are negative (blue), 10-12cm below the vertical mean. A gradual fall transition occurs in October and November. SSHA maximums inside the sanctuary occur during January and minimums occur primarily in June/July, with a secondary peak in September.

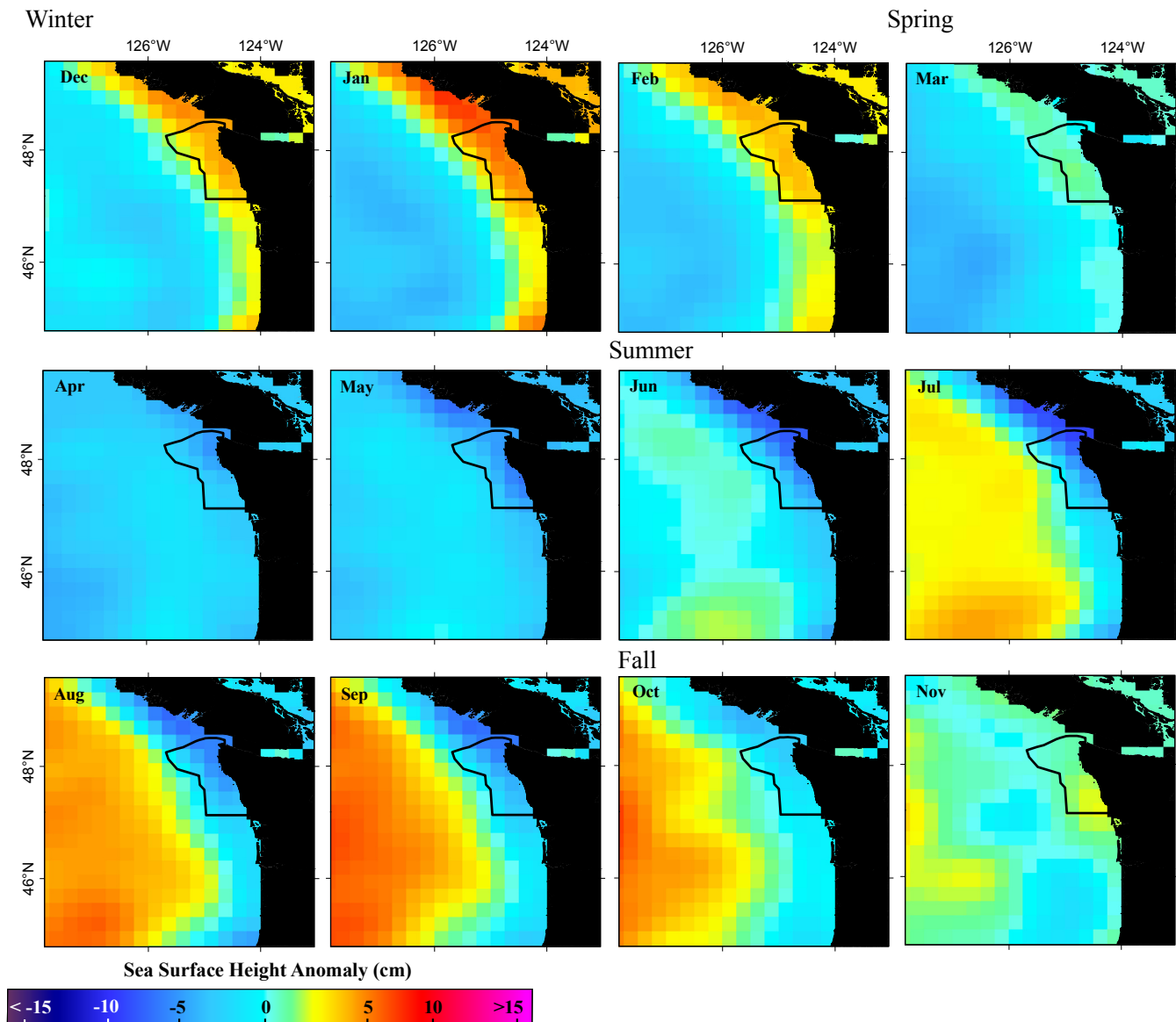


Figure 8. AVISO SSHA monthly climatologies (1992-2006) showing typical SSHA distribution during the winter (December-February), spring (March-May), summer (June-September), and fall (October-November) periods.

### East-west summary

Hovmöller diagrams of expected weekly SST and SSHA reveal the dramatic spring SST increases (cyan to green) up until a mid-late summer maximum (orange-red), followed by the dramatic cooling effect in November (Figure 9). A significant transition occurs starting in May (cyan to green approximates a transition of 1.5 °C; Figure 9). A similar SST transition maximum occurs in November. Warmer waters penetrating northward in spring reveal earlier transition in near-shore areas than in the open ocean (Figure 9, top). Fall transition is more gradual nearshore than in offshore areas (Figure 9, bottom).

SSHA signal strength and sign (+/-) are highly dynamic near shore versus offshore. A wintertime maximum (yellow-orange; Figure 9) near shore occurs during January with a peak of approximately 7cm above mean sea level. In offshore areas, SSHA seasonal variability is more gradual, trending towards a September-October maximum. SSHA minimum inside the sanctuary typically occurs during mid-late September, coincident with increased upwelling at that time. Spring surface height transition occurs before SST transition with maximum sea-level transition in March (Figure 9). Fall sea-level transition occurs in November. SSHA-derived surface geostrophic currents reveal north-northwestward flow in winter and southward flow in summer/fall. Strongest currents occur in late September and January.

### Cross-shelf summary

Hovmöller diagrams illustrate generally lower SST associated with the Juan de Fuca Strait outflow and the eddy feature during summer (Figure 10). Mean SST along the transect reveal summer temperatures to be 14.6°C (red line; figure 10), approximately 2°C colder than in areas of the continental slope (blue line). Lower SST in shelf waters forms an SST frontal boundary in early fall, generally associated with the 200 m isobath.

Strong near-shore variations in SSHA signals are apparent along the

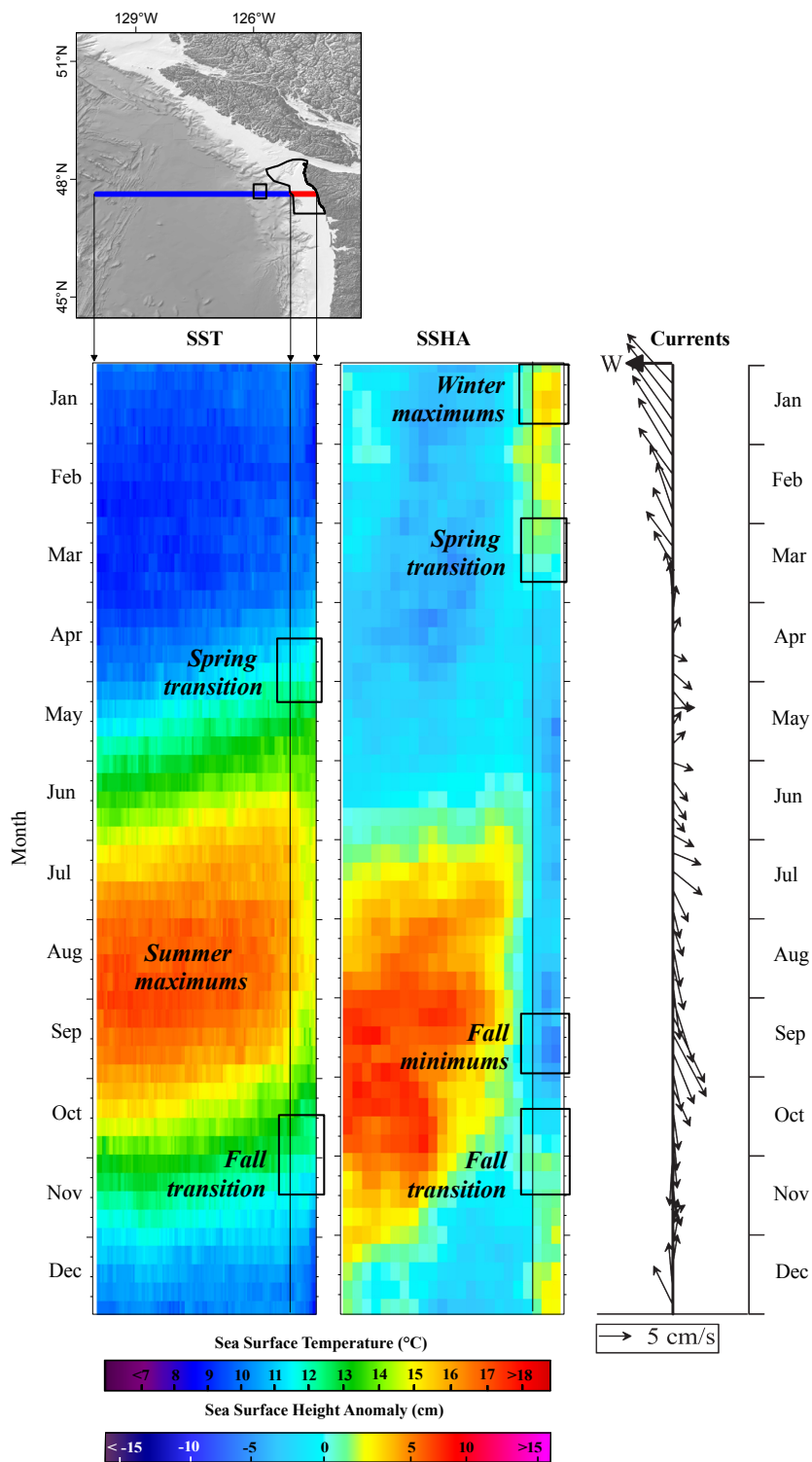


Figure 9. Climatological summary of weekly averaged (expected) conditions of SST and SSHA during a typical annual cycle along an East-West longitudinal (47°N) transect line for the continental shelf (<200m isobath; red line) and continental slope, open ocean (>200m isobath; blue line). SSHA-derived general surface currents are depicted from extracted data along the shelf break of the study area (box).

cross-shelf transect, where summer minimums can exceed 10cm below mean sea level in areas outside of the Juan de Fuca Strait (Figure 10). Of note are the pronounced maximum heights in January, especially in nearshore areas, where heights can exceed 10cm above the vertical mean. Decreased salinities and coastal impingement are speculated as the predominant drivers to elevated sea heights. Spring sea-level transition typically occurs two months earlier than SST transition (Figure 10; boxes). Fall sea-level transition is typically one month after SST transition. Maximum differences between near-shore and offshore heights are slightly exaggerated in January and September (Figure 10), coincident with stronger surface currents during these months. Geostrophic currents along the continental slope (Figure 10) reveal north-northwestward flow in winter, and southward flow in summer/fall.

*Alongshore summary*

Hovmöller diagrams reveal notable differences in SST and SSHA inside the sanctuary, with cooler waters persistent in June-July just south of Bamfield, BC, near the mouth of the Juan de Fuca Strait (Figure 11). Fall SST minimums occur in September just south of Cape Flattery. Wintertime SST differences between northern and southern sections of the transect are negligible, with a February minimum of 8.5°C.

Longshore variations in SSHA patterns are evident inside the sanctuary, with a maximum in January and minimums throughout the upwelling season. A mainly neutral SSHA pattern is evident near the mouth of the Columbia River. Of note are the dramatic differences between SST minimum and SSHA maximum in January. Fluctuations in sea level are influenced by changes in temperature, salinity, and winds. The heightened seasonal SSHA patterns in winter suggest a strong salinity and wind-driven influence, especially since the colder wintertime seawater is less dense than it is during summer.

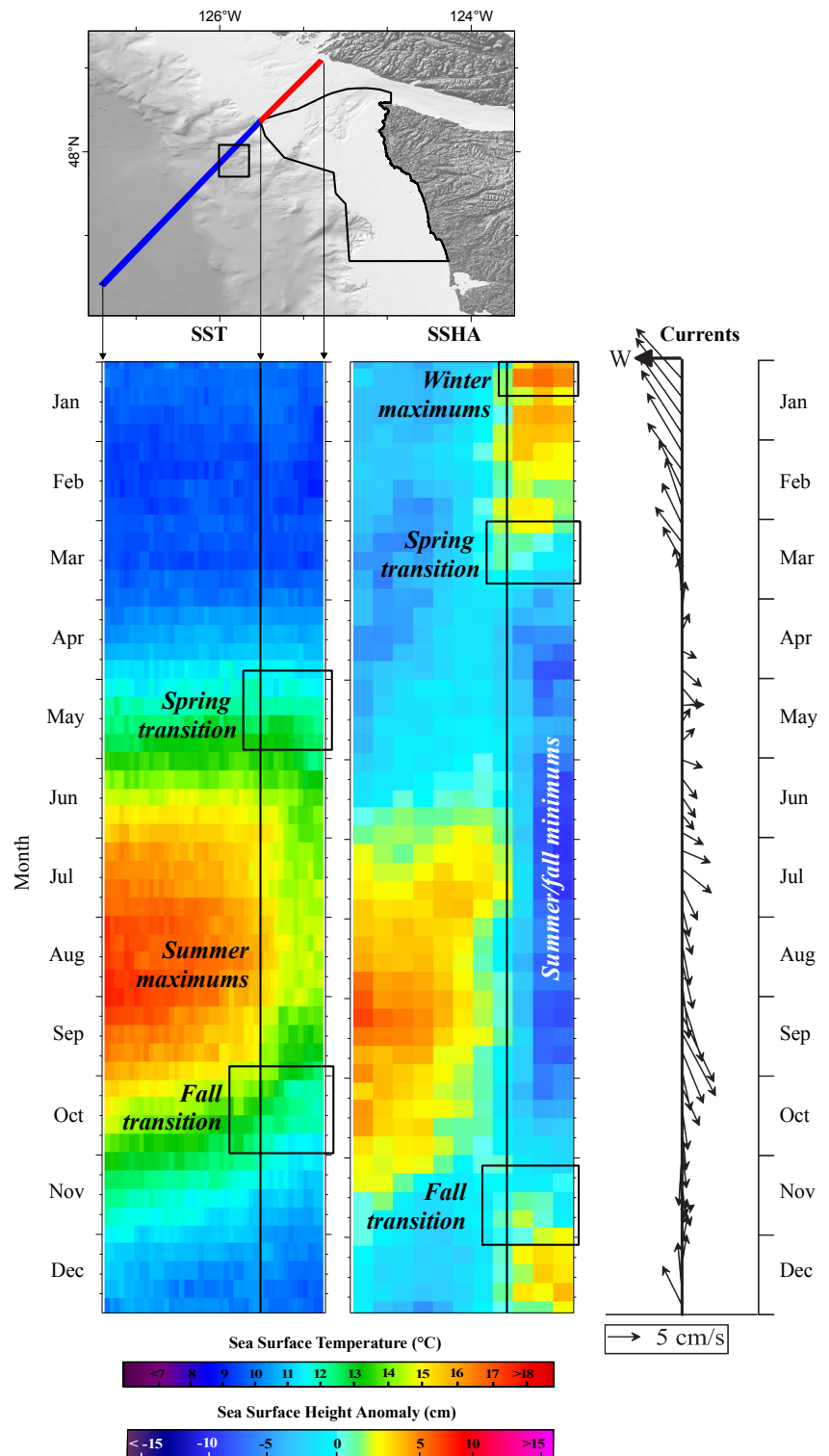


Figure 10. Climatological summary of weekly averaged (expected) conditions of SST and SSHA during a typical annual cycle along a cross-shelf transect line for the continental shelf (<200m isobath; red line) and continental slope, open ocean (>200m isobath; blue line). SSHA-derived general surface currents are depicted from extracted data along the shelf break of the study area (box).

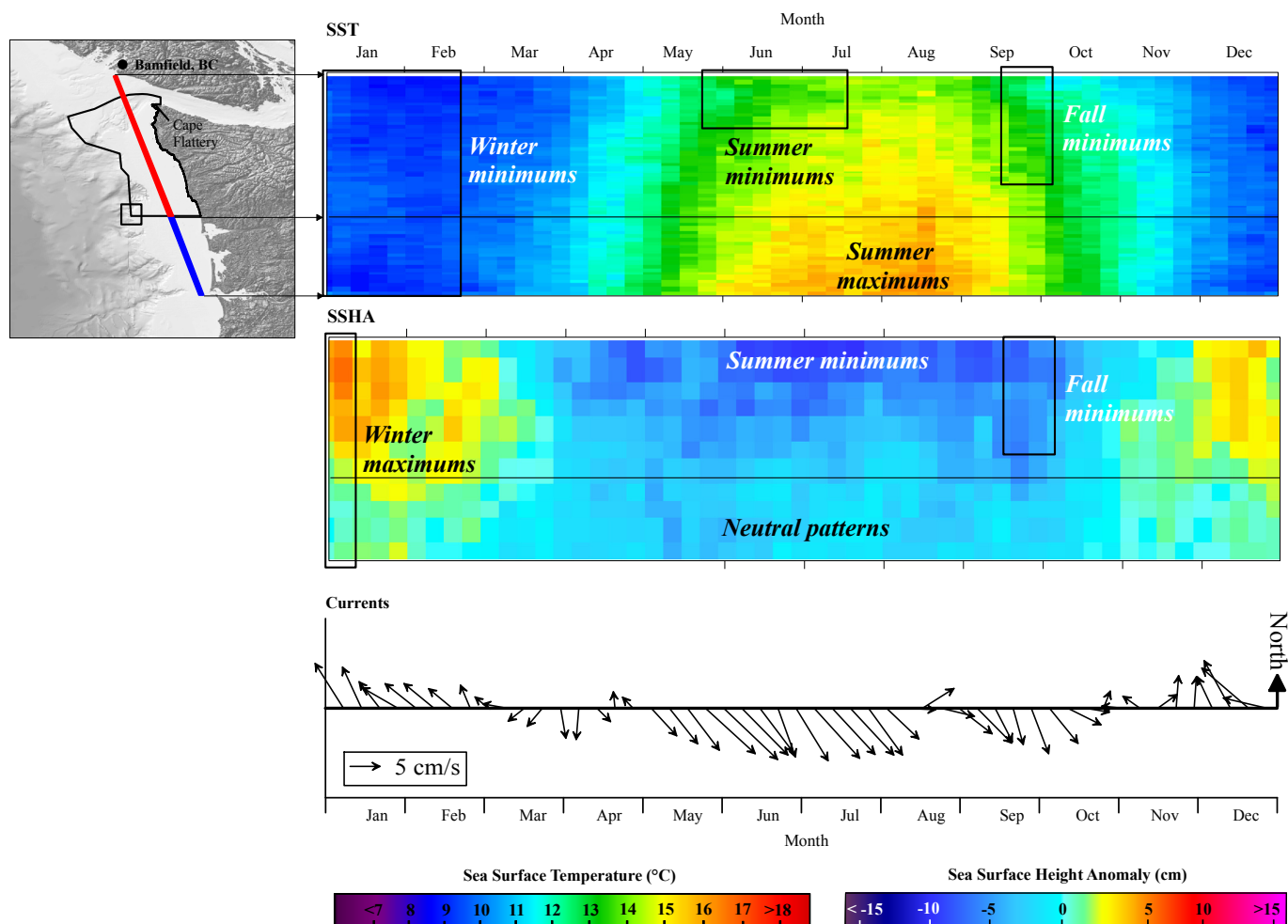


Figure 11. Climatological summary of weekly averaged (expected) conditions of SST and SSHA during a typical annual cycle along a North-South transect line for Olympic Coast shelf waters (red line) and Washington Coast shelf waters (blue line). SSHA-derived general surface currents are depicted from extracted data along the shelf break of the study area (box).

### Summary of seasonal processes influencing SST and SSHA

Patterns of SST and SSHA for the Olympic Coast reflect responses caused by a combination of physical factors. During a strong upwelling period in September 2001, regional SST minimums corresponded with sea surface height minimums (Figure 12). The suppressed SSHA summer signals are indicative of upwelling pulses injecting cooler dense waters to the surface, creating lower sea surface heights (Figure 12; top row). Lower SST is generally shoreward of maximum equatorward flow (Figure 12). During the downwelling period of January 2004 (Figure 12; bottom row), northward wind-induced coastal impingement, Juan de Fuca outflow, and coastal/estuarine influence were likely to have resulted in positive SSHA patterns inside the sanctuary. A more thorough investigation of processes influencing surface temperatures and sea level fluctuations will be presented in section 3.4 and 3.5.

Depictions of both SST and SSHA, derived from infrared and radar altimetry estimates, respectively, reveal dominant seasonally induced processes affecting the region, i.e., wind-driven upwelling and downwelling. Since radar altimetry is not cloud-dependent, subtleties in SSHA variability are captured in the AVISO data, which are sometimes lost in the SST signals due to cloud obscurement. SSHA appears to be less responsive to summer air/sea heating and more responsive to upwelling-induced mixing and wind influences. In summary, these variables could be used in combination to isolate upwelling response for the region.

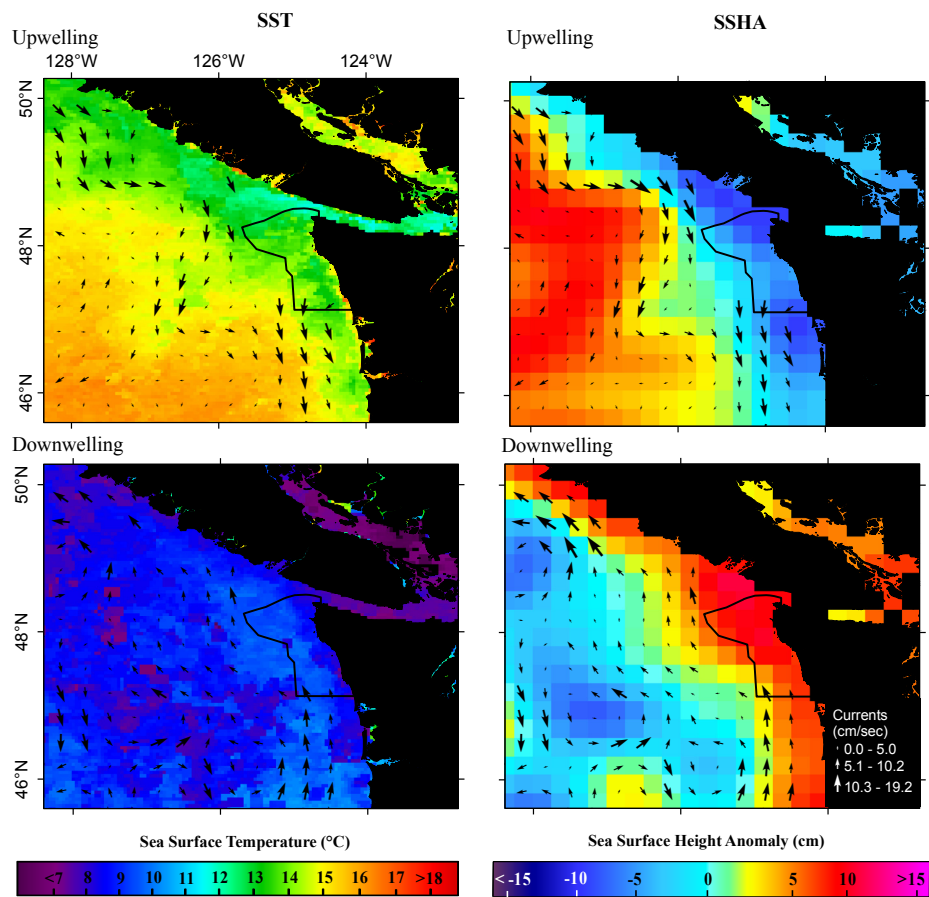


Figure 12. Monthly mean SST distribution, SSHA, and SSHA-derived surface current velocities for September 2001 and January 2004, during the height of the upwelling and downwelling periods, respectively.

### 3.2 Seasonal Patterns of Ocean Color Chlorophyll, Turbidity and Winds

Ocean color data were used to reveal seasonal characteristics for the PNW region, addressing spatial and temporal variability inside and outside of sanctuary boundaries. The climatological monthly mean images shown illustrate the dynamic nature of the spatial distribution of monthly and seasonal chlorophyll (Figure 13). Lower chlorophyll (cooler colors) is indicative of the downwelling season (Figure 13; top row), most apparent during December through February, followed by a gradual spring transition starting in March. In May, coastal chlorophyll concentrations north of the sanctuary increase dramatically, exhibiting a peak in the 6.0- 10.0  $\mu\text{g/L}$  range during the start of the upwelling season. During August to October, a primary peak occurs inside the sanctuary, when highest chlorophyll typically appears for the season. A fall transition typically occurs in November, when chlorophyll production significantly diminishes, falling to lows of around 1.5  $\mu\text{g/L}$  from November through January (Figure 13; bottom row).

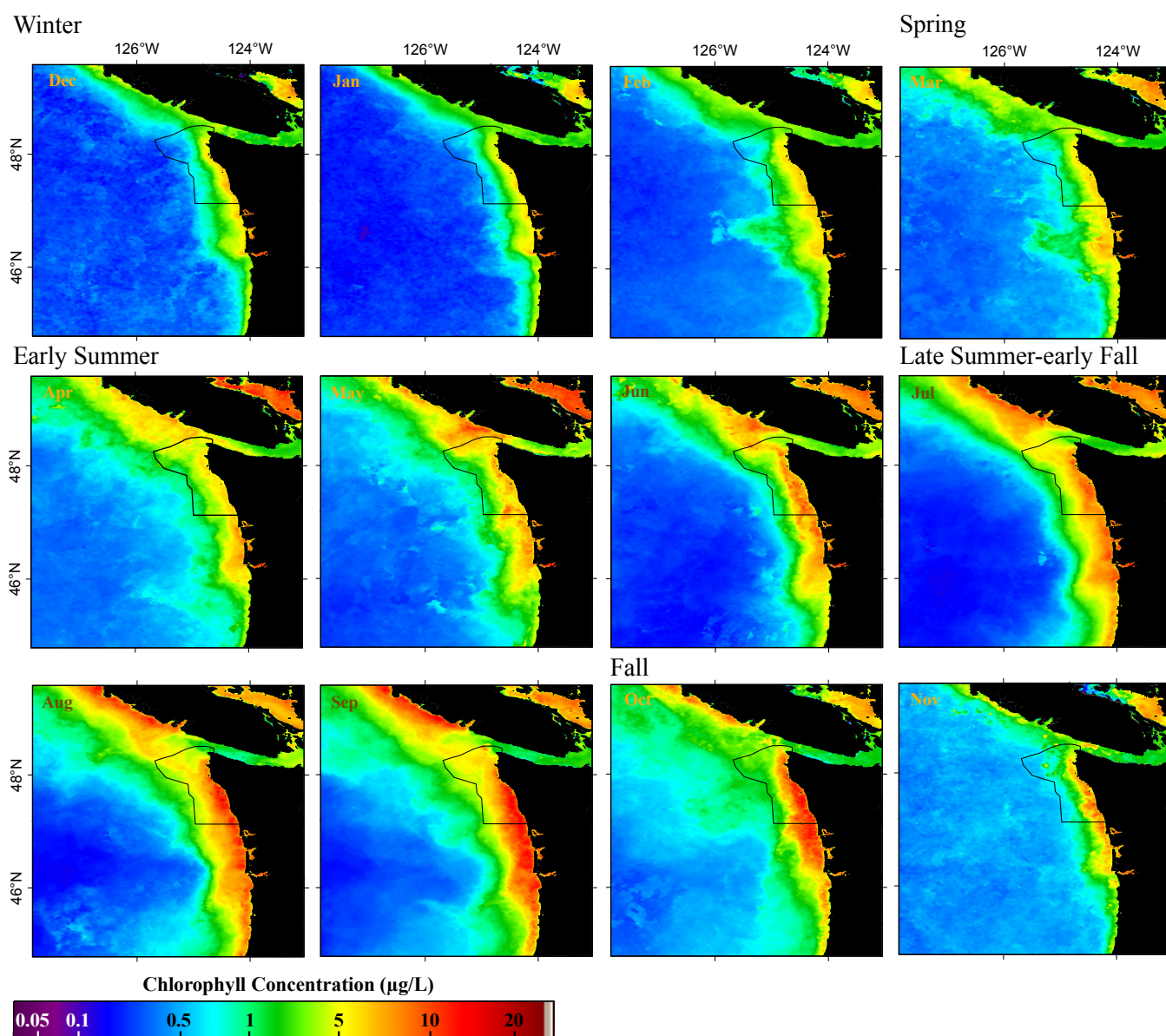


Figure 13. SeaWiFS monthly climatologies (1997-2007) showing typical chlorophyll distribution during the winter (December-February), spring (March), early summer (April-September), late summer-early fall (July-September) and fall (October- November) periods.

Ocean color turbidity, as measured by remote sensing reflectance at 670nm (Rrs670) is a proxy for light availability and particulate (inorganic) loading in the upper water column (Figure 14). This surface effect can be caused by runoff, wind-generated resuspension of sediments, or upwelling currents. Turbidity values are generally very low for the PNW; high values are relatively uncommon and spatially limited. Regions of persistently high values are associated with river plumes and the sediment generated by coastal runoff west of the Olympic Mountains. The highest median turbidity values are the lighter colors (greens to yellows), and lower values are depicted by cooler colors decreasing from greens to blues (Figure 14). The patterns for light availability are divided into two main seasons—wet and dry. Coastal areas south of the Juan de Fuca Strait experience their highs in the winter wet season when rainfall is at its highest, while areas to the west of the Strait, along the continental shelf, experience a primary peak in summer (Figure 14), during the dry season. Values for near-shore areas in the sanctuary are highest from December through March, with a spring transition evident in April, falling to a seasonal low in May. The fall months of September and October are characterized by transition, marking the end of the dry season and start of the wet season.

*East-West summary*

Hovmöller plots of SeaWiFS data extractions along the E-W transect reveal expected chlorophyll

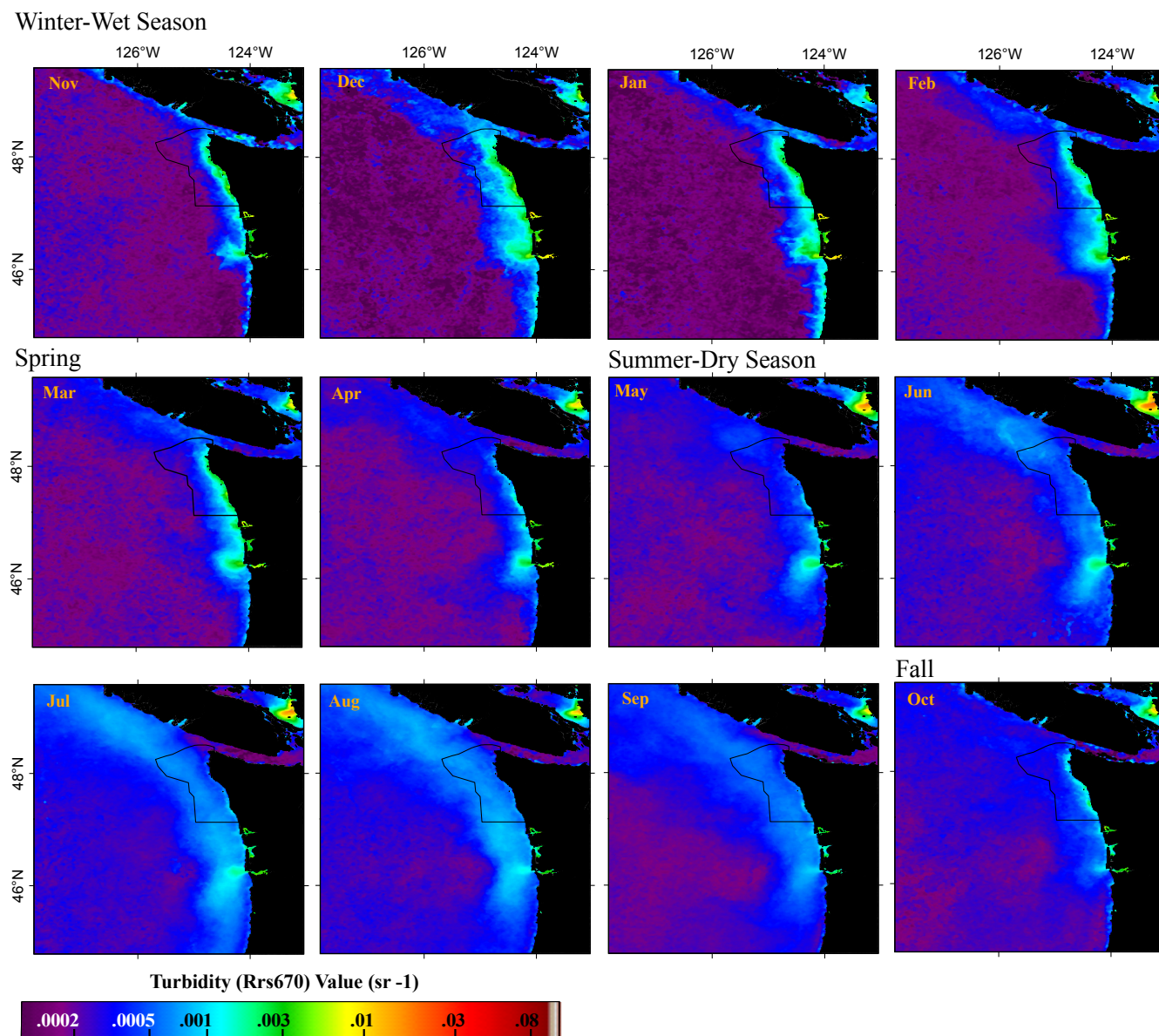


Figure 14. SeaWiFS monthly climatologies (1997-2007) showing typical Rrs670 value distribution during the winter wet season (December-February), spring (March-April), summer dry season (May-September), and fall (October- November) periods.

concentrations and Rrs670 values for the climatological period of January-December (Figure 15). Values represent expected conditions based on the 10-year climatology. A climatological minimum near shore occurs from November through early February, where the width of coastal chlorophyll is restrained to extreme coastal areas and concentration peaks at  $\sim 5 \mu\text{g/L}$ . Slight increases in concentration are evident in late February, with significantly stronger peaks beginning in late July through early October inside the sanctuary (Figure 15, red line). In July, the width of coastal chlorophyll widens significantly. Climatological maximum near shore occurs during late September-early October, when maximum concentrations can reach  $8 \mu\text{g/L}$ . Of note are the chlorophyll responses offshore in mid-October extending into the open ocean environment, where chlorophyll can increase from  $0.1 \mu\text{g/L}$  to  $0.5 \mu\text{g/L}$  during a two-week period (Figure 15, blue line). The onshore-offshore chlorophyll enhancement ends fairly abruptly in November.

The differences in remotely sensed signals of turbidity versus chlorophyll are evident in Figure 15. From November through March, a band of turbidity  $> 0.002$  Steradian $^{-1}$  can be seen during the wet season. Between the end of April to mid October, turbidity near the coast reduces by an order of magnitude to  $\sim 0.0005$  Steradian $^{-1}$ , with a minimum occurring in May. Minimal turbidity increases are evident near the shelf break in summer, with coastal increases building in late October and peaking in December.

Winds show strong seasonal patterns with east-south-eastward directions in spring and early summer, south-eastward directions in mid-summer to early fall, and northward winds in winter (Figure 15).

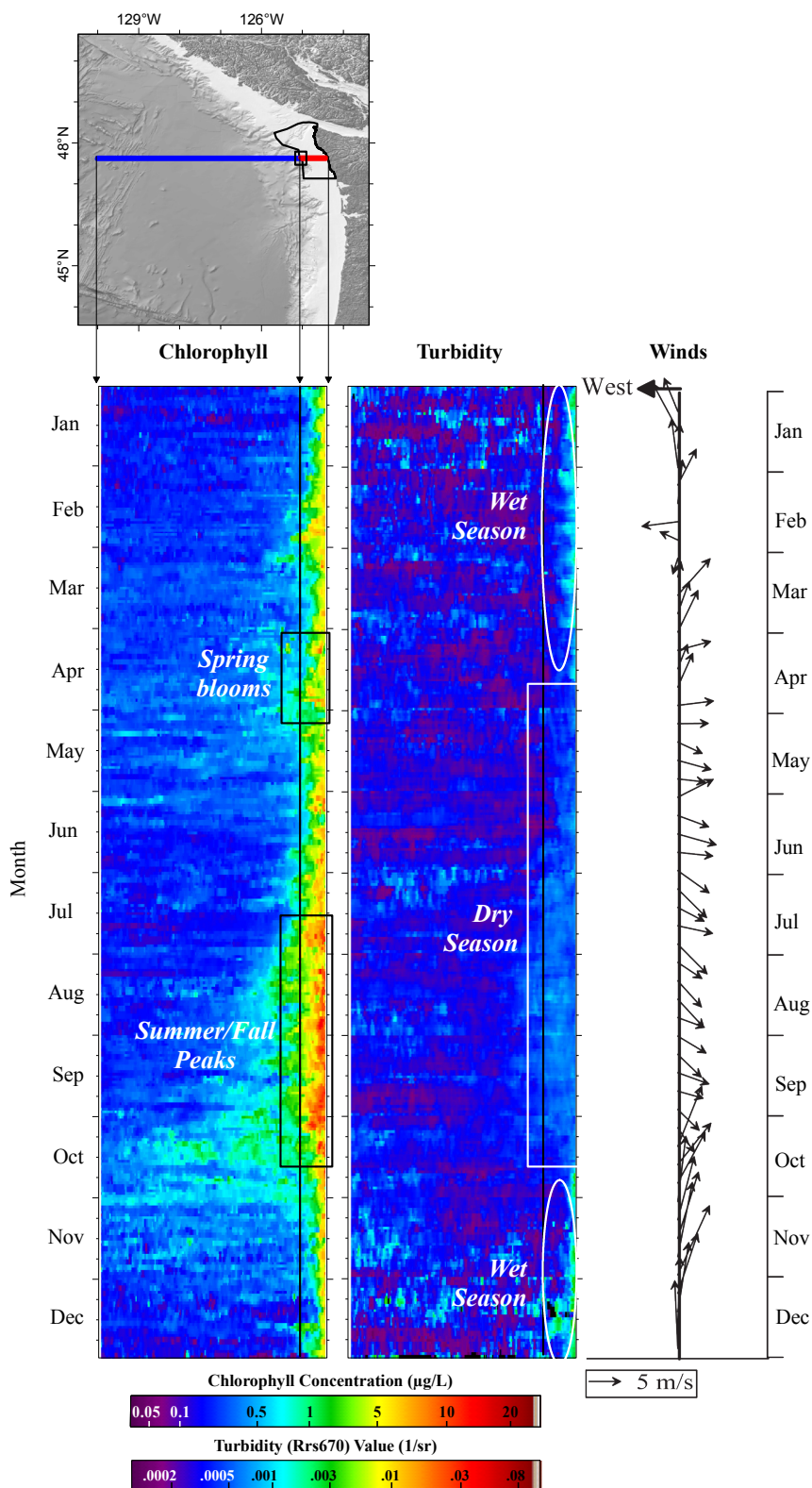


Figure 15. Climatological summary of weekly averaged (expected) conditions of SeaWiFS chlorophyll, turbidity and QuikSCAT winds during a typical annual cycle along an East-West longitudinal ( $47^{\circ}\text{N}$ ) transect line for the continental shelf ( $<200\text{m}$  isobath, red line) and continental slope, open ocean ( $>200\text{m}$  isobath, blue line). Winds were extracted along the transect line near the shelf break (box) and vectors plotted to reveal direction in oceanographic convention.

**Cross-shelf summary**

Through pixel extractions along the cross-shelf transect, Hovmöller diagrams illustrate spring chlorophyll blooms as well as the influences of the Juan de Fuca outflow in spring and summer. Chlorophyll along the coast is near 1 µg/L from December through March. Starting in early April, chlorophyll increases of up to 6 µg/L are observed (Figure 16). The chlorophyll maximums indicative of the spring bloom period can be seen (Figure 16, red line). Nutrient buildup in the cross-shelf area is likely influenced more strongly by spring river runoff out of the Juan de Fuca strait at this time. Of note are the fall peaks evident off the shelf break in October prior to the fall transition period (Figure 16).

A spatially homogeneous area of more turbid water persists just inside of the shelf break from May to September. Slight increases in Rrs670 returns during upwelling could be caused by resuspended sediments churned up by the strong upwelling currents. Of note is the near-shore area around the Juan de Fuca Strait outflow, which exhibits decreased turbidity starting in June and ending in October (Figure 16).

Winds show stronger magnitudes offshore, with eastward directions shifting southeastward in summer and early fall (Figure 16). During fall transition, a fairly abrupt shift from eastward to northward occurs in November and December.

**Alongshore summary**

Longshore variability in chlorophyll signals along the N-S transect line highlight the distinct spring bloom periods to the north of the sanctuary, the summer/fall peaks inside the sanctuary, and the Columbia River outflow influence to the south (Figure 17). During fall transition (November) and winter downwelling, chlorophyll decreases significantly near shore. A distinct transition occurs in late February along the mid-transect, where general increases are seen over a two-week period, and

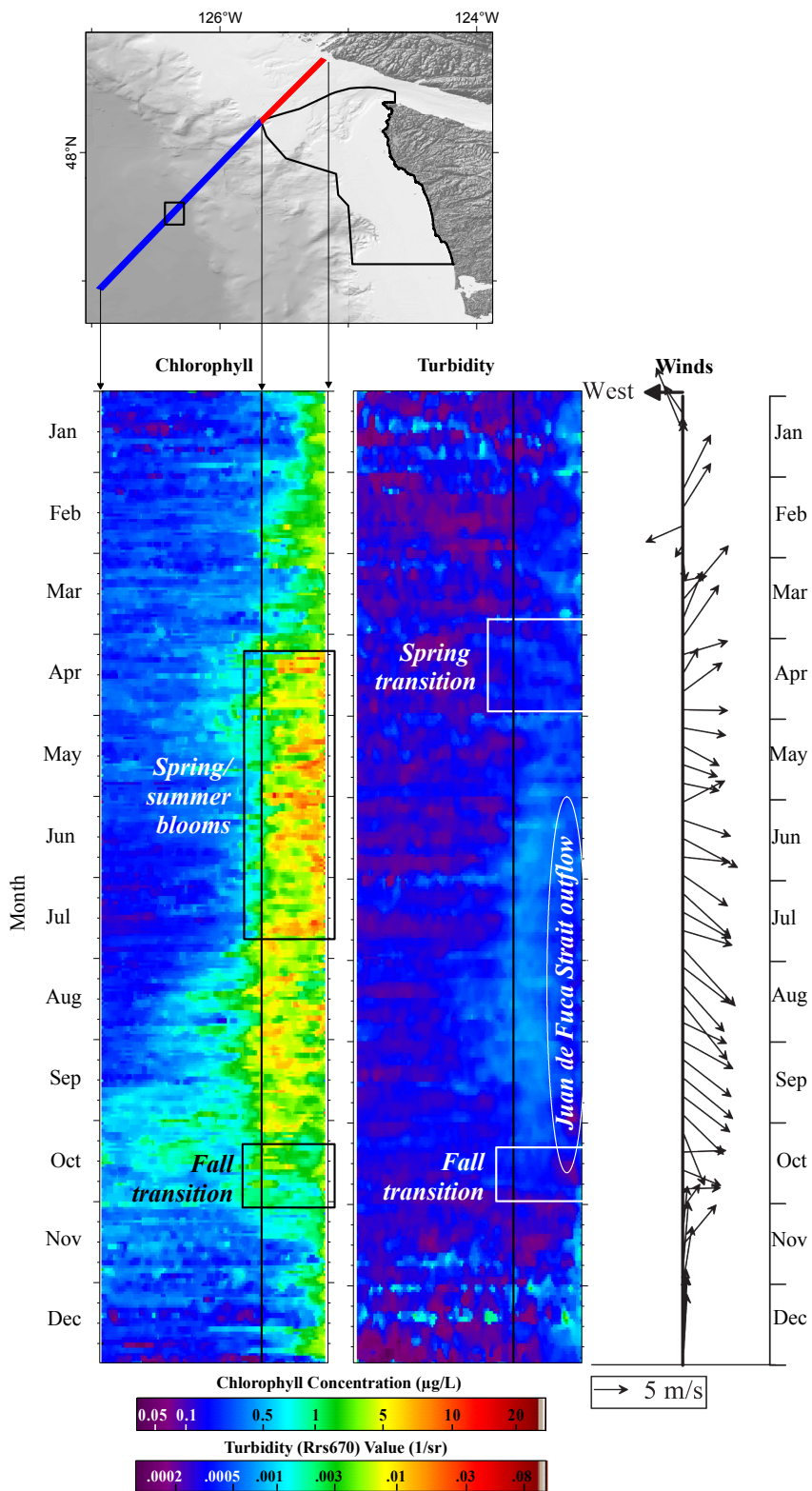


Figure 16. Climatological summary of weekly averaged (expected) conditions of SeaWiFS chlorophyll, turbidity and QuikSCAT winds during a typical annual cycle along a cross-shelf transect line for the continental shelf (<200m isobath, red line) and continental slope, open ocean (>200m isobath, blue line). Winds were extracted along the transect line off the shelf break (box) and vectors plotted to reveal direction in oceanographic convention.

then a flattening occurs until late March (Figure 17). By early April, distinct blooms consistently  $>6 \mu\text{g/L}$  are evident in northern sections (Figure 17, red line), lasting until July. By August, the northern enhancement edge dissipates, with more southerly enhancement persisting through mid October, with maximums ranging from 8-10  $\mu\text{g/L}$  inside sanctuary boundaries. Of note is the implied influence of nutrients from the Columbia River plume affecting the nearshore, remotely sensed chlorophyll signals in the immediate vicinity of the plume (Figure 17). Also of note is the apparent break in the elongated signal band and decreased chlorophyll of  $<0.5 \mu\text{g/L}$  predominantly inside the sanctuary in November and December.

Turbidity values in the alongshore direction reveal influences of the wet season in fall and winter (Figure 17). From the second half of December to the end of March, the magnitude on the southern end of the transect is  $\sim 0.002 \text{ 1/sr}$ . While this magnitude will remain constant until August, the northward extent of coastal influence from the Columbia River varies. The northward extent increases from December through February, and then recedes in March through May. The northbound extent dissipates until the last week of August, and then drops an order of magnitude to  $0.0005 \text{ 1/sr}$ . The strong precipitation influence west of the Olympic Mountains may be attributed to the increased Rrs670 signal in November and December, where land-sea runoff may play a significant role in elevated Rrs670 distribution.

Winds reveal three prevailing patterns, with slightly lighter winds in spring and early summer, stonger upwelling favorable winds southeastward in mid-summer, and northward winds in fall and winter (Figure 17). Fall wind shifts to the north typically occur during October after the fall primary chlorophyll peak.

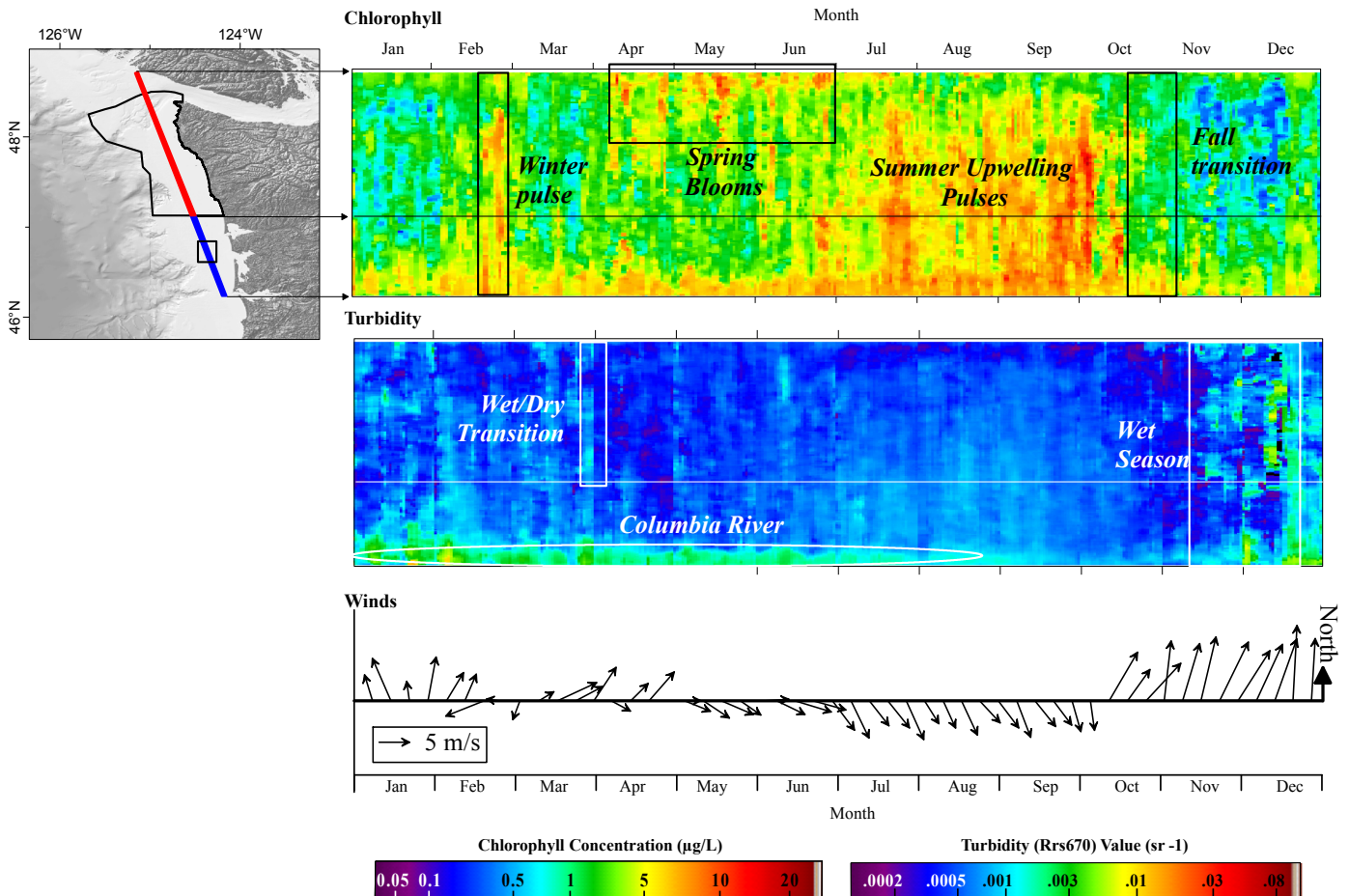


Figure 17. Climatological summary of weekly averaged (expected) conditions of SeaWiFS chlorophyll, turbidity and QuikSCAT winds during a typical annual cycle along a North-South transect line for Olympic Coast shelf waters (red line) and Washington Coast shelf waters (blue line). Winds were extracted along the transect line along the shelf (box) and vectors plotted to reveal direction in oceanographic convention.

The Juan de Fuca Strait outflow and circulation eddy has been shown to be a significant source of nutrients for the region (Hickey and Banas 2003, Trainer et al. 2002). Using SeaWiFS Rrs670 values representing typical low conditions (less turbid) during summer, a narrow band of less turbid waters is evident in areas just outside and to the south of Cape Flattery (Figure 18, purple). These lower Rrs670 values could represent a proxy to nutrient source for this area.

*Summary of ocean color response characteristics*

Ocean color chlorophyll and turbidity estimates provide information on algal production, light availability, and river/estuarine plume influence inside and outside of the sanctuary. Chlorophyll conditions during a strong upwelling period in May 2002 revealed spatially distinct pulses outside of the Juan de Fuca Strait with slight increases in Rrs670 values (Figure 19). Strong fall upwelling-induced pulses were evident during September 2006 inside sanctuary boundaries, with fairly stable Rrs670 values (Figure 19). Chlorophyll maximum typically occurs along the Olympic Coast in late September and early October. Although Rrs670 values are low year-round, values generally exhibit a cyclical temporal variability, with late fall-winter peaks generally occurring during the precipitation maximum for the region. Columbia River plume influence on ocean color is most evident in southern sections of the study area. Juan de Fuca outflow in summer induces clearer water conditions inside the sanctuary.

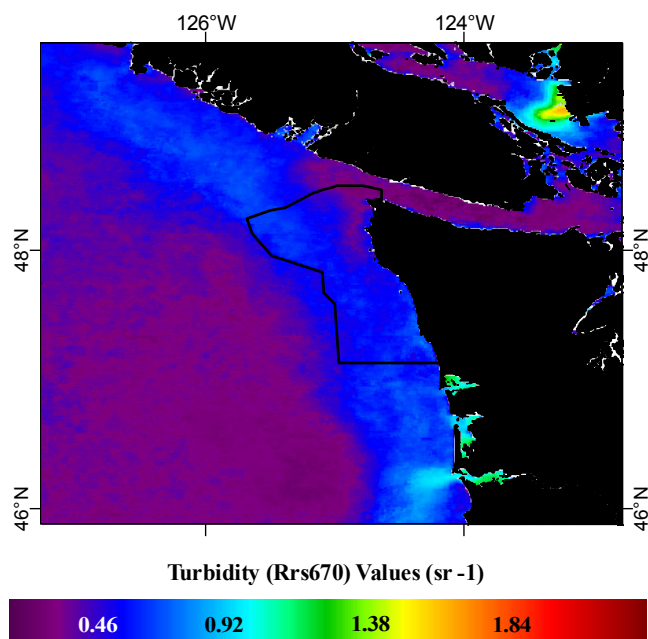


Figure 18. SeaWiFS-derived climatological estimates of Rrs670 20th quantile values during July revealing decreased turbidity associated with Juan de Fuca outflow inside sanctuary boundaries. Note bifurcation near the mouth of the Strait.

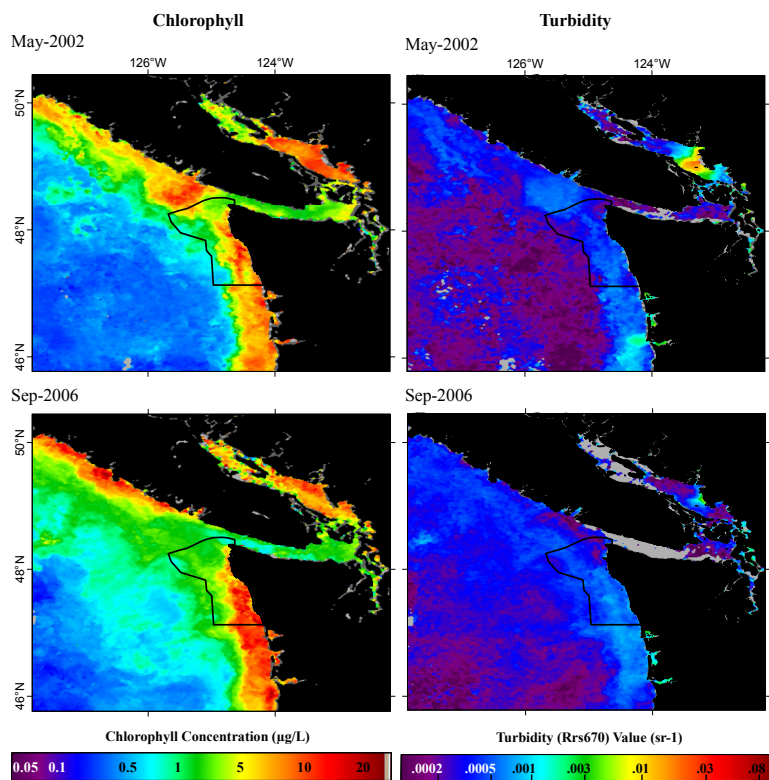


Figure 19. Monthly mean SeaWiFS chlorophyll and turbidity (Rrs670 values) for May 2002, and September 2006 during the spring bloom period and enhanced fall upwelling periods, respectively.

### 3.3 OCNMS Seasonal Cycles and Transition Periods

Through analysis of surface patterns of chlorophyll, currents, and winds, five seasonal cycles were documented for the Olympic Coast region. Seasonal cycles and transition periods were noted for sanctuary waters only, and may or may not be indicative for other areas outside the sanctuary.

- (1) *Winter (November through mid-February)*
- (2) *Spring transition (late February through March)*
- (3) *Spring/early summer bloom period (April through June)*
- (4) *Late summer/early fall transport and upwelling period (July through early October)*
- (5) *Fall transition (October through November)*

(1) *Winter (November through mid-February)*—This period is dominated by strong winds from the south, on-shore Ekman transport, northward mean flow, and downwelling. The present study depicts surface patterns consistent with previous investigation summarized by Hickey and Banas (2003) and Hickey (pers. comm). Chlorophyll patterns are lowest for the year in December (present study). Currents and winds reveal predominantly north-northwest patterns during the height of the downwelling cycle (Figure 20). The region can also undergo diminishing cross-shelf and alongshore currents, causing a reduction in onshore transport at times during the winter season (Allen and Newberger 1996; Austin and Barth 2002).

(2) *Spring transition (late February through March)*—This period reveals variable winds and currents, with generally mean northward flow. Surface pattern climatologies reveal general shifts in currents, winds and chlorophyll production during this time (Figure 20). Upwelling of deep nutrient-rich waters begins after the transition and continues through the fall (Landry et al. 1989). An “early spring” period is evident in a February chlorophyll pulse depicted inside the sanctuary, and could be representative of a transition of fair, upwelling-favorable wind conditions, followed by increased volatility and storminess. A somewhat distinct 2-3 week westward wind shift is evident (Figure 20).

(3) *Spring/early summer bloom period (April through June)*—During this period, upwelling continues, bringing deep waters to the surface near the coast in some areas. Surface flows over much of the shelf and slope are generally southeastward, especially later in the period (Figure 20). Spring chlorophyll enhancement occurs as upwelled nutrients reach the surface near the coast and in the Strait of Juan de Fuca and its eddy (MacFadyen et al., 2005; Hickey and Banas, 2003). The period is associated with increasing SST regionally.

(4) *Late summer/early fall transport and upwelling period (July through early October)*—This period is dominated by southeastward mean surface flow (Hickey 1989, present study), Ekman-induced cross-shelf transports, and upwelling. Coastal upwelling and transport are the dominant processes controlling Olympic Coast water property variability during this time (Lentz 1992, Kirincich et al. 2005). Increases in chlorophyll production are evident during this period. Both currents and winds are generally lighter during this time (Figure 20).

(5) *Fall Transition (October through November)*—During the fall transition, winds shift to more downwelling-favorable (northward), and mean monthly surface currents begin to transition more northward with corresponding changes in water-column stratification (Hickey 1989). The upwelled waters relax downward offshore across the shelf and nutrient supply thus diminishes. A fairly abrupt decrease in chlorophyll concentration occurs during this time.

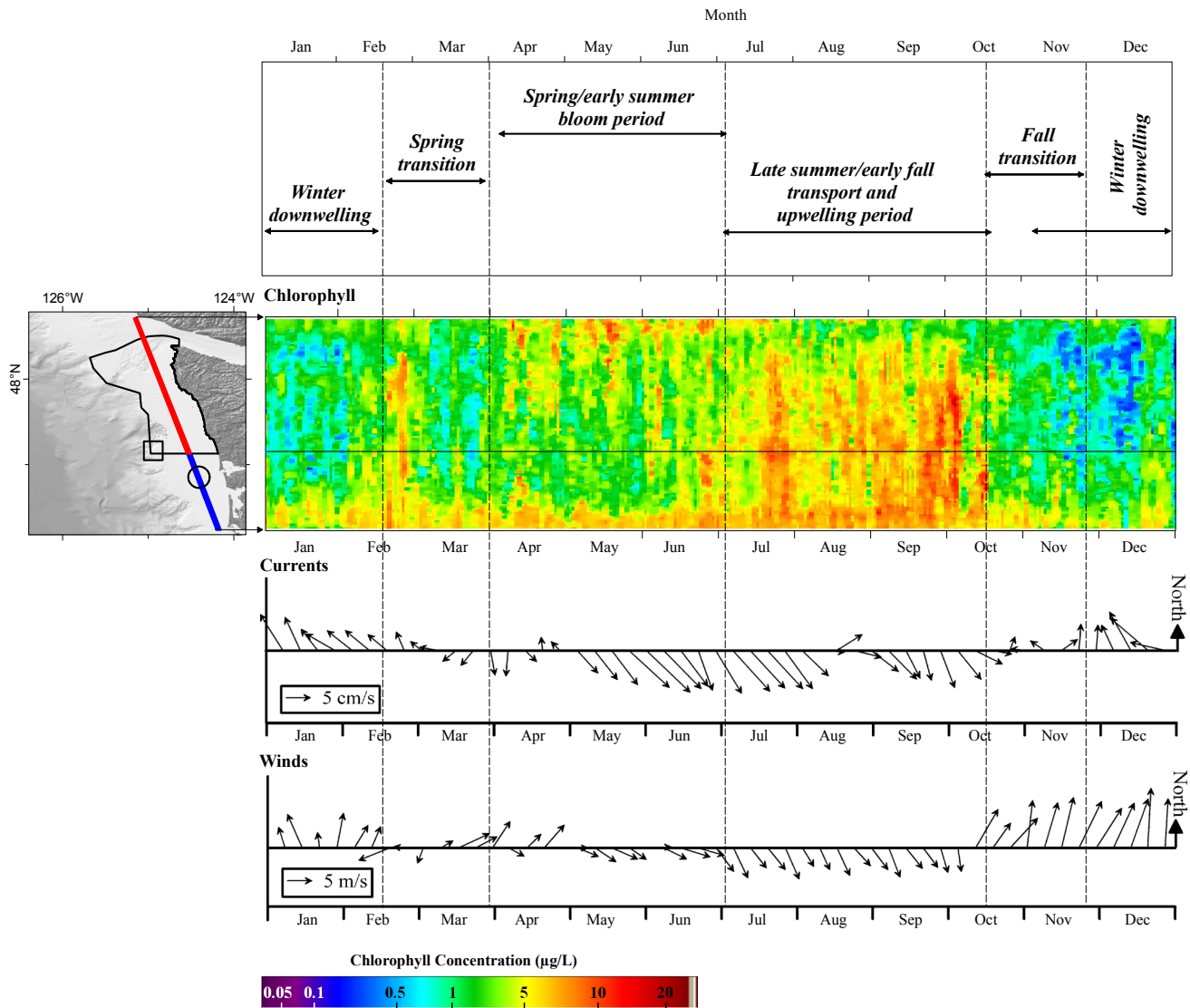


Figure 20. Diagrams of seasonal breakouts and periods of transition for the Olympic Coast Sanctuary. Average (expected) weekly SeaWiFS median chlorophyll data extracted along a North-South transect line, AVISO geostrophic currents (box), and QuikSCAT winds (circle) depict weekly patterns over the calendar year. Breakouts are characterized by surface chlorophyll patterns and circulation drivers for the Olympic Coast region.

### 3.4 Seasonal Patterns of Oceanic Fronts, Gradients, and Ocean Color Variability

Ocean fronts are boundary features typically associated with intensified motion, sharp gradients, decreased stability, and increased convergence at the ocean surface. Efforts to characterize fronts using satellite-derived edge detection methods are well documented (Castelao et al. 2006, Breaker et al. 2005). In PNW marine environments, fronts can be placed into three general classes: (1) small-scale fronts associated with estuarine/river discharge, (2) upwelling fronts associated with strong thermal and salinity gradients, and (3) open ocean fronts caused by wind-forcing. Fronts in the PNW are most apparent during and slightly after the heightened upwelling season.

In OCNMS ocean environments, fronts initially develop in May (Figure 21), coincident with SST undergoing the greatest temporal transition. Coastal upwelling intensity increases dramatically in June, and fronts strengthen during this time. By July, frontal intensity is centered inside the shelf break near the Juan de Fuca eddy circulation, and by September, persistent fronts set up near the shelf break. The most intense offshore fronts occur in October and November. Frontal activity inside the sanctuary decreases significantly during the November transition, reaching a minimum between February and April (Figure 21). Small-scale fronts are also associated with estuarine/river discharge.

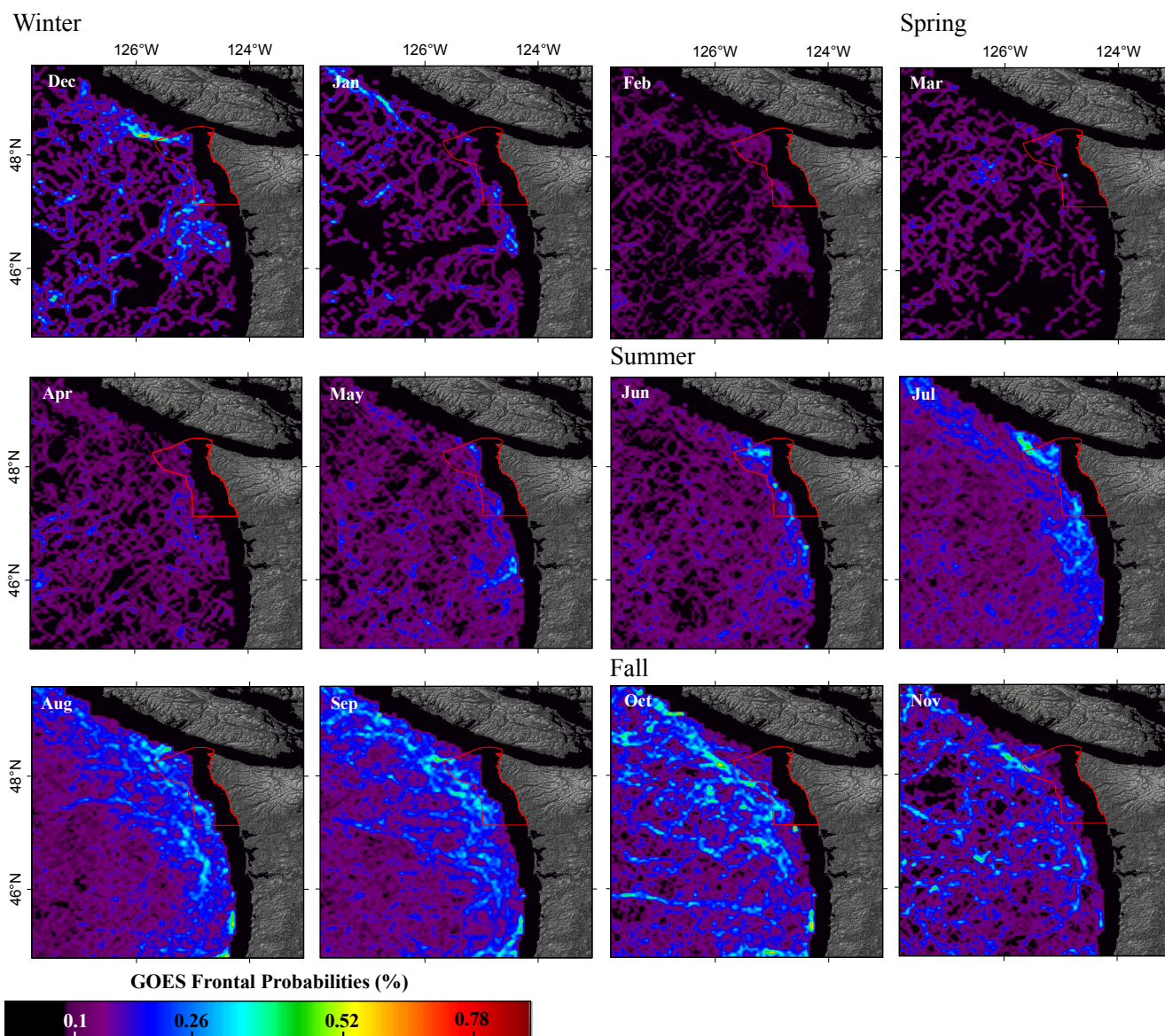


Figure 21. GOES climatological (2000-2007) SST monthly frontal probabilities showing long-term frontal persistence during the winter (December-February), spring (March-May), summer (June-September), and fall (October-November) periods.

Ocean color chlorophyll variability estimates the level of change of chlorophyll concentration over a monthly interval. Assessing variability from satellite data provides added spatial context into ocean phytoplankton activity and physical processes that limit or enhance biological production at the surface. Using differences between the 75<sup>th</sup> and 25<sup>th</sup> quantiles, resulting maps show the spatial distribution of months with the highest variability, revealing distinct and sometimes pronounced areas of enhancement.

At the height of the “turbid season” in January, chlorophyll variability is lowest for the year. A distinguishable area of increased chlorophyll variability is evident in the February image (Figure 22). April patterns of heightened chlorophyll variability exhibit a narrow band of heightened variability inside the sanctuary (Figure 22). Variability then decreases in the sanctuary in late summer, when upwelling pulses are speculated as the dominant process of influence. In September, during the peak of seasonal chlorophyll production, variability also increased and was more widespread, mainly confined outside of sanctuary boundaries (Figure 22).

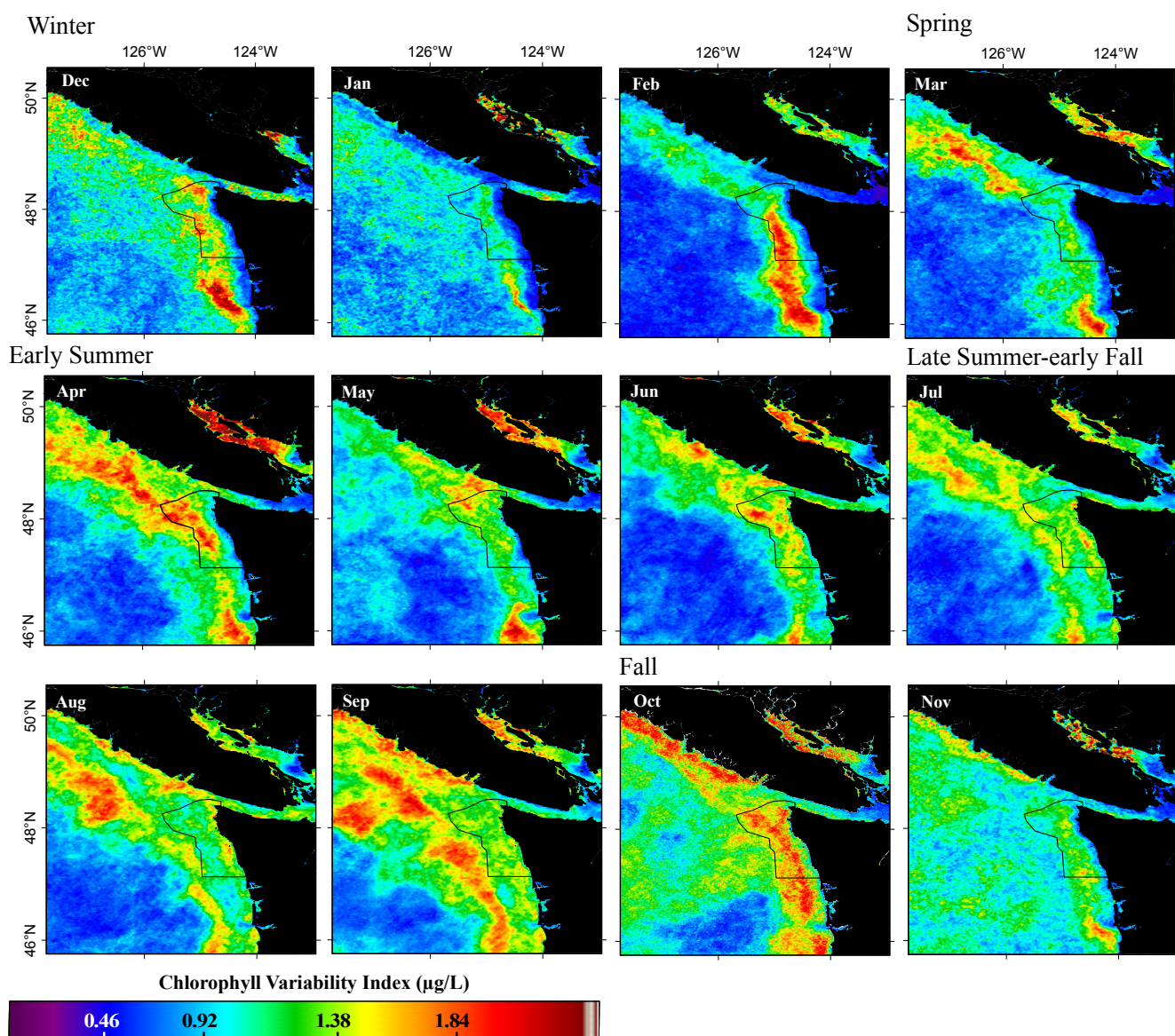


Figure 22. SeaWiFS- derived climatological (1997-2007) estimates of chlorophyll variability during the winter (December-February), spring (March), early summer (April-September), late summer-early fall (July-September) and fall (October-November) periods. Variability was determined using the difference of the 75<sup>th</sup> and 25<sup>th</sup> quantiles for the distribution of chlorophyll and turbidity values, respectively.

Ocean color variability speaks to enhanced transition in biotic response. It is assumed that chlorophyll response can be measured not only through algal abundance (using chlorophyll *a* as a proxy), but through temporal change in abundance, which may be more useful for coupling with other parameters. Figure 23 depicts these heightened chlorophyll transition periods effectively. Specifically highlighted are the changes associated with the time periods of late March (Figure 23a), depicting a calm period, and mid-April (Figure 23b), showing significant enhancement in chlorophyll variability.

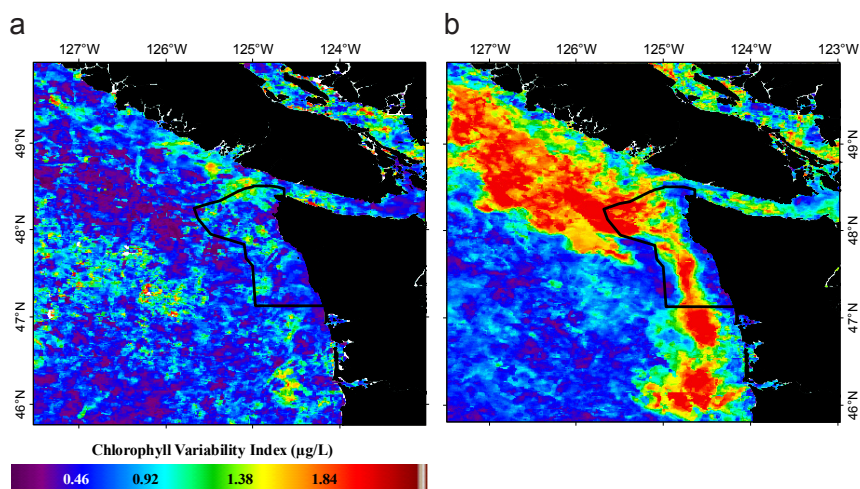


Figure 23. Comparison of climatological chlorophyll variability estimates during a) late March, versus b) mid-April. Note the significant enhancement in variability inside the sanctuary.

### *Juan de Fuca Eddy*

The Juan de Fuca eddy is a semi-permanent cyclonic feature located off the coast of Vancouver Island and the Juan de Fuca Strait. The extreme diversity in habitats and zones of convergence of ocean currents accounts for the rich biodiversity in the eddy.

The counterclockwise cold-core eddy is situated west of the Strait of Juan de Fuca, southwest of Bamfield, BC. The eddy is a dominant feature of circulation around the OCNMS with a diameter ranging from 50-100km, and is visible in summertime satellite imagery in seasonal minimum low SST and, generally, minimums and maximums in chlorophyll. The seasonal eddy is a result of the interaction between effluent from the Strait, southward wind-driven upwelling processes, and underlying topography—a spur of the Juan de Fuca submarine canyon (Hickey and Banas 2003). The eddy forms in spring and declines in fall (Freeland and Denman 1982). The eddy was defined by using density profiles (MacFadyen et al. 2005). Decreases in SST in the center of circulation are most apparent in July, when climatological SST gradient magnitudes are most distinct. In days prior to and during Eddy SST enhancement, light to moderate NW winds prevail in near-shore zones, indicative of fair weather conditions.

A well-documented edge detection algorithm (Canny 1986) was used to delineate SST frontal gradient edges associated with eddy boundaries using both the CoRTAD and GOES long-term data series. In addition to gradients, frontal orientation was also computed to provide a reasonable proxy of circulation around the center of circulation. Climatological gradients and along-front directions reveal implied circulation around the eddy during climatological June and July (Figure 24), indicating a slight westward shift in eddy orientation from June to July in the long-term data series. Spatial patterns of frontal directions, climatological median chlorophyll, and eddy location are shown in Figure 25, with implied circulation around the center depicted through along-front direction.

### *Summary of SST fronts and chlorophyll variability*

SST fronts for the region show distinct patterns indicative of the Juan de Fuca eddy circulation, upwelling fronts, offshore wind forced events, and the Columbia River plume effect. Ocean color chlorophyll variability estimates the level of change of chlorophyll over a temporal interval. Heightened monthly chlorophyll variability is typically oriented along the eastern edges of SST frontal boundaries, hinting at increased convergence and enhanced biological activity. Westward shifts in eddy circulation are evident in the long-term SST data series. Spatial patterns of near-shore and offshore frontal boundaries and chlorophyll infer zones of increased upwelling, and possible habitat niches for biological assemblages.

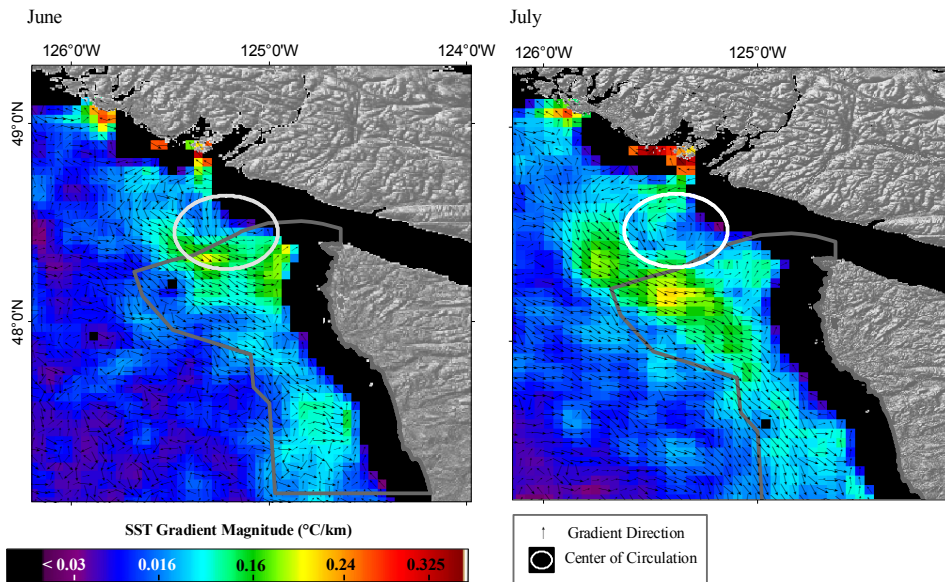


Figure 24. CoRTAD SST climatological (1985-2005) monthly gradients and along-front directions for June and July.

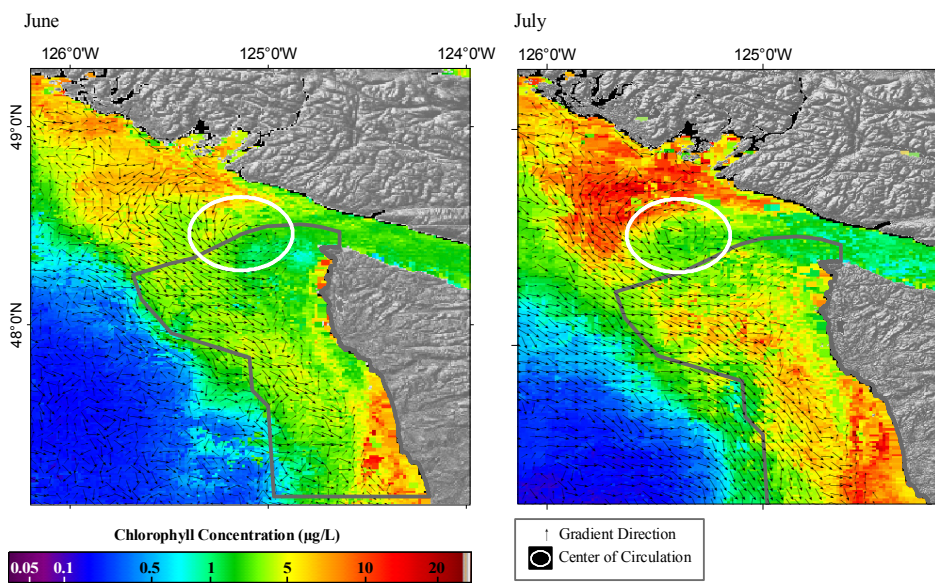


Figure 25. CoRTAD SST climatological (1985-2005) monthly along-front directions and climatological monthly median chlorophyll for June and July.

### 3.5 OCEAN CLIMATE DATA SUMMARY

In this section, previously shown Hovmöller diagrams of remotely sensed SST, SSHA, chlorophyll, turbidity, currents, and winds are presented in combination to visually depict average (expected) conditions for the climatological period covering January to December. Extracted data along the three transect lines were compared across the four variables, and inferences were made on the dominant factors influencing surface response.

#### East-West Summary

Suppressed near-shore SST values are evident starting in early June and ending in October, indicative of seasonal upwelling processes (Figure 26). Suppressed SSHA values inside the sanctuary (Figure 26, cyan-blue) are likely the result of density-driven (temperature/salinity) processes related to seasonal upwelling. In winter, heightened SSHA values along the coast are likely caused by precipitation/runoff, the Columbia River, and coastal impingement (wind forcing). Spring chlorophyll blooms typically start in mid-April. Chlorophyll pulses are much more pronounced in late summer and early fall, typically ending in mid-October (Figure 26). Wind-induced effects can lead to SST fronts in offshore areas with the most persistent frontal features setting up in October and November, coincident with increased chlorophyll production offshore. Slight influence of localized precipitation and sediment resuspension can be seen in expected turbidity conditions (Figure 26). Of note are the strong northwestward-dominated mean currents and winds in January and

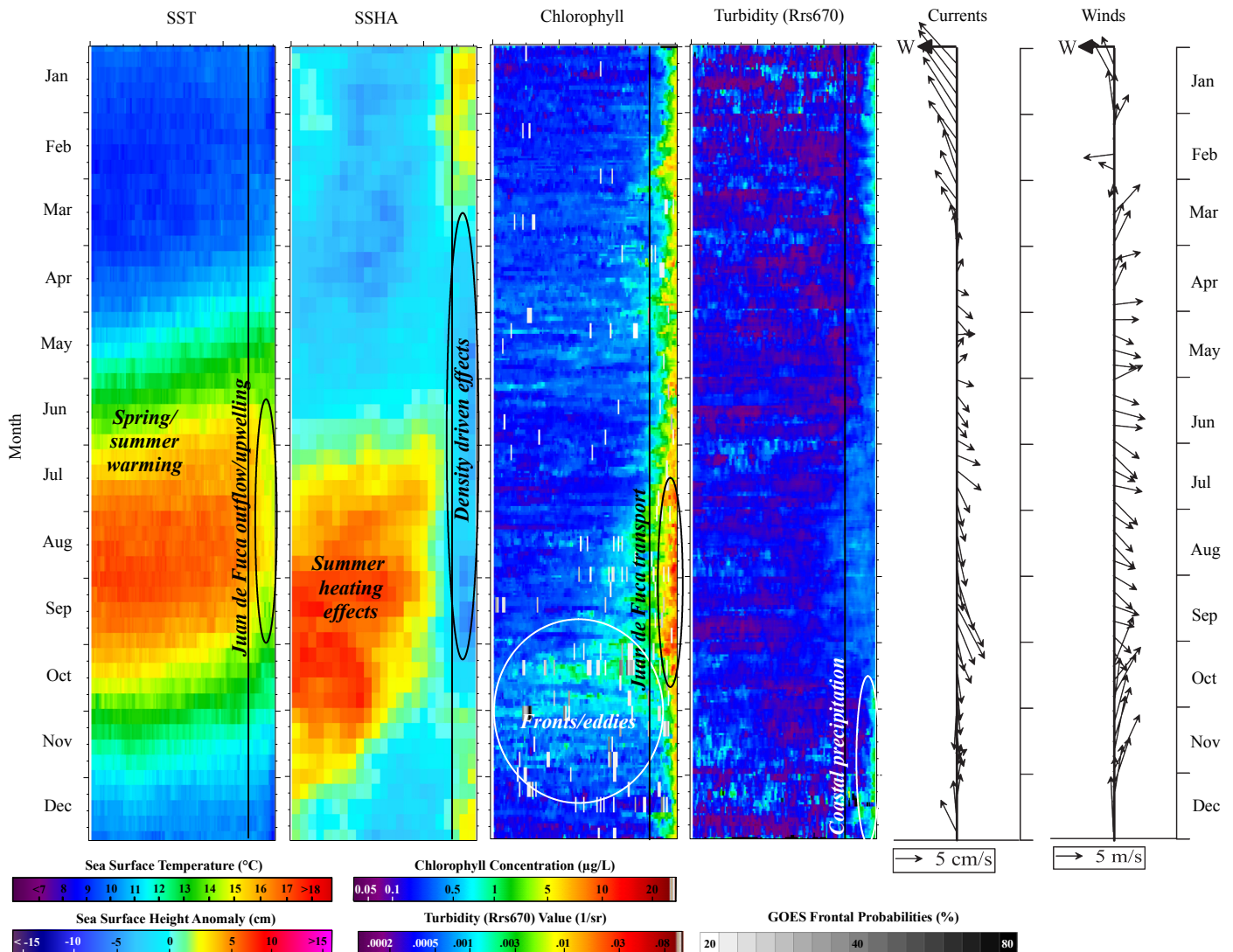


Figure 26. Diagrams of averaged (expected) daily-weekly AVISO SSHA, CoRTAD SST, SeaWiFS chlorophyll and turbidity (Rrs670), AVISO geostrophic currents, and QuikSCAT winds along an East-West transect line over the calendar year. Plots reveal typical conditions of remotely sensed surface response characteristics for OCNMS waters.

southeastward currents in September (Figure 26).

**Cross-shelf Summary**

Cross-shelf patterns in ocean climate reveal distinct transitions between near-shore and offshore surface water property responses. Outflow from the Juan de Fuca Strait causes suppressed SST during summer (Figure 27). Negative SSHA in summer is likely caused by dips in temperature due to Juan de Fuca outflow in combination with upwelling processes (Figure 27). Spring chlorophyll blooms typically start in mid-April and diminish slightly by mid-summer. Wind-induced effects can lead to SST fronal development (frontogenesis) in offshore areas. Of note are the SST and SSHA spatial transition areas coincident with increased chlorophyll production (and fronts) in October. Influence of the Juan de Fuca outflow can be seen in expected turbidity conditions promoting lower turbidities directly adjacent to the Strait (Figure 27). A summer/fall turbidity maximum is also noted near the shelf break (Figure 27). Of note are the southeastward-dominated currents during July, with a transition to more southward mean flow in August and September (Figure 27).

**Alongshore Summary**

Ocean climate patterns in the alongshore direction reveal seasonal warming, density-driven, and wind effects along the Olympic Coast. Outflow from the Juan de Fuca strait is evident, where SST differences between extreme northern and southern sections typically reach 2-3°C during summer. Sea-level

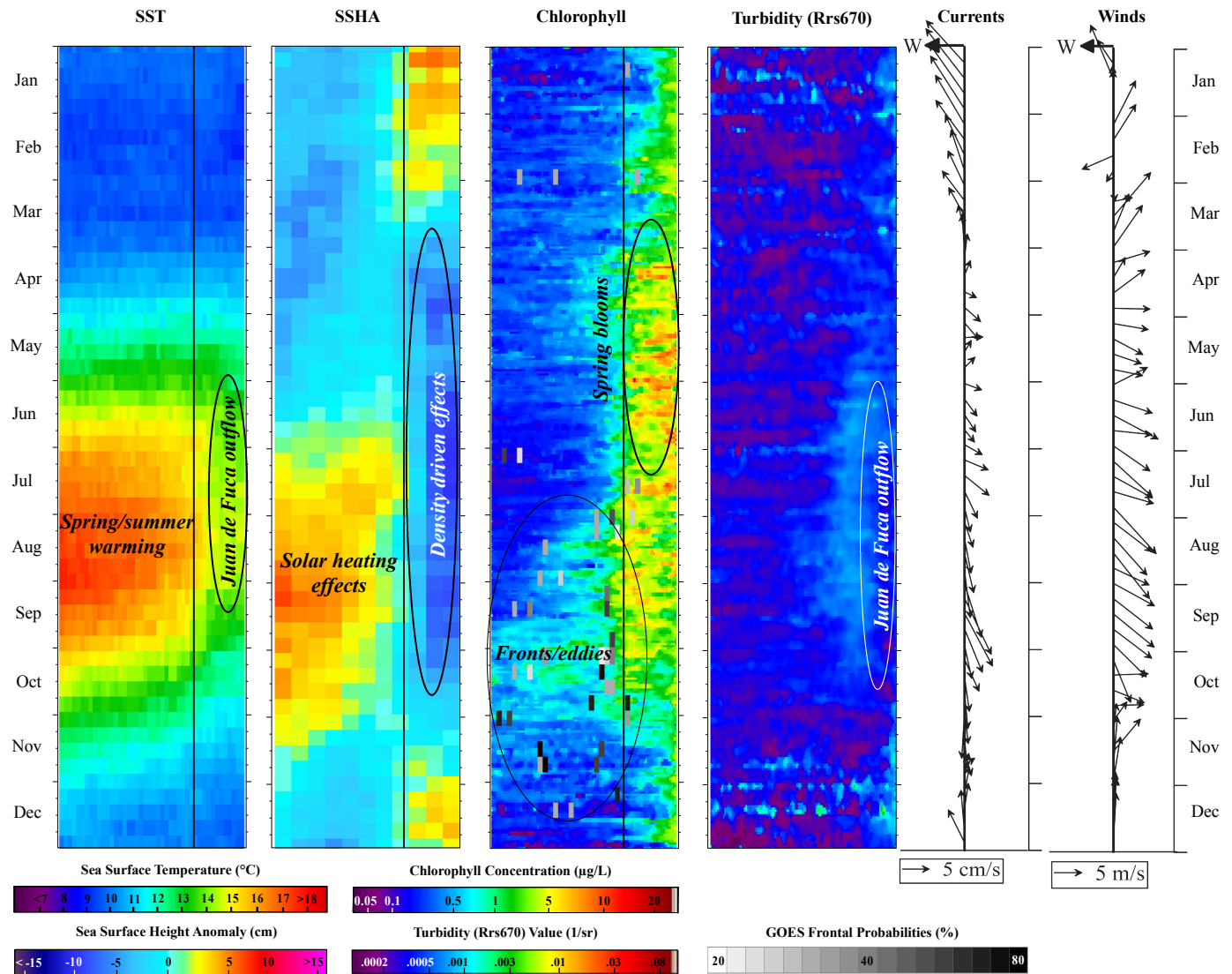


Figure 27. Diagrams of averaged (expected) daily-weekly AVISO SSHA, CoRTAD SST, SeaWiFS chlorophyll and turbidity (Rrs670), AVISO geostrophic currents, and QuikSCAT winds along a cross-shelf transect line of each data series over the calendar year. Plots reveal typical conditions of remotely sensed surface response characteristics for OCNMS waters.

fluctuations between summer and winter are most exaggerated along this transect. Wind-induced coastal impingement, Juan de Fuca outflow, and upwelling processes appear to have significant influence on SSHA signals in northern sections, with decreased influence near the Columbia River mouth (Figure 28). From ocean color values, the evidence of spring bloom events is most apparent in northern sections of the study area from early April through mid-June (Figure 28). Near shore Ekman-induced pulses then dominate the region; this is most apparent during mid-July through early October when chlorophyll reaches an annual maximum. Of note is the Columbia River outflow influence on chlorophyll concentrations and turbidity in extreme southern sections, and heightened chlorophyll (low Rrs670) during a brief period in February (Figure 28). February is typically a time of pre-transition, when frequent, severe cold-front passages could cause bottom resuspension and subsequent increased chlorophyll at the surface. Although Rrs670 signals are generally low to moderate year-round, a coastal runoff effect is noted across northern and southern sections from November through December. General transition periods are depicted well with altimetry-derived geostrophic currents (Figure 28, bottom). Coastal currents become redirected from typical wintertime patterns (north-northwestward) to southeastward starting in early March through April. Summer-time southeastward flow remains fairly consistent through October until the November transition period.

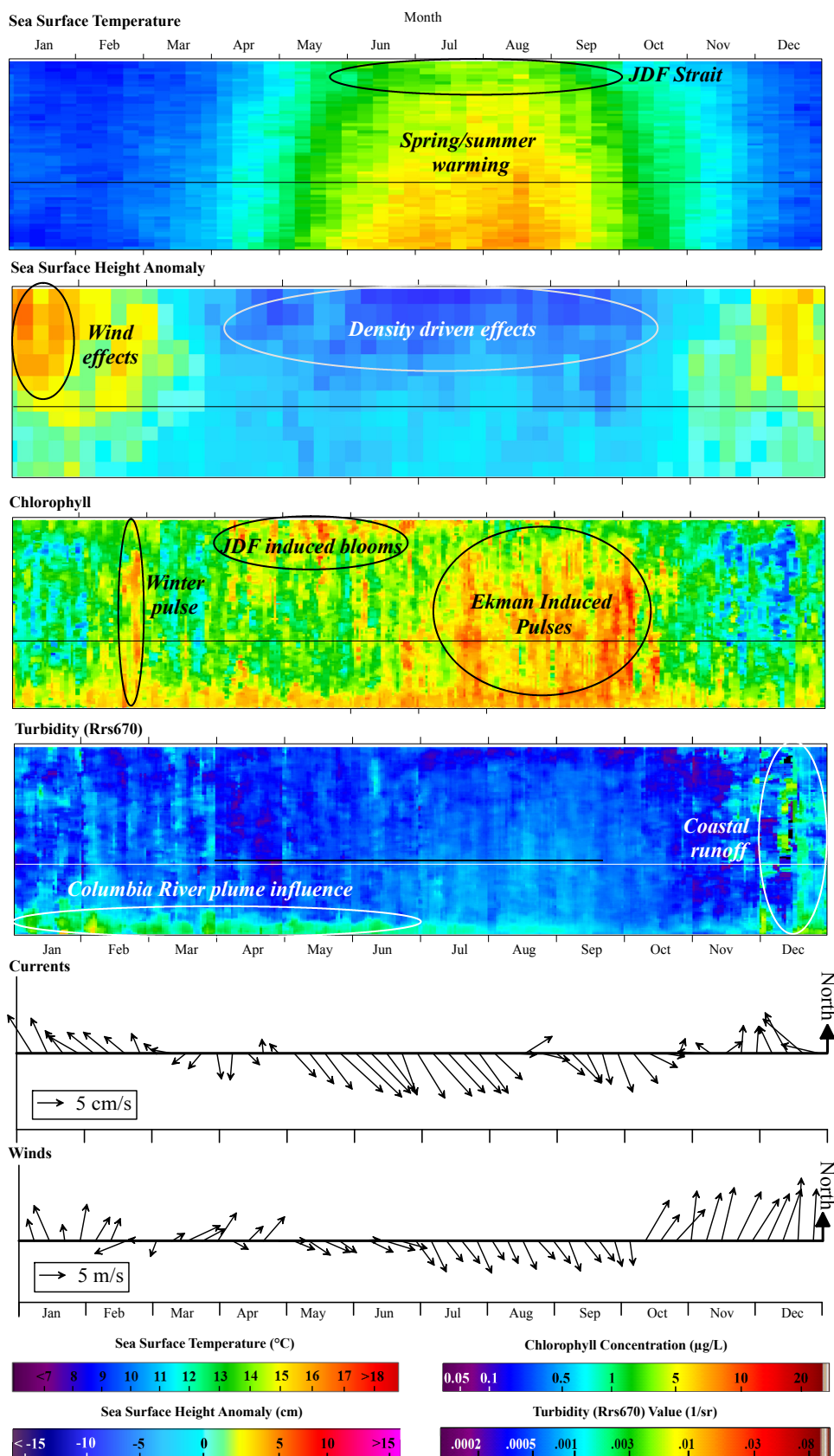


Figure 28. Diagrams of averaged (expected) daily-weekly AVISO SSHA, CoRTAD SST, SeaWiFS chlorophyll and turbidity (Rrs670), AVISO geostrophic currents, and QuikSCAT winds along a North-South transect line of each data series over the calendar year. Plots reveal typical conditions of remotely sensed surface response characteristics for OCNMS waters.

### 3.6 Surface Property Relationships and Processes Affecting the OCNMS

The relationship between surface layer properties provides information on bio-physical coupling, and local versus regional processes affecting OCNMS waters. For example, global studies investigating the co-variability of chlorophyll and SST have demonstrated the effects of large-scale climate cycles on heightened or suppressed signals over expansive ocean regions (Yoder and Kenelly 2003, McGillicuddy et al. 2001). In the Pacific Ocean basin, El Niño periods generally favor lower chlorophyll and higher SST, while La Niña years favor high chlorophyll and low SST. Localized spatial patterns of SST and chlorophyll have been linked to hemispheric climate cycles and have been used to identify feeding grounds for many commercially important species (Valavanis et al. 2004). In this section, monthly SST, SSHA, ocean color chlorophyll and turbidity, Columbia River discharge, and land-based precipitation data will be used to help define spatio-temporal correlation peaks during downwelling and upwelling periods. Multiple rho maps will be used to depict select spatial correlation patterns of interest in both local and regional ocean environments.

#### *SST and SSHA Co-variability*

Through pair-wise correlation approaches using Spearman's rho ( $\rho$ ), the association of monthly SST and SSHA image data values were tested. When all months were tested, SST/SSHA relationship was positive, indicating that thermal expansion properties have a strong influence on SST/SSHA relationship year-round. During upwelling in July (Figure 29a), slightly neutral to negative patterns are evident near the Juan de Fuca Strait outflow. The density-driven processes related to upwelling appear to reinforce a positive relationship in October (Figure 29b). Seasonal heating (thermal expansion effects) is the likely contributor to positive SST/SSHA correlation regionally in both summer and winter.

#### *SST, SSHA, and Chlorophyll Co-variability*

The overall correlation pattern between SST and chlorophyll anomaly values reveal mostly negative  $\rho$  in open ocean waters with neutral patterns along the Olympic Coast. That is, cooler SST co-varies with increased chlorophyll regionally. Strength and direction of association between these two variables are generally moderate and negative when averaged over the entire upwelling period, but reveal unique spatial-temporal patterns within the upwelling season.

At the start of upwelling season in May, distinct spatial patterns arise in SST/chlorophyll correlation fields (Figure 30). May shows a distinct negative association along the Olympic Coast shelf, specific to areas along the Vancouver Island and Washington coastlines. This pattern represents a time when solar radiation effects are in transition and upwelling pulses of nutrient-rich, cooler waters become more evident. Differences between offshore and nearshore pixels is evident when monthly mean SST and median chlorophyll values are extracted from selected clusters (boxes, Figure 30). Trend lines of fit are added to emphasize opposing relationship in offshore (Figure 31a) and coastal (Figure 31b) environments. The nearshore relationship (Figure 31b) emphasizes low SST values ( $10.5^{\circ}\text{C}$ ) corresponding with a heightened chlorophyll signal up to  $3\mu\text{g/L}$ . SSHA and chlorophyll correlations (not shown) reveal similar pat-

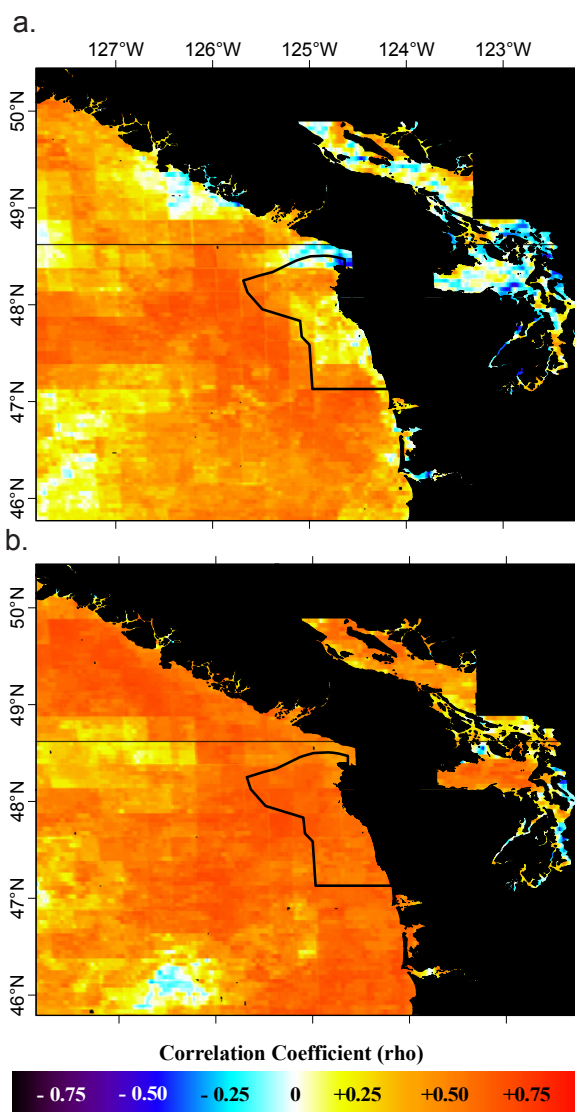


Figure 29. Monthly SST vs. SSHA Spearman correlation coefficients ( $\rho$ ) showing strength and direction (+/-) of spatio-temporal relationship for the months of (a) July and (b) October.

terns in May although negative correlation fields are not as spatially homogeneous.

July correlations along the Olympic Coast reveal typical summer conditions, with increases in light availability and sea surface heating acting to limit chlorophyll production at the surface. Nutrient availability in July increases overall due to increased upwelling and other localized processes. An opposing pattern from May is shown in the July plots, with a negative trend offshore (Figure 32a) versus a positive trend near shore (Figure 32b). Chlorophyll concentration reached 14µg/L for extracted pixels in the sample when temperatures were greater than 15°C. Rho was moderate to strongly positive near-shore, and negative offshore (Figure 33). The overall pattern offshore is strongly negative. SSHA and chlorophyll rho maps (not shown) show a similar near-shore versus offshore relationship in strength and direction.

In September/October, SST/chlorophyll correlation patterns reveal negative association regionally (Figure 34), with a small cluster of positive rho associated with Juan de Fuca outflow and eddy circulation inside the

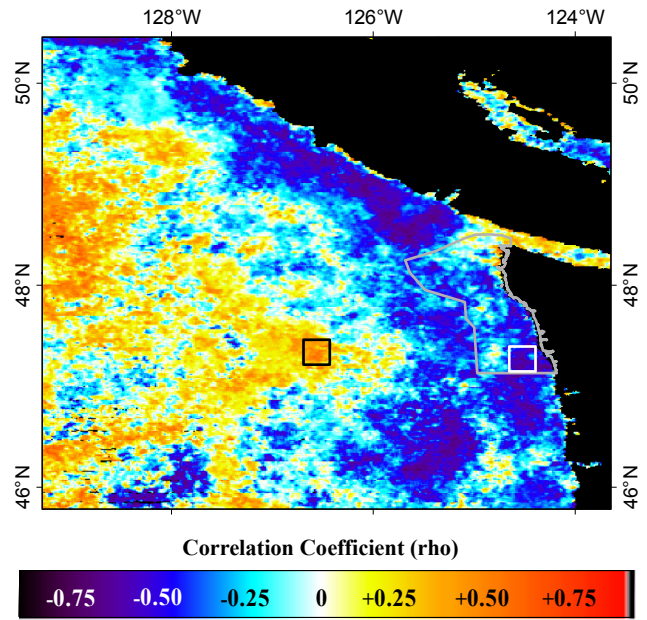


Figure 30. Spearman correlation coefficients (rho) showing strength and direction (+/-) of spatio-temporal relationship between CoRTAD monthly SST and chlorophyll for May.

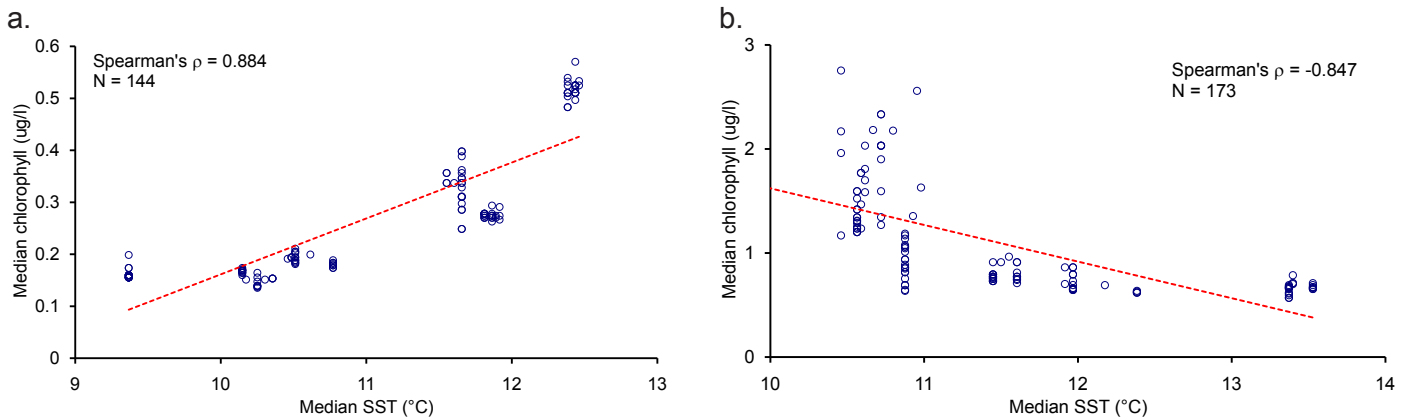


Figure 31. Scatterplot displaying the relationship between CoRTAD SST and SeaWIFS chlorophyll during climatological May for waters (a) outside and (b) inside the sanctuary. Values are extracted from boxes shown in Figure 30.

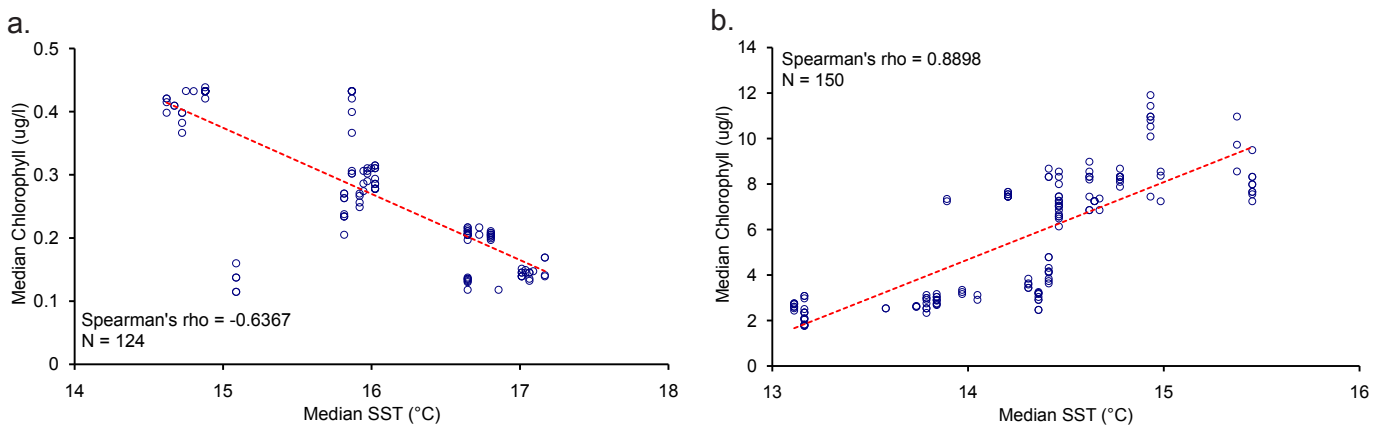


Figure 32. Scatterplot displaying the relationship between CoRTAD SST and SeaWIFS chlorophyll during climatological July for waters (a) outside and (b) inside the sanctuary. Values are extracted from boxes shown in Figure 33.

sanctuary. This pattern would indicate that localized processes related to the Juan de Fuca eddy may have more influence on SST/chlorophyll relationship inside the sanctuary. Differentiating the dominant physical processes that limit chlorophyll and sediment characteristics will be addressed in the following sections.

#### *Nutrient/sediment Sources and Ocean Color Covariability*

Outflow from the Columbia River plume, Juan de Fuca Strait, and other land-sea interactions have a significant effect on biological activity and sediment response in the OCNMS (Thomas and Weatherbee 2006). In this section, co-variability of chlorophyll, turbidity, precipitation, and discharge will be presented to highlight sources (and sinks) of nutrient and sediments impacting OCNMS marine environments.

The Columbia River plume is highly dynamic with variation in direction, depth, and width of response (Hickey and Banas 2003). The Columbia River plume core flows northward on the inner shelf in fall and winter and southward in spring and summer, offshore of the Oregon shelf. Through spectral classification techniques, Thomas and Weatherbee (2006) depicted the Columbia River plume core to reach near sanctuary boundary waters in winter. Spearman's rank correlation of monthly Rrs(670) and Columbia River discharge values exhibit a similar pattern during the winter period (Figure 35a). A distinct "plume" of high rho (Figure 35a, deep orange) is evident from the Columbia River mouth northwards along the coast. Of note is the negative association (deep blue) in coastal areas south of Cape Flattery (Figure 35a).

Increased precipitation and runoff play significant roles in the transport and distribution of sediments and nutrients out of Olympic Coast river systems, estuarine plumes, and the Juan de Fuca Strait (Thomas and Weatherbee 2006, Newton et al. 2003). A strong potential exists for precipitation-effect on sediment and nutrient characteristics along the OCNMS inner shelf. Through pair-wise approaches, a significant portion of turbidity in near-shore zones co-varies with coastal precipitation during the winter wet season (Figure 35b). These correlation patterns support the premise that seasonal runoff from areas to the north of the Columbia River plume contribute significantly to higher turbidity values in OCNMS waters, relative to the influence of the Columbia Plume itself. The results speak to other factors, such as more localized coastal precipitation, as substantial contributors to seasonal Rrs670 response.

The association of precipitation and chlorophyll should differ based on the amount of light available for algal stimulation. It is speculated that negative precipitation/chlorophyll correlation in September (Figure 36a) indicates that optimal light conditions (less precipitation) could yield more production at the surface. In October, the relationship is positive but limited to an area around the mouth of the Juan de Fuca Strait, includ-

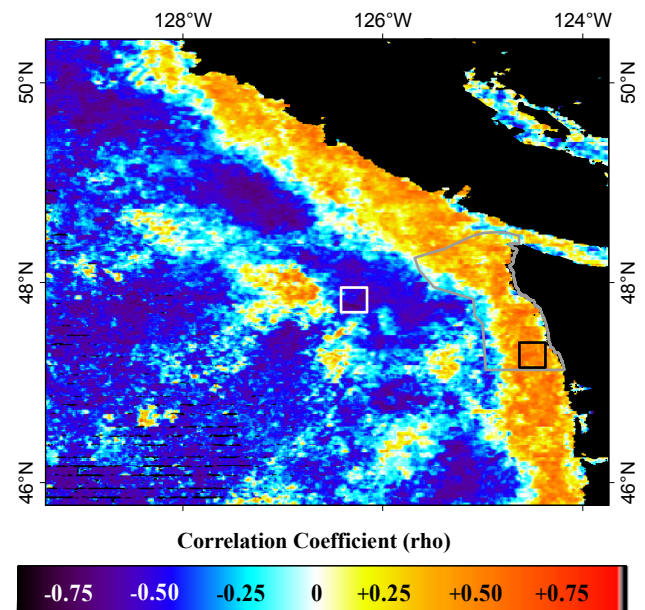


Figure 33. Spearman correlation coefficients ( $\rho$ ) showing strength and direction (+/-) of spatio-temporal relationship between CoRTAD monthly SST and chlorophyll for July.

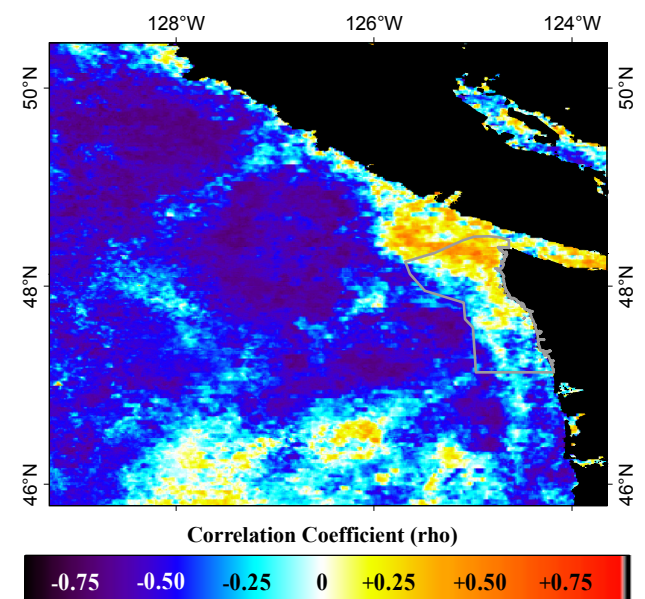


Figure 34. Spearman correlation coefficients ( $\rho$ ) showing strength and direction (+/-) of spatio-temporal relationship between monthly SST and chlorophyll for September.

ing the sanctuary (Figure 36b). October is more indicative of increased precipitation, which could influence correlation patterns together with the possible influence of both the Strait and coastal runoff processes.

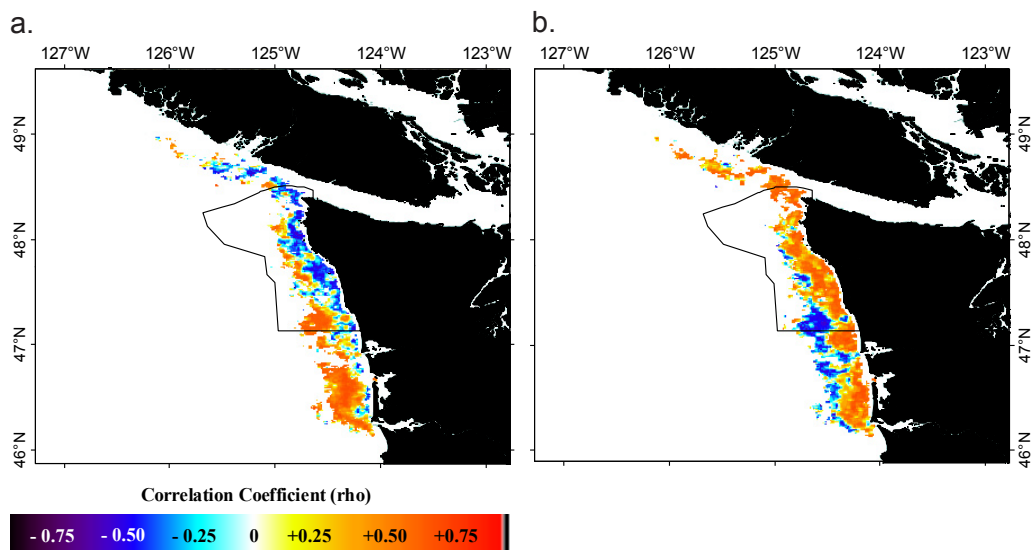


Figure 35. Spearman correlation coefficients ( $\rho$ ) showing strength and direction (+/-) of spatio-temporal relationship between SeaWiFS January turbidity and (a) USGS gauged Columbia River January discharge and (b) GPCC January precipitation.

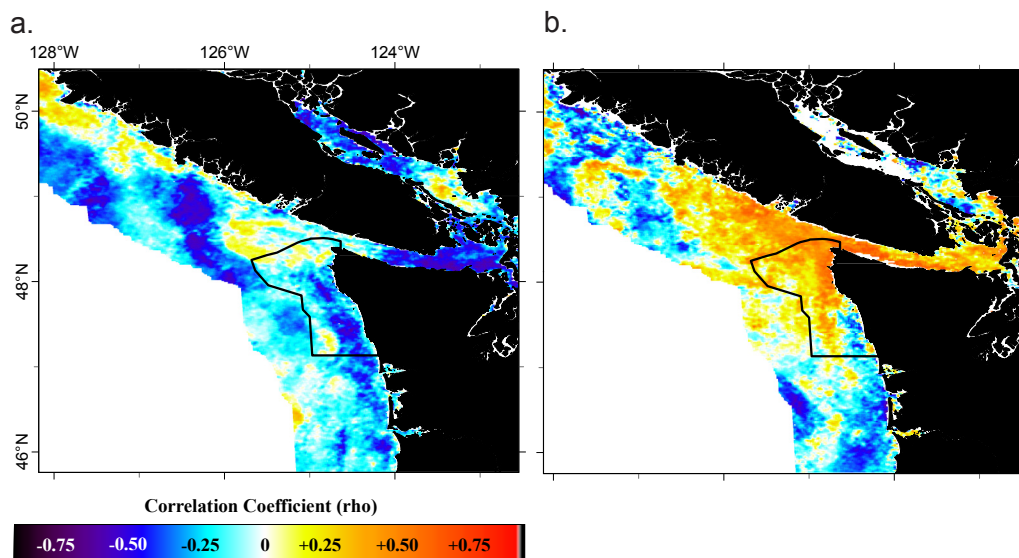


Figure 36. Spearman correlation coefficients ( $\rho$ ) showing strength and direction (+/-) of spatio-temporal relationship between SeaWiFS chlorophyll and GPCC precipitation for (a) September and (b) October.

*Summary of intraseasonal (within season) processes influencing surface layer relationships*

To report on processes affecting surface layer responses inside and outside OCNMS waters, a correlation matrix revealing level and direction of association between remote sensing parameters and other physical-hydrometeorological variables is presented (Table 2). Correlation patterns of surface water properties are spatially and temporally tied to upwelling/downwelling cycles (mixing processes), increased light availability, and changes in land-based physical forcing mechanisms. In this section, the dominant mechanisms influencing surface layer characteristics inside the OCNMS will be interpreted from sign (+/-) and strength of selected relationships from Table 2, and from the climate summaries of expected conditions (Figures 26-28).

For all months, a positive relationship is evident for SST and SSHA (row 1, Table 2). Thermal expansion properties and upwelling reinforces positive SST/SSHA relationship. During the start of the upwelling season in May, SST/chlorophyll and SSHA/chlorophyll relationship is negative inside the sanctuary and positive regionally (row 2, 3; Table 2). Nutrient-rich, colder water being forced to the surface during upwelling enhances negative SST/chlorophyll relationship. In July, the SST/chlorophyll relationship is highly influenced by localized heating effects, inducing a positive relationship. During September and October, SST/chlorophyll relationship is negative at regional scales, suggesting that chlorophyll is heavily influenced by physical circulation (water mass characteristics) in addition to upwelling (mixing processes). The relationship between ocean color chlorophyll/turbidity and precipitation is positive during January inside the sanctuary (row 6, 7; Table 2). Columbia River discharge and turbidity reveals both a negative and positive relationship inside sanctuary boundaries (row 5, Table 2).

Table 2. Levels of association between remote sensing parameters, Columbia River discharge, and land-based precipitation inside and outside OCNMS boundaries. Possible regional and local processes influencing spatial-temporal levels of association are added for reference.

Parameter Association	Jan	May	July	Sep	Oct	Inference to dominant processes affecting relationships
SST/ SSHA	OCNMS	Positive	Positive	Positive	Positive	Thermal expansion and density driven processes reinforce positive relationship inside sanctuary and in open ocean environments. During upwelling, colder subsurface waters forced upwards induces suppressed SST and SSHA mainly confined to areas east of the shelf break.
	Regional	Positive	Positive	Positive	Positive	
SST/ Chlorophyll	OCNMS	Not enough data	Negative	Positive	Negative	Physical circulation and mixing processes influence negative relationship during upwelling months. Chlorophyll is partially enhanced by seasonal heating effects in July inducing positive relationship. In May, a positive offshore relationship generally occurs due to warmer waters penetrating northward promoting algal stimulation. A split correlation pattern exists locally with Juan de Fuca outflow influencing negative relationship inside sanctuary boundaries.
	Regional	Not enough data	Negative	Negative	Negative	
SSHA/ Chlorophyll	OCNMS	Not enough data	Negative	Negative	Negative	Same as above. Negative relationship during upwelling months possibly linked to geostrophic transport and advection processes. Additional data testing needed.
	Regional	Not enough data	Negative	Negative	Negative	
Chlorophyll/ Rrs670	OCNMS	Positive	Not enough data	Not enough data	Not enough data	Terrestrial sources (coastal and Columbia River) reinforce positive relationship in January. During dry season, relationship is mainly neutral to slightly positive.
	Regional	Not enough data	Not enough data	Not enough data	Not enough data	
Rrs670/ Columbia R. Discharge	OCNMS	Negative	Not enough data	Not enough data	Not enough data	Columbia River plume influences turbidity inside sanctuary during January- Negative relationship exists nearshore- positive relationship offshore. During May, Juan de Fuca Strait outflow southward reinforces negative relationship.
Rrs670/ Precipitation	OCNMS	Positive	Not enough data	Not enough data	Positive	Precipitation (coastal runoff) induces positive relationship in nearshore areas during January, October and November (not shown).
Chlorophyll/ Precipitation	OCNMS	Positive	Negative	Not enough data	Negative	Precipitation (coastal runoff) induces positive relationship in nearshore areas during January and October. Juan de Fuca Strait outflow to the south in May and September possibly reinforces negative relationship during the dry season.

	Positive correlation (> 0.77 rho)
	Negative correlation (< - 0.77 rho)
	Not enough data or no relationship

Monthly differences in localized processes and limiting factors affecting surface layer relationships from remote sensing are visually depicted in map form (Figure 37). During January, surface layer response inside the OCNMS is heavily influenced by downwelling conditions (poleward currents, onshore Ekman transport), precipitation (coastal/estuarine runoff), and Columbia River discharge (Figure 37). The positive association of precipitation, discharge, chlorophyll and turbidity suggests that the turbid source is from estuarine/coastal waters, mainly west of the Olympic Mountains.

During May, surface layer responses inside the sanctuary are mainly influenced by strengthened upwelling and Juan de Fuca Strait outflow (Figure 37). The negative May correlation patterns of chlorophyll and SST are indicative of these limiting factors, where colder, nutrient-rich waters are forced upwards through upwelling processes promoting algal stimulation at the surface. Negative association of precipitation and chlorophyll suggests that the nutrient source is not from coastal/estuarine runoff processes. Flow out of the Juan de Fuca Strait is less turbid during spring and summer, which would indirectly support the negative association between decreased precipitation (with increased light availability) and increased chlorophyll. Results were inconclusive on the influence of the Columbia River during May, but southward circulation would support lesser affect inside the sanctuary.

During July, surface layer responses are indicative of increased light and temperature, with available nutrients promoting chlorophyll production along the entire Olympic coast. Although upwelling persists in the region at promoting enhanced chlorophyll, SST appears to be more sensitive to seasonal heating than to mixing processes. A negative association between chlorophyll and precipitation suggests that blooms are induced by either upwelled water or Juan de Fuca Strait outflow (Figure 37).

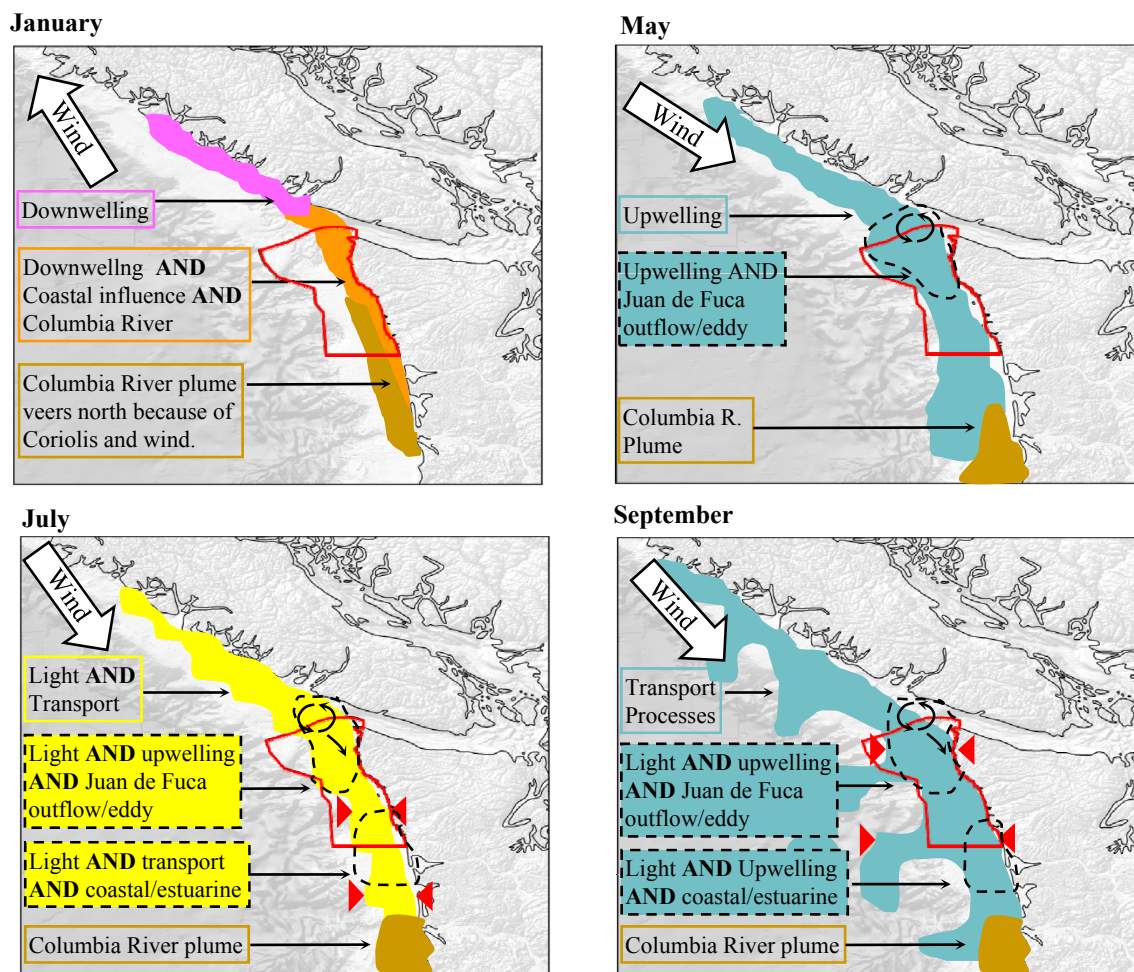


Figure 37. Schematic representation of physical factors limiting nutrient availability and chlorophyll production during (a) winter (January), (b) spring (May), (c) mid summer (July), and (d) early fall (September) periods.

September chlorophyll peaks (annual maximums) inside the sanctuary are likely tied to localized processes, including Juan de Fuca outflow and eddy circulation (Figure 37). In fall, nutrient availability remains high, when Juan de Fuca outflow is circulated and recirculated, heated, and forced southward, causing increased production south of Cape Flattery (Figure 37). It is speculated that increases in Ekman transport leads to increased production at the surface in September/October.

Through correlation results and analysis of expected surface characteristics for the OCNMS, the governing physical limiting factors on surface layer responses were assessed and documented for the sanctuary (Table 3). Contribution levels for these limiting factors are based on spatial and temporal sign and strength of relation for the months of January, May, July, and September, and are relative to five broad-scale physical factors: Columbia River, Coastal/Estuarine, Juan de Fuca Strait, Upwelling/Marine, and Light/Temperature. The Columbia River shows moderate influence in January, with lower influence for the remaining months (column 1, Table 3). Coastal/Estuarine influence shows a high level of contribution on response characteristics for January and October, with moderate influence during July and September. Juan de Fuca Strait outflow and circulation shows significant influence during all upwelling months analyzed. Mixing processes associated with upwelling/marine influence is strong during spring, summer and fall. Light- and temperature-promoting conditions necessary for algal bloom activity are most pronounced in July, with moderate effect occurring in spring and fall. The information in Table 3 is intended to provide a process-driven conceptual framework on governing processes at low-frequency (monthly) time scales, but does not infer higher-frequency (daily-weekly) patterns of co-variability.

In summary, using 12 calendar months and six different variables, nearly 100 correlation maps were produced and analyzed. Tables 2 and 3 condense these patterns and governing processes that are most apparent from visual interpretation and quantitative-based analysis. Many of the correlation patterns documented in this report support existing local knowledge of the physical and biological factors that limit production on seasonal time scales. However, the month-to-month differences in relation between variables reveal the importance of long-term satellite data series in further dissecting month-to-month variability in this dynamic ocean environment. The long-term relationship with remotely sensed bio-physical properties allows for more robust synoptic-scale interpretations and inferences to be made on estuarine-near shore interaction between

Table 3. Relative level of contribution of physical limiting factors on surface layer response inside OCNMS boundaries. Determination of contribution level based on analysis of expected conditions and intra-seasonal correlation patterns.

	Limiting Factors/Mode of Influence				
	<u>Columbia River</u>	<u>Coastal/Estuarine</u>	<u>Juan de Fuca Strait</u>	<u>Upwelling/Marine</u>	<u>Light and Temperature</u>
January	Moderate	High	Not enough data or not applicable	Not enough data or not applicable	Low
May	Not enough data or not applicable	Low	High	High	Moderate
July	Low	Moderate	High	High	High
September	Low	Moderate	High	High	Moderate
October	Low	High	High	High	Low

	High
	Moderate
	Low
	Not enough data or not applicable

light, nutrient availability, and surface production. General year to year water mass characteristics outside the sanctuary are significant contributors to the overall relationship between variables and more study is needed to fully address local and regional variability of surface properties and their impacts on living marine resources.

### 3.7 Interannual Patterns of Surface Properties as Indicators to Environmental Perturbations

Ocean climate anomalies for the PNW region reflect deviations from expected (normal) conditions that are sometimes strongly affected by interannual variability in climate. Through climatological anomalies, seasonal variability is, in part, removed, so that the anomalies can be assessed in relation to environmental perturbations with a higher degree of confidence. In this section, patterns of local to regional interannual variability of surface water properties will be presented through climatological anomalies using SST, SSHA, chlorophyll and turbidity data. General patterns involving anomaly patterns for these surface level properties will be visually interpreted for extremes (positive and negative) during the period of record of each data-set. Comparisons will be made with heightened periods of ENSO using the Multivariate ENSO Index from NOAA's Earth System Research Laboratory, Climate Analysis Branch (Wolter and Timlin, 1998).

#### Interannual patterns of SST and SSHA

SST Hovmöller plots reveal anomalous conditions inside the sanctuary during the well documented ENSO warm (Figure 38, orange) El Niño phases in winter 1997-1998 and 2003 and the cool (blue, Figure 38) La Niña phases in 1988-89 and 1998-99. Cold events can be associated with positive ENSO index values (Figure 38, SST hovmoller), as was the case in July 2002. This period featured moderate to strong negative anomalies and an intrusion of cold subarctic waters (Grantham et al. 2004). SST anomaly maps for warm and cold ENSO and non-ENSO periods are depicted (Figure 39) with mainly positive (top row, orange patterns) anomalies evident during warm El Niño. During cool La Niña phases, negative anomalies are common (middle row, blue patterns, Figure 39). During non-ENSO periods, anomalous patterns tend to be slightly more spatially limited and shorter in duration. For example, extreme positive anomalies occurred in September 1990, August 1994, and negative anomalies were evident in December 1985 and June 1991. Typically, these patterns result from large-scale physical circulation fluctuations related to the CCS (Goericke et al. 2005).

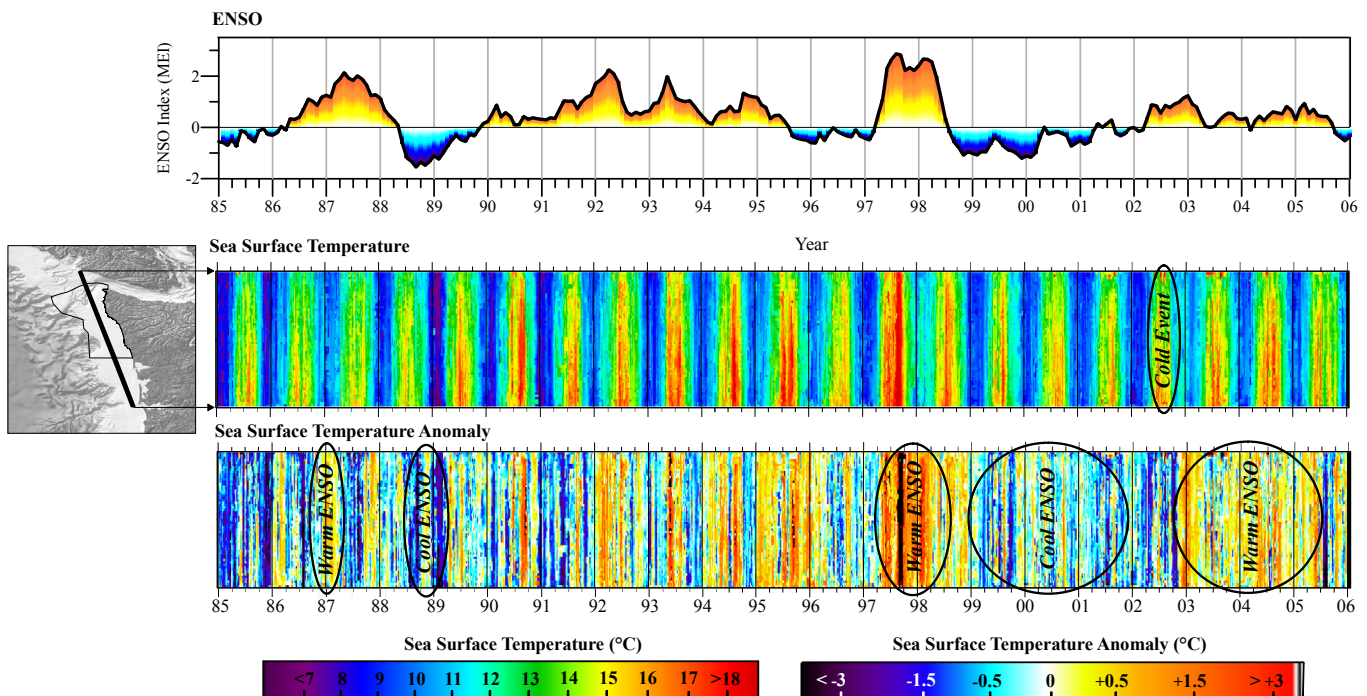


Figure 38. Time-series plot (Hovmöller) along a North-South transect line revealing weekly gap-filled CoRTAD SST, and weekly SST anomaly values for the period 1985-2005.

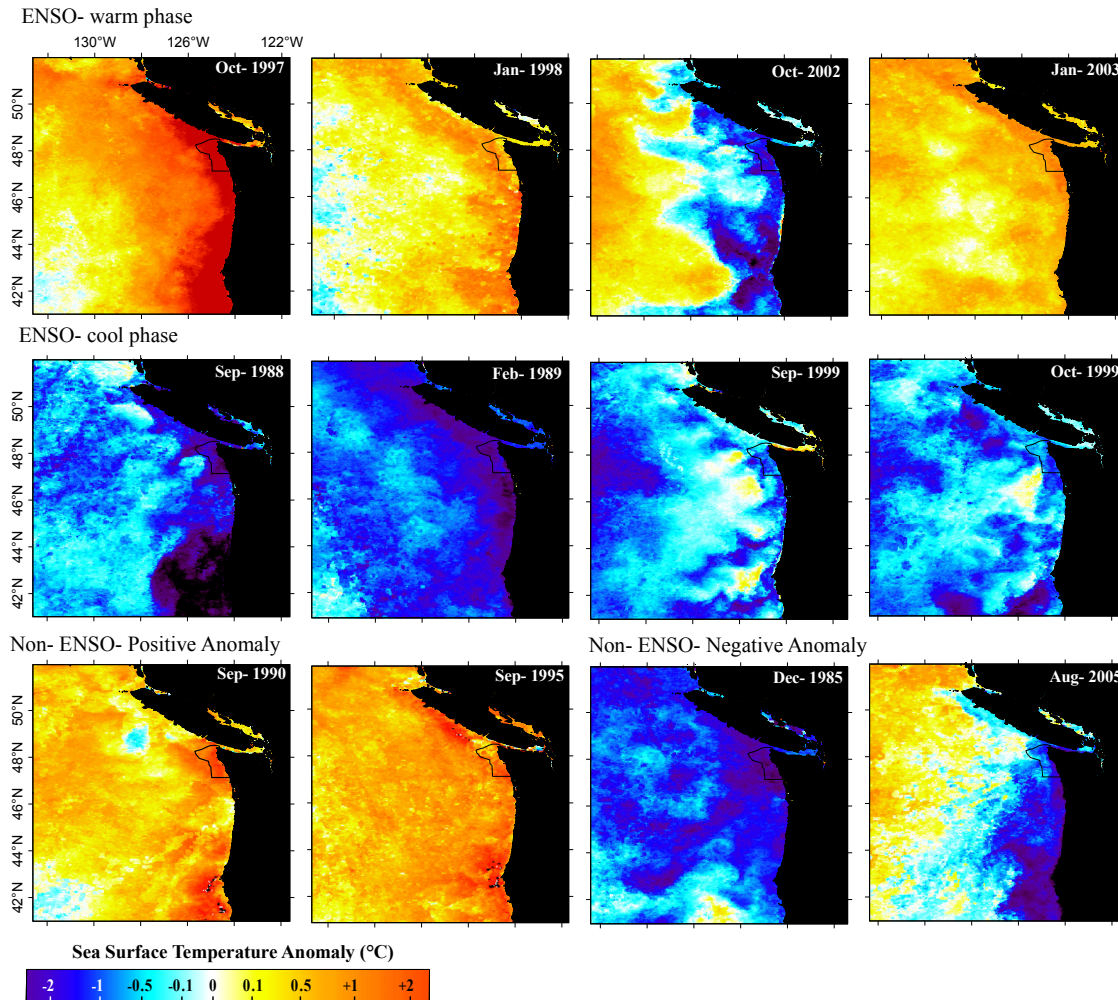


Figure 39. CoRTAD monthly mean SST anomaly image maps during ENSO and non-ENSO periods.

Sea surface height deviation was particularly evident during the ENSO warm (Figure 40, orange) phase in winter 1997-1998, and the strong anomalously cool (Figure 40, blue) spring of 1999. A general lag associated with SSHA temporal deviation from the end of El Niño through the start of La Niña is evident from the Hovmöller and the image maps, where heights remained positive until late 1998 (Figure 40). Spatial patterns of both negative and positive SSHA deviation revealed strong regional signals for most of the eastern North Pacific basin (Figure 41). Anomalously lower sea heights were evident from January 1999 until late summer 2002. Also evident is the moderate El Niño in 2003 (top row, Figure 41). Similar to SST anomaly, during non-ENSO periods, SSHA temporal deviation patterns tend to be slightly more spatially limited and shorter in duration (bottom row, Figure 41).

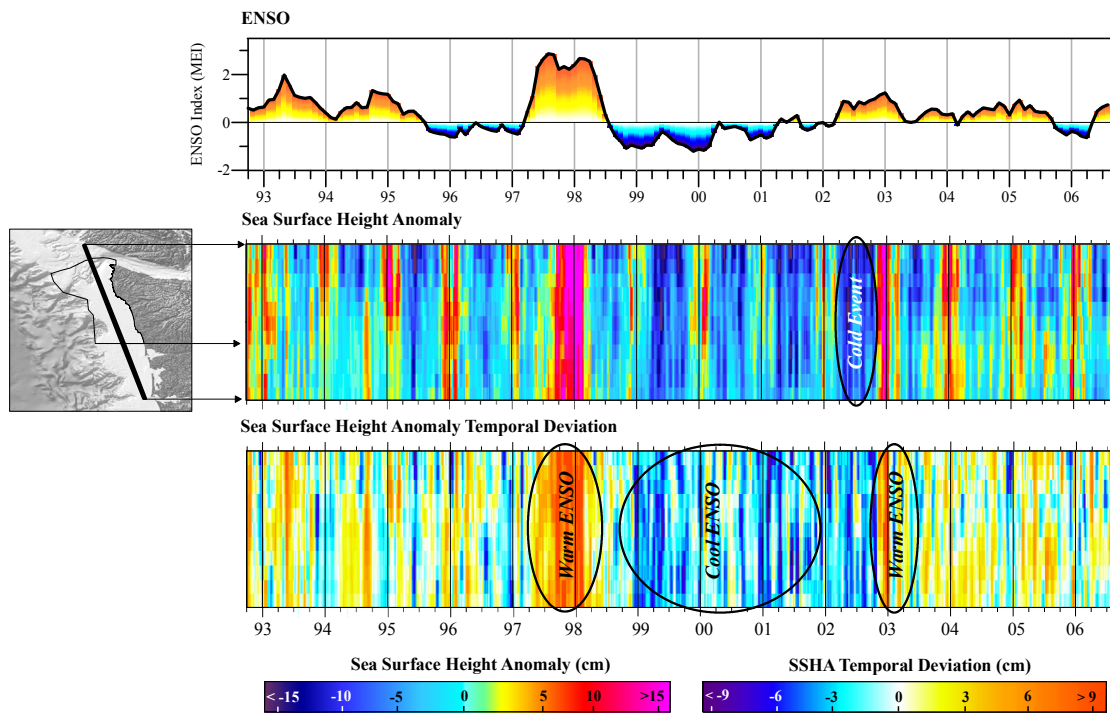
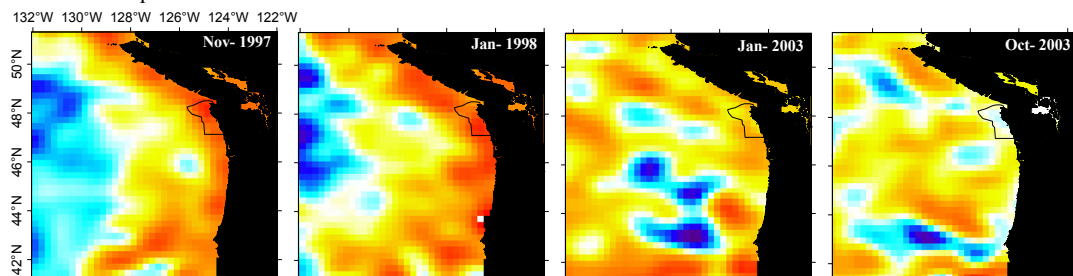
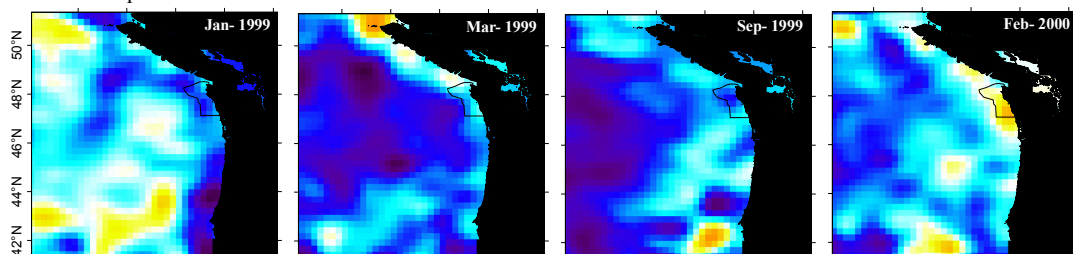


Figure 40. Time-series plot (Hovmöller) along a North-South transect line revealing (a) weekly AVISO SSHA; (b) climatological weekly SSHA; and (c) weekly SSHA temporal deviation for the period 1992-2006. Multivariate ENSO index values added for reference. Source: NOAA/NWS.

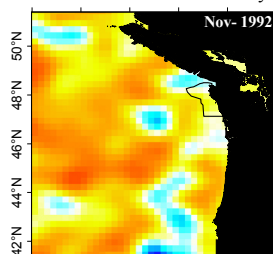
ENSO- warm phase



ENSO- cool phase



Non- ENSO- Positive Anomaly



Non- ENSO- Negative Anomaly

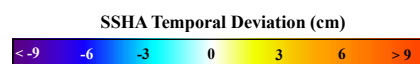
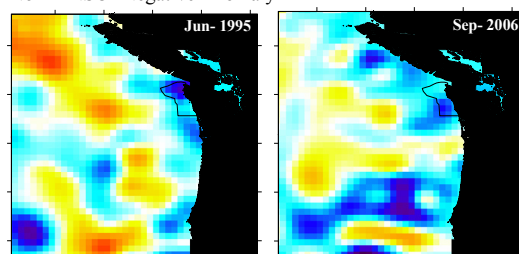


Figure 41. AVISO monthly mean SSHA temporal deviation image maps during ENSO and non-ENSO periods.

### Interannual Patterns of chlorophyll and turbidity

Monthly chlorophyll concentrations are strongly influenced by interannual variability in climate. The phase and strength of climate signals, such as the Pacific Decadal Oscillation (PDO), ENSO, and the North Pacific Gyre Oscillation (Thomas et al. 2003, Sackmann et al. 2004, Di Lorenzo et al. 2008), can lead to large-scale anomalies in chlorophyll concentration. This section presents patterns of local to regional interannual variability of climatological anomalies using SeaWiFS chlorophyll and turbidity data. General patterns involving stronger anomaly signals will be visually interpreted for select months in the 10-year climatology.

Specific OCNMS anomalous chlorophyll “events” for the period were in the fall of 1999, September 2000, and May and June 2007 (Figure 42). A strong negative chlorophyll anomaly was measured in the fall of 1997, associated with the strong El Niño event. Weaker negative anomalies were also evident in the fall of 1998, 2002, 2003, and 2005. Image maps generally representing warm and cool periods of ENSO are depicted in Figure 43, with strong positive anomalies generally associated with La Niña conditions, and negative PDO. During warm ENSO phases, open ocean characteristics in the North Pacific basin reveal positive chlorophyll to the west of the study area, with negative anomalies inside the sanctuary. Strong non-ENSO events occurred in October 2001 and the summer of 2006, when anomalous chlorophyll was evident along the entire length of the study area (Figure 43, bottom row) that persisted through August 2006. Overall, chlorophyll anomalies appear to have only slight association with the large scale climate indices, such as the Multivariate ENSO Index (MEI) and PDO Index, particularly at localized scales.

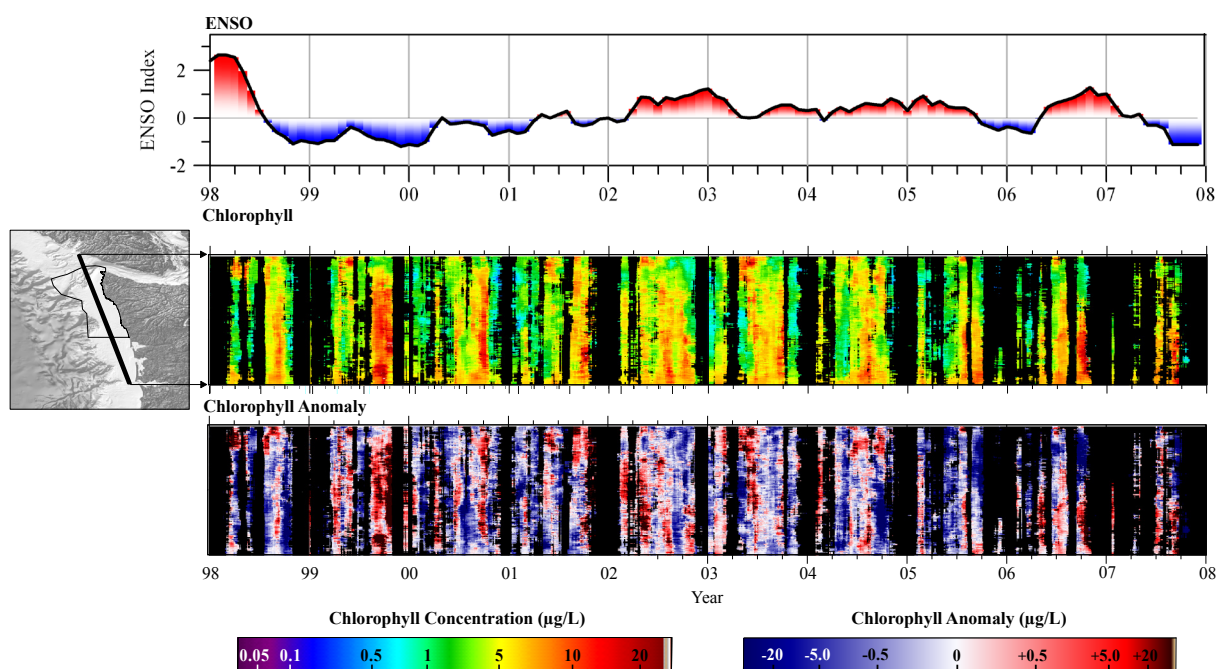


Figure 42. Time series plot (Hovmöller) along a North-South transect line revealing filtered SeaWiFS chlorophyll and chlorophyll anomaly values for the period 1997-2007. Multivariate ENSO index values added for reference. Source: NOAA/NWS.

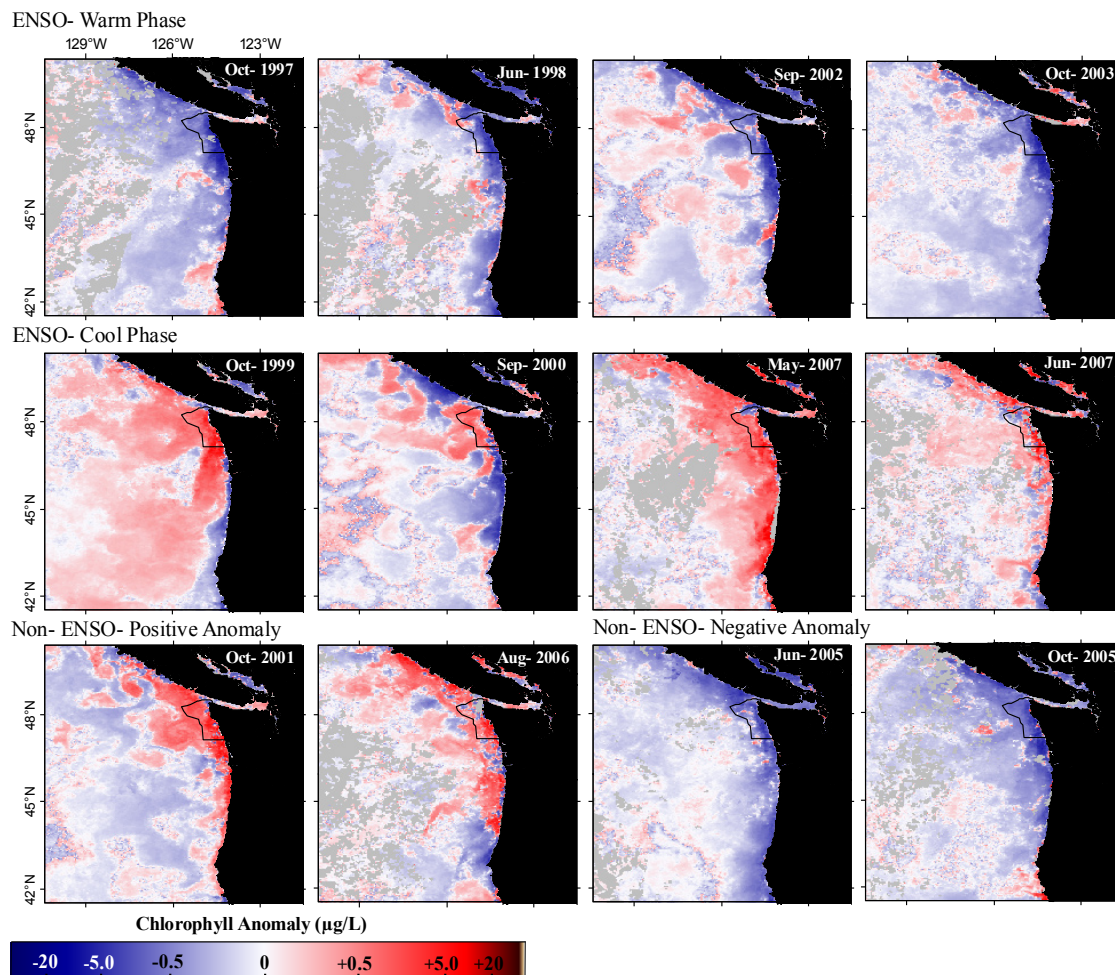


Figure 43. SeaWiFS monthly mean chlorophyll anomaly image maps during ENSO and non-ENSO periods.

Monthly turbidity anomaly levels are extremely moderate for the region, but vary according to interactions with other physical drivers related to seasonal rainfall/runoff patterns. Higher values were observed in the 1998, 1999, 2001, 2006, and 2007 winters south of the Juan De Fuca Strait (Figure 44). Small-scale anomalies in Rrs670 were observed within the OCNMS in the winter-spring of 1999 and 2007 during La Niña conditions (Figure 45, middle row). Turbidity anomalies are mainly restricted to areas along the mid- to inner shelf and can span consecutive months. This was the case in early 1999, when elevated turbidity occurred over a 4-month interval inside the sanctuary (Figure 44). An abnormally low turbidity winter occurred in 2005.

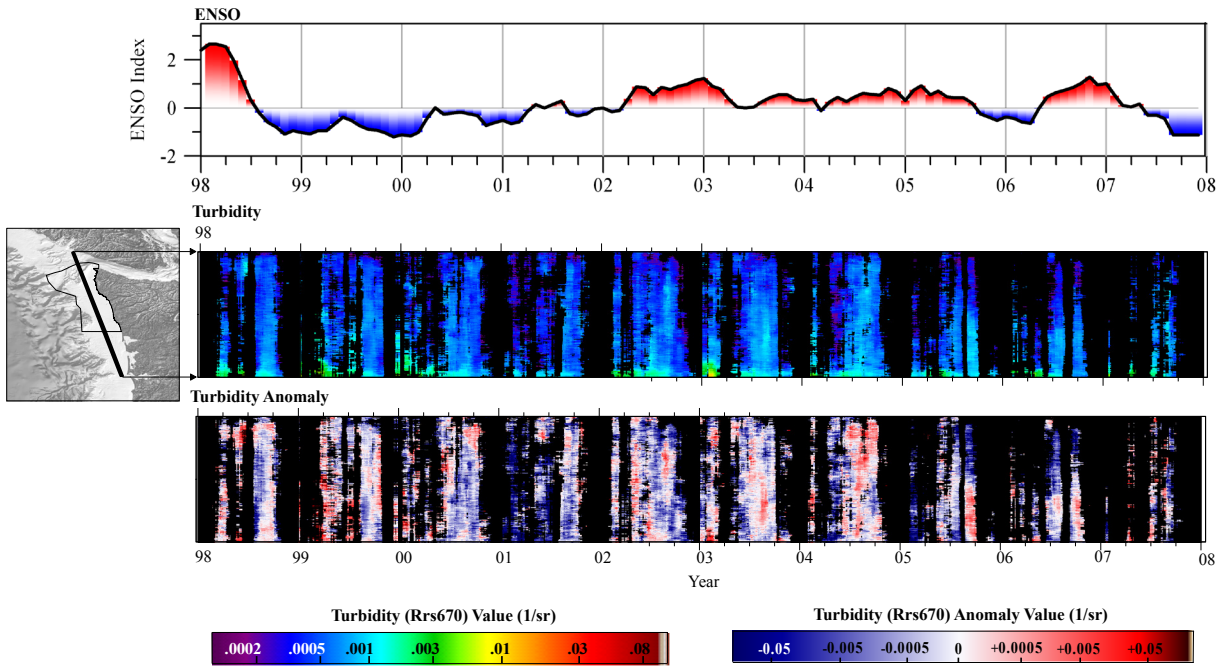


Figure 44. Time series plot (Hovmöller) along a North-South transect line revealing filtered SeaWiFS turbidity and turbidity anomaly values for the period 1997-2007. Multivariate ENSO index values added for reference. Source: NOAA/NWS.

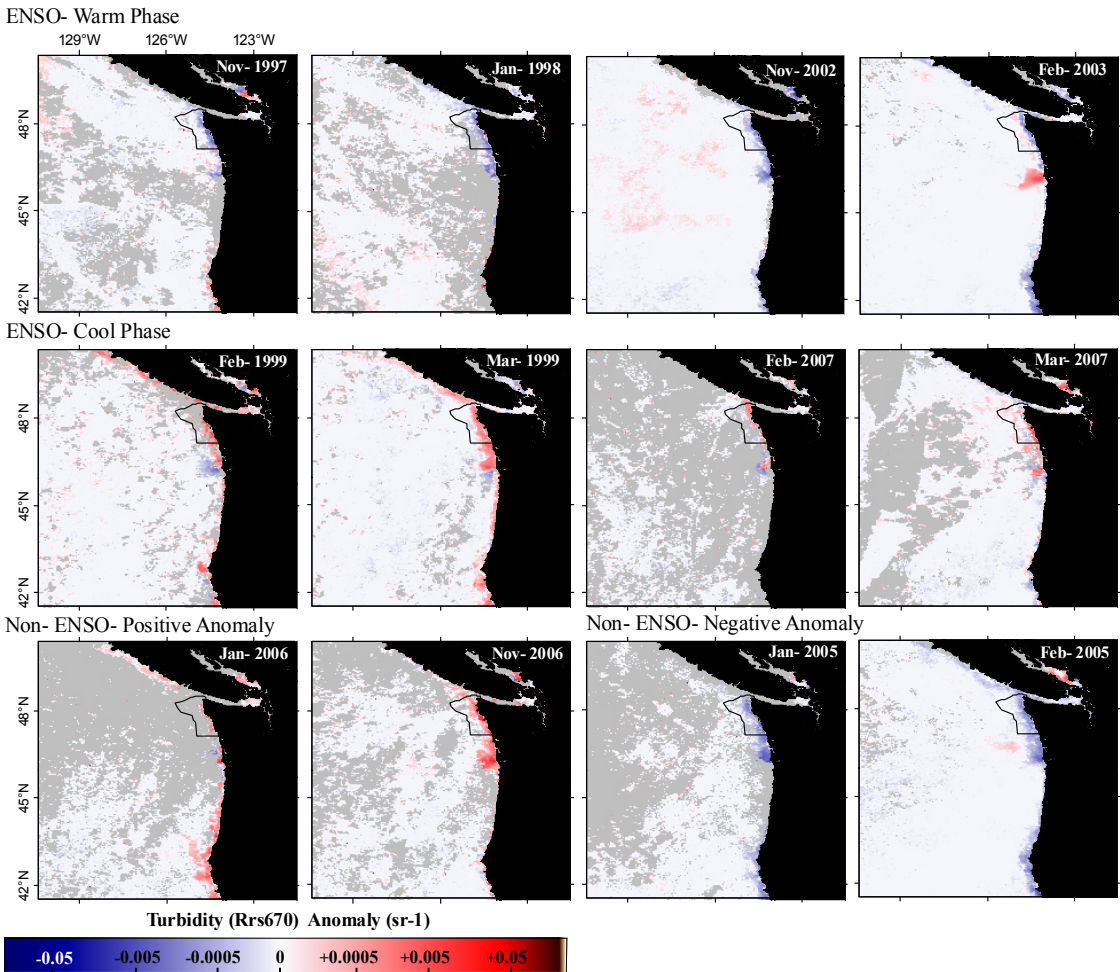


Figure 45. SeaWiFS monthly mean turbidity anomaly image maps during ENSO and non-ENSO periods.

### Summary of Surface Anomalies for the OCNMS

Ocean climate anomalies developed from long-term data series were found to be associated with both large-scale climate cycles and localized perturbations in OCNMS environments. Selected data extractions of climate anomalies inside the sanctuary are summarized (Table 4) to reveal general coincidence with ENSO indices. For example, during the strong El Niño period in fall 1997 through summer 1998, high SST and increased vertical SSHA deviation were detected inside the sanctuary for all months selected. Chlorophyll concentrations revealed strong negative anomalies at the beginning of the period, with alternating patterns at the end of the period. Turbidity anomalies revealed negative anomalies at the beginning of the period, with slight positive anomalies at the end. During the strong La Niña period in 1999, SST and SSHA were found to be negative, while chlorophyll and turbidity were strongly positive. During a 6-month period in 2001, negative anomalies were recorded for all variables analyzed. The ENSO index was positive again in 2002, with unexpectedly colder water (negative SST anomaly) evident and decreased sea surface heights inside the sanctuary<sup>5</sup>. Lower turbidity and less chlorophyll production were evident inside the Sanctuary during the 2002 fall period. In 2004, neutral ENSO conditions were evident, with warmer than expected SST and SSHA, coupled with stronger than normal chlorophyll present in the sanctuary. Significant alternating patterns of ocean color variability reveal the potential volatility of ocean color signals inside the sanctuary. The extreme positive and negative anomalies of SSHA and SST are usually well separated and can last for years, generally revealing similar patterns to the ENSO index. However, heightened ENSO does not always imply extreme anomalous surface patterns, as seen in 2002 and 2004 (Table 4).

Table 4. Comparison of ENSO index values and remotely sensed variable anomalies from extracted data averaged for the Olympic Coast National Marine Sanctuary

Date	ENSO	SST anomaly	SSHA deviation	Turbidity anomaly	Chlorophyll anomaly	ENSO	SST anomaly	SSHA deviation	Turbidity anomaly	Chlorophyll anomaly	
Sep-97	2.83	3.75	9.84	-0.00025	-2.24196	May-02	0.88	-1.24	-4.65	0.00002	0.30555
Oct-97	2.22	2.06	9.30	0.00022	-3.18499	Jun-02	0.84	-0.44	-3.16	0.00000	0.51718
Nov-97	2.33	1.69	8.60	-0.00025	-0.05153	Jul-02	0.56	-0.16	-2.11	0.00002	0.12283
Dec-97	2.22	1.60	10.10	-0.00009	-0.22234	Aug-02	0.86	-0.96	-5.39	0.00000	1.30825
Jan-98	2.40	1.25	8.64	-0.00035	0.05643	Sep-02	0.77	-0.35	-3.60	-0.00002	-1.80847
Feb-98	2.67	2.28	10.85	0.00031	-0.47932	Oct-02	0.91	-1.57	-5.49	-0.00022	-0.44078
Mar-98	2.65	1.46	3.65	-0.00012	0.56345	Nov-02	0.98	-0.03	4.69	-0.00027	-0.66917
Apr-98	2.56	0.80	2.53	0.00001	-0.87637	Dec-02	1.15	0.84	6.72	-0.00025	-0.23135
May-98	1.97	0.48	1.91	0.00010	0.29000	Jan-03	1.23	1.60	4.83	-0.00010	-0.12747
Jun-98	1.14	0.30	2.40	0.00029	-2.10982	Feb-03	0.91	0.80	-0.23	-0.00035	0.24995
Jul-98	0.34	0.26	-1.81	0.00008	0.45776	Mar-03	0.80	0.61	1.45	0.00018	0.18309
Apr-99	-0.96	-0.56	-5.73	0.00011	1.00066	Feb-04	0.36	0.33	2.41	-0.00019	1.54079
May-99	-0.68	-0.75	-6.42	0.00009	0.35166	Mar-04	-0.11	0.24	1.32	-0.00013	0.17599
Jun-99	-0.39	-0.66	-4.49	0.00001	-0.11754	Apr-04	0.25	0.68	2.01	-0.00009	0.15430
Jul-99	-0.53	-0.83	-3.43	-0.00004	-1.65118	May-04	0.44	1.20	0.35	-0.00008	-1.32536
Aug-99	-0.74	0.73	-0.24	0.00001	0.02917	Jun-04	0.27	0.61	1.70	-0.00005	-0.47355
Sep-99	-0.88	-1.04	-3.85	0.00007	3.99553	Jul-04	0.46	0.66	1.18	-0.00002	0.22001
Oct-99	-0.92	-1.08	-1.48	0.00003	5.17155	Aug-04	0.61	0.45	-0.37	0.00013	1.63739
Jan-01	-0.52	0.03	-4.67	-0.00036	-0.10192	Feb-05	0.74	0.18	2.74	-0.00048	0.51114
Feb-01	-0.66	-0.26	-6.83	-0.00050	-0.30537	Mar-05	0.93	0.67	2.40	-0.00013	-0.56225
Mar-01	-0.59	-0.33	-3.71	-0.00028	-0.41193	Apr-05	0.54	0.35	0.84	0.00011	-0.91012
Apr-01	-0.14	-0.58	-6.30	-0.00011	-1.23980	May-05	0.71	0.70	4.93	-0.00007	-1.53243
May-01	0.15	-0.85	-2.35	-0.00002	-0.15311	Jun-05	0.46	0.67	0.84	-0.00010	-1.65062
Jun-01	0.00	-0.10	-2.87	-0.00018	-0.98320	Jul-05	0.42	0.19	3.49	-0.00005	0.47946

Positive anomaly  
 Negative anomaly  
 Neutral or slightly positive/negative



## 4. CONCLUSIONS AND RECOMMENDATIONS

This work was intended to summarize surface layer conditions (both typical and atypical) as depicted from long-term satellite data series. The suite of remote sensing data, presented as conventional maps, Hovmöller diagrams, and statistical plots, afforded simplicity in summarizing conditions for the region. In particular, merged satellite oceanographic data revealed information on:

- seasonal cycles and transition periods
- linkages between seasonal warming and cooling, upwelling/downwelling, transport, and wind influences
- seasonal nutrient sources and physical limiting factors controlling surface layer responses
- interannual cycles and general response to climate oscillations (ENSO)

All surface layer data collected and analyzed near the Olympic Coast National Marine Sanctuary exhibited change during a typical annual cycle. Using climatological summaries of average (expected) conditions, and through correlation maps and Hovmöller diagrams along three respective transect lines, periodic seasonal and subseasonal shifts in surface conditions affecting the OCNMS were interpreted. Five fairly distinct seasonal cycles were evident in the ocean climate data summaries and were consistent with the known literature.

Insights on underlying processes and limiting factors controlling surface response and nutrient sources affecting the sanctuary were documented. The correlation patterns of surface water properties were found to be spatially and temporally tied to upwelling/downwelling cycles, outflow from the Juan de Fuca Strait, the Columbia River, coastal/estuarine influence, and increased light availability (Figure 37).

There is general agreement that January is typically dominated by downwelling favorable winds, precipitation influence (coastal/estuarine), and Columbia River discharge. During May, strengthened upwelling, increased regional heating and Juan de Fuca outflow influence surface layer characteristics most dramatically. In July, surface layer responses are indicative of enhanced upwelling, increased light and temperature, with available nutrients out of the Juan de Fuca Strait promoting chlorophyll production along the entire Olympic Coast. Late September/early October is typically dominated by increased chlorophyll production and westward propagation of SST fronts and eddies. Increased Ekman transport, driven by local alongshore winds, appears to be the governing forcing mechanism on this early fall chlorophyll peak enhancement (Strub, pers. comm.). Numerous surface reflections appear to be coincident with primary chlorophyll peak including decreases in localized SST, suppressed SSHA, and lower turbidity conditions that are evident in a 2-week interval prior to and during chlorophyll peaks. Further investigation is needed to assess the periodicity and predictability of this phenomenon.

The remote sensing data also provided insights on isolating upwelling responses and the nature of frontal features for the region. Since the surface patterns that were represented revealed periodicity and co-variability, further testing of relationships could be used to discern specific cues involving upwelling response, based on a combination of surface and subsurface characteristics. In addition, chlorophyll variability indicators were identified as a proxy for phytoplankton activity at specific time periods during the upwelling cycle. This information could also be used to discern specific timing cues for individual species assemblages.

This report reviewed and summarized remotely sensed proxies needed for building appropriate decision support tools, including integrated assessments. General uses of core variables estimated from satellite are shown (Figure 46) as a basis for environmental characterization, resource evaluation and problem detection. Characterization and resource evaluation involve developing baselines of environmental parameters for trend detection, where data is extracted and subsequently integrated with biological and habitat information. Problem detection involves using remote sensing data to identify physical oceanographic and climatological conditions (and/or processes) directly and indirectly related to coastal water quality issues (e.g. low DO conditions and harmful algal blooms). It is suggested that a thorough analysis of expected surface conditions using a suite of merged information is critical in characterization and resource evaluation, problem detection, and trend determination. Assimilation of remotely sensed data for environmental modeling purposes will con-

tinue to evolve through improvements in satellite engineering and optics.

An essential requirement for marine resource evaluation and assessment involves the integration of spatially and temporally resolved oceanographic datasets. Through this work, a merged suite of oceanographic data was summarized to provide a foundation for building assessment capability and design, wherein merged data types are of more significance than singular data types. Integration of this form works in many ways to improve remote sensing utilization through a more spatially and temporally comprehensive assessment of surface patterns and variability, and an increased understanding of interactions between processes, habitats, and resources necessary for sustained ecosystem function. Development of indicators of biological response using a full suite of remote data types should be a priority for future work involving marine resource evaluation and assessments.

NOAA's National Center for Coastal Ocean Science (NCCOS), Office of National Marine Sanctuaries, and National Marine Fisheries Service have consistently worked to merge datasets (and disciplines) for improved ecosystem-based management. As an example, NCCOS's Biogeography Program relies on multifaceted data to study the relationship of species distribution patterns relative to geographical differences in the environment, with added specificity to marine-managed boundary concepts (NCCOS, 2005). For many protected areas, basic biological and physical data are lacking in spatial and/or temporal resolution. This remote sensing baseline is central for understanding the region in a broader context and how the biology and oceanographic conditions of a region change through time.

In summary, the data and analysis presented here were intended to be the first of many steps to address present and future management questions posed by the OCNMS. The intent was to demonstrate how long-term data series could contribute to a better understanding of oceanographic variability and processes along the Pacific Northwest and elsewhere. This summary should be used as a vehicle for future discussions and work posed by joint partnerships between funding agencies, including NOAA and the research community vested in ocean science.

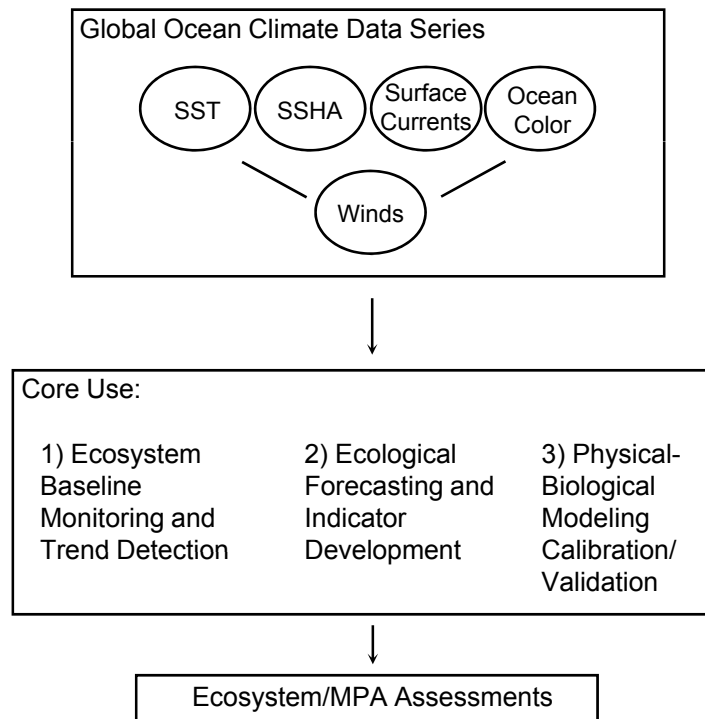


Figure 46. Schematic describing general uses of remotely sensed parameters (proxies) outlined in this report for ecosystem resource evaluation, problem identification, and management decision support.

## REFERENCES

- Airamé, S., J.E. Dugan, K.D. Lafferty, H. Leslie, D.A. McArdele, and R.R. Warner. 2003. Applying ecological criteria to marine reserve design: A case study from the California Channel Islands. *Ecological Applications* 13(1):S170-S184.
- Adler, R.F., G.J. Huffman, A. Chang, R. Ferraro, P-P. Xie, J.E. Janowiak, B. Rudolf, U. Schneider, S. Curtis, D. Bolvin, A. Gruber, J. Susskind, P.A. Arkin, and E. Nelkin. 2003. The Version-2 Global Precipitation Climatology Project (GPCP) monthly precipitation analysis (1979-Present). *Journal of Hydrometeorology* 4:1147-1167.
- Allen, J.S. and P.A. Newberger. 1996. Downwelling circulation on the Oregon continental shelf. Part I: Response to idealized forcing. *Journal of Physical Oceanography* 26:2011-2035.
- Austin, J.A. and J.A. Barth. 2002. Drifter behavior on the Oregon-Washington shelf during downwelling-favorable winds. *Journal of Physical Oceanography* 32:3132-3144.
- Breaker, L.C., T.P. Mavor, and W.W. Broenkow. 2005. Mapping and monitoring large-scale ocean fronts off the California Coast using imagery from the GOES-10 geostationary satellite. Publication T-056 San Diego: California Sea Grant College Program, University of California, 25 pp.
- Bruno, J.F., E.R. Selig, K.S. Casey, C.A. Page, B.L. Willis, C.D. Harvell, H. Sweatman, and A. Melendy. 2007. Thermal stress as a driver of coral disease dynamics on the Great Barrier Reef. *PLoS Biology* 5(6):e124.
- Canny, J. 1986. A computational approach to edge-detection. *IEEE Transactions on Pattern Analysis and Machine Intelligence* 6:679-698.
- Castelao, R.M., T.P. Mavor, J.A. Barth, and L.C. Breaker. 2006. Sea surface temperature fronts in the California Current System from geostationary satellite observations. *Journal of Geophysical Research* 111(C09026) doi:10.1029/2006JC003541.
- Conlan, R. and R. Service. 2000. *El Niño and La Niña: Tracing the Dance of Ocean and Atmosphere*. Washington, DC: National Academy of Science Office on Public Understanding of Science.
- Dall'Olmo, G., and A. A. Gitelson. 2005. Effect of bio-optical parameter variability on the remote estimation of chlorophyll-a concentration in turbid productive waters: experimental results. *Applied Optics* 44:412-422.
- Di Lorenzo, E., N. Schneider, K.M. Cobb, P.J. S. Franks, K. Chhak, A.J. Miller, J.C. McWilliams, S.J. Bograd, H. Arango, E. Curchitser, T.M. Powell, and P. Rivièrè. 2008. North Pacific Gyre Oscillation links ocean climate and ecosystem change. *Geophysical Research Letters* 35:1-6.
- Freeland, H.J. and K.L. Denman. 1982. A topographically controlled upwelling center off southern Vancouver Island. *Journal of Marine Research* 40:1069-1093.
- Goericke, R., E. Venrick, A. Mantayla, S.J. Bograd, F.B. Schwing, A. Huyer, R.L. Smith, P.A. Wheeler, R. Hooff, W.T. Peterseon, G. Gaxiola-Castro, C. Collins, B. Marinovic, R. Durazo, F. Chavez, N. Lo, K.D. Hyrenbach, W.J. Sydeman. 2005. The State of the California Current, 2004-2005: Still cool? California Cooperative Oceanic Fisheries Investigations Report 46: 32-71.
- Gordon, A.L. and C.F. Giulivi. 2004. Pacific decadal oscillation and sea level in the Japan/East Sea. *Deep-Sea Research I* (51): 653-663.
- Grantham, B.A., F. Chan, K.J. Nielsen, D.S. Fox, J.A. Bart, J. Huyer, J. Lubchenco, and B.A. Menge. 2004. Upwelling-driven nearshore hypoxia signals ecosystem and oceanographic changes in the northeast Pacific.

Nature 429:749-754.

Gregg, W.W. and N.W. Casey. 2004. Global and regional evaluation of the SeaWiFS chlorophyll data set. *Remote Sensing of Environment* 93: 463-479.

Halliwell Jr., G.H. and J.S. Allen. 1987. Large-scale coastal wind field along the west coast of North America, 1981-1982. *Journal of Geophysical Research* 92(C2):1861-1884.

Halpern, B.S., S. Walbridge, K.A. Selkoe, C.V. Kappel, F. Micheli, C. D'Agrosa, J.F. Bruno, K.S. Casey, C. Ebert, H.E. Fox, R. Fujita, D. Heinemann, H.S. Lenihan, E.M.P. Madin, M. Perry, E.R. Selig, M. Spalding, R.S. Steneck, and R. Watson. 2008. Assessing and mapping the global impact of human activities on marine ecosystems. *Science* 319:948-952.

Halpin, P.M., P.T. Strub, B. Peterson, and T. Baumgartner. 2004. An overview of interactions among oceanography, marine ecosystems, climatic and human disruptions along the eastern margins of the Pacific Ocean. *How Landscapes Change: Human Disturbance and Ecosystem Disruptions in the Americas* (G.A. Bradshaw, P.A. Marquet, and H. A. Mooney, eds.) Special edition of *Revista Chilena de Historia Natural* 77:371-409.

Hickey, B.M. 1979. The California current system – hypotheses and facts. *Progressive Oceanography* 8:191-279.

Hickey, B.M. 1989. Patterns and processes of circulation over the shelf and slope. In *Coastal Oceanography of Washington and Oregon* (M.R. Landry and B.M. Hickey eds.). New York:Elsevier. pp. 41-115.

Hickey, B.M., R.E. Thomson, H. Yih, P.H. LeBlond. 1991. Velocity and temperature fluctuations in a buoyancy-driven current off Vancouver Island. *Journal of Geophysical Research* 96 (C6) 10:507-10,538.

Hickey, B.M. 1998. Coastal Oceanography of western North America from the tip of Baja California to Vancouver Island. In *The Sea* (A.R. Robinson, A.R. and K.H. Brink eds.). New York: Wiley and Sons, 11 345-393.

Hickey, B.M. and N.S. Banas. 2003. Oceanography of the U.S. Pacific Northwest coastal ocean and estuaries with application to coastal ecology. *Estuaries* 26(4B): 1010-1031.

Kirincich, A.R., J.A. Barth, B.A. Grantham, B.A. Menge, and J. Lubchenco. 2005. Wind-driven inner-shelf circulation off central Oregon during summer. *Journal of Geophysical Research* 101(C10S03), doi10.1029/2004JC002611.

Landry, M.R., J.R. Postel, W.K. Peterson, and J. Newman. 1989. BROADSCALE PATTERNS IN THE DISTRIBUTION OF HYDROGRAPHIC VARIABLES. In *Coastal Oceanography of Washington and Oregon* (M.R. Landry and B.M. Hickey eds.). New York: Elsevier. pp. 1-41.

Lehmann, E.L. and H.J.M. D'Abrera. 1998. *Nonparametrics: Statistical Methods Based on Ranks*. Englewood Cliffs, NJ: Prentice-Hall. pp 292, 300, 323.

Lentz, S., 1992. The surface boundary layer in coastal upwelling regions. *Journal of Physical Oceanography* 22:1517-1539.

MacFadyen, A., B.M. Hickey, and M.G.G. Foreman. 2005. Transport of surface waters from the Juan de Fuca eddy region to the Washington coast. *Continental Shelf Research* 25:2008-2021.

Mantua, N.J., and S.R. Hare. 2002. The Pacific Decadal Oscillation. *Journal of Oceanography* 58(1):35-44.

McGillicuddy, D.J., V.K. Kosnyrev, J.P. Ryan, and J.A. Yoder. 2001. Covariation of mesoscale ocean color

- and sea-surface temperature patterns in the Sargasso Sea. *Deep Sea Research, Part II*, 48:1823-1836.
- Newberger, P.A. and J.S. Allen. 1996. On the use of the Boussinesq equations, the reduced system, and the primitive equations for the computation of geophysical flows. *Dynamics of Atmospheres and Oceans* 25(1):1-24.
- Newton, J.A., E. Siegel, and S.L. Albertson. 2003. Oceanographic Changes in Puget Sound and the Strait of Juan de Fuca during the 2000-01 Drought. *Canadian Water Resources Journal* 28 (4):715-728.
- NOAA National Ocean Service/Special Projects. 1999. Coastal Assessment Framework, N/SPO, 9th Floor 1305 East-West Highway, Silver Spring, MD:NOAA.
- NOAA National Centers for Coastal Ocean Science. 2003. A Biogeographic assessment off north/ central California: To support the joint management plan review for Cordell Bank, Gulf of the Farallones, and Monterey Bay National marine sanctuaries: Phase I-Marine fishes, birds, and mammals. Silver Spring, MD:NOAA 145 pp.
- NOAA National Centers for Coastal Ocean Science. 2005. A Biogeographic Assessment of the Channel Islands National Marine Sanctuary: A Review of Boundary Expansion Concepts for NOAA's National Marine Sanctuary Program. NOAA Technical Memorandum NOS NCCOS 21. Silver Spring, MD:NOAA DVD.
- NOAA Office of National Marine Sanctuaries. 2008. Olympic Coast National Marine Sanctuary Condition Report 2008. Silver Spring, MD:NOAA 72 pp.
- NOAA National Centers for Coastal Ocean Science. 2006. An Ecological Characterization of the Stellwagen Bank National Marine Sanctuary Region: Oceanographic, Biogeographic, and Contaminants Assessment. NOAA Technical Memorandum NOS NCCOS 45. Silver Spring, MD:NOAA 356 pp.
- NOAA National Centers for Coastal Ocean Science. 2007. Characterization of the Benthos, Marine Debris and Bottom Fish at Gray's Reef National Marine Sanctuary. NOAA Technical Memorandum NOS NCCOS 50. Silver Spring, MD:NOAA 82 pp. + Appendices.
- Office of National Marine Sanctuaries. 2008. Olympic Coast National Marine Sanctuary Condition Report 2008. Silver Spring, MD:NOAA. 72 pp.
- Peterson, W.T. and F.B. Schwing. 2003. A new climate regime in northeast Pacific ecosystems. *Geophysical Research Letters* 30(17):1896, doi:10.1029/2003GL017589.
- Sackman, B., L. Mack, M. Logsdon, and M.J. Perry. 2004. Seasonal and inter-annual variability of SeaWiFS-derived chlorophyll a concentrations in waters off the Washington and Vancouver Island coasts, 1998-2002. *Deep Sea Research, Part II*, 51(10-11):945-965.
- Saraceno, M., P.T. Strub, and P.M. Kosro. 2008. Estimates of sea surface height and near-surface along-shore coastal currents from combinations of altimeters and tide gauges. *Journal of Geophysical Research* 113 (C11013), doi:10.1029/2008JC004756.
- Schwing, F.B., M. O'Farrell, J.M. Steger, and K. Baltz. 1996. Coastal upwelling indices, west coast of North America, 1946-95. NOAA Technical Memorandum NOAA-TM-NMFS-SWFSC-231. Silver Spring, MD: NOAA 207 pp.
- Strub, P.T. and C. James. 1988. Atmospheric conditions during the spring and fall transitions in the coastal ocean off western United States. *Journal Geophysical Research* 93(C12)15:561-584.
- Strub, P.T., J.S. Allen, A. Huyer, R.L. Smith, and R.C. Beardsley. 1987. Seasonal cycles of currents, temperatures, winds and sea level over the NE Pacific continental shelf: 35N to 48N. *Journal of Geophysical*

Research 92:1507-1526.

Strub, P.T., and C. James, 2002. Altimeter-derived surface circulation in the large-scale NE Pacific Gyre: Part 1. Seasonal variability. *Progress In Oceanography* 53(2-4):163-183.

Strub, P.T. and C. James. 2003. Altimeter estimates of anomalous transports into the northern California Current during 2000-2002. *Geophysical Research Letters* 30(15):8025, doi:10.1029/2003GL017513.

Sydeman, W.J., and M.L. Elliott. 2008. Developing the California Current Integrated Ecosystem Assessment, Module I: Select Time-Series of Ecosystem State. Marine Ecology Division, PRBO Conservation Science, 3820 Cypress Drive, # 11, Farallon Institute for Advanced Ecosystem Research, Petaluma, California 94954. 37 pp.

Thomas A.C., P.T. Strub, and P. Brickley. 2003. Anomalous chlorophyll concentrations in the California Current in 2001-2002. *Geophysical Research Letters* 30(15):8022, doi:10.1029/2003GL017409.

Thomas, A.C., D.W. Townsend, and R. Weatherbee. 2003. Satellite-measured phytoplankton variability in the Gulf of Maine. *Continental Shelf Research* 23:971-989.

Thomas, A.C. and R.A. Weatherbee. 2006. Satellite-measured temporal variability of the Columbia River plume. *Remote Sensing of the Environment* 100(2):167-178.

Trainer, V.L., B.M., Hickey, and R.A. Horner. 2002. Biological and physical dynamics of domoic acid production off the Washington U.S.A. coast. *Limnology and Oceanography* 47(5):1438-1446.

Trainer, V.L. and M. Suddleson. 2005. Monitoring approaches for early warning of domoic acid events in Washington State. *Oceanography* 18(2):228-237.

Trainer, V.L., B.M. Hickey, E.J. Lessard, W.P. Cochlan, C.G. Trick, M.L. Wells, and A. MacFadyen. 2009. Variability of *Pseudo-nitzschia* and domoic acid in the Juan de Fuca eddy region and its adjacent shelves. *Limnology and Oceanography* 54(1):289-308.

Yoder, J.A. and M.A. Kennelly. 2003. Seasonal and ENSO variability in global ocean phytoplankton chlorophyll derived from 4 years of SeaWiFS measurements. *Global Biogeochemical Cycles* 17(4):1112, doi:10.1029/2002GB001942.

Valavanis, V.D., I. Katara, and A. Palialexis. 2004. Critical regions: A GIS-based modeling approach for the mapping of marine productivity hotspots. *Aquatic Sciences* 36(66):234-243.

Wilson, C., and V.J. Coles. 2005. Global climatological relationships between satellite biological and physical observations and upper ocean properties. *Journal of Geophysical Research* 110(C10001), doi:10.1029/2004JC002724.

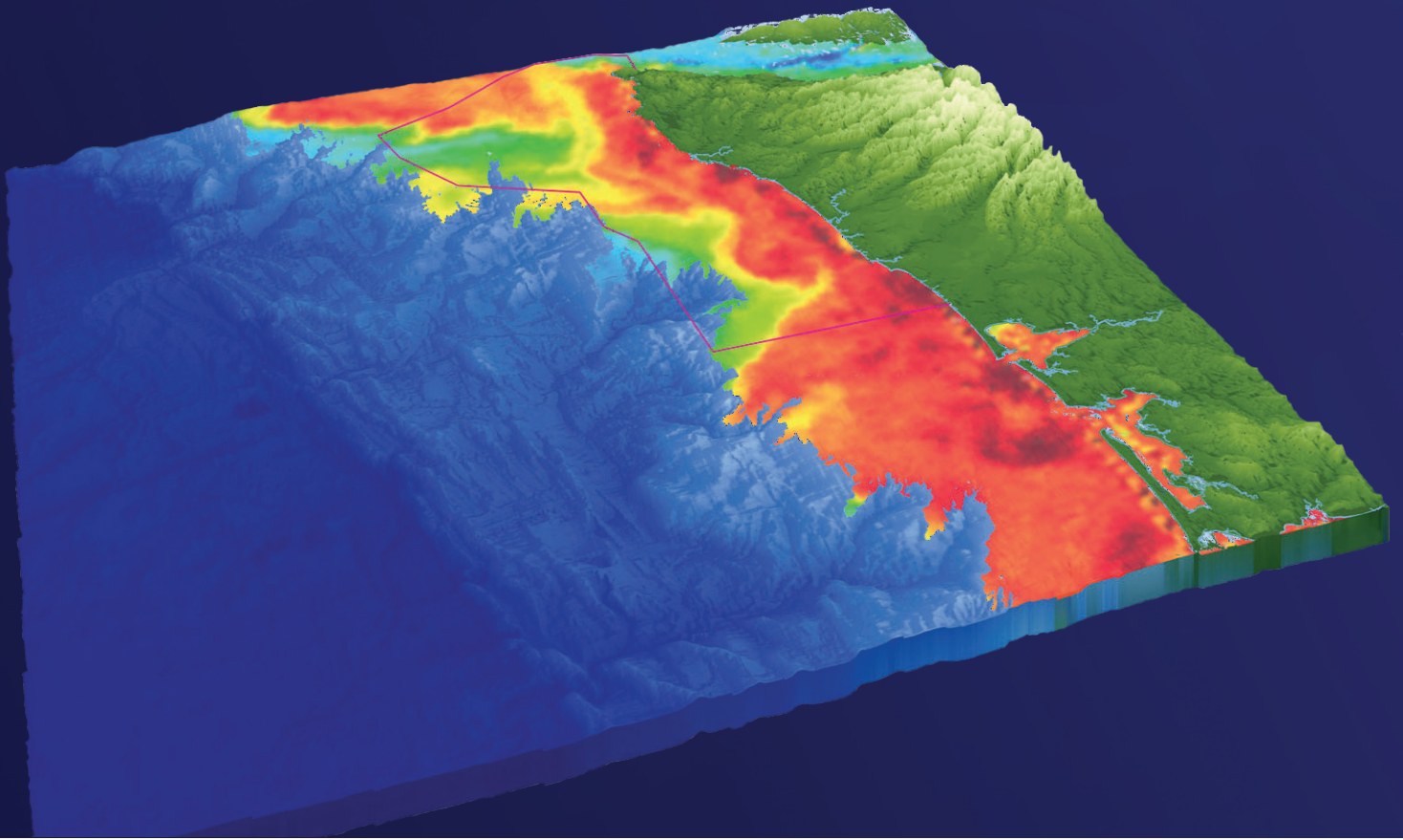
Wolter, K. and M.S. Timlin. 1998. Measuring the strength of ENSO – how does 1997/98 rank? *Weather* 53:315-324.

## ACKNOWLEDGMENTS

The authors are indebted to the following individuals, who represent many State/Federal agencies, tribal staff, and research entities, and who provided guidance and review of this document:

Barbara Hickey	University of Washington, School of Oceanography
Sue Geier	University of Washington, School of Oceanography
Jan Newton	University of Washington, School of Oceanography
James Postel	University of Washington, School of Oceanography
Kate Edwards	University of Washington, Applied Physics Laboratory
Terrie Klinger	University of Washington, School of Marine Affairs
Ted Strub	Oregon State Univ., Coop. Inst. for Ocean. Satellite Studies
Maria Kavanaugh	Oregon State Univ., Coop. Inst. for Ocean. Satellite Studies
Roberto Venegas	Oregon State Univ., Coop. Inst. for Ocean. Satellite Studies
Andrew Thomas	University of Maine, School of Marine Sciences
Dana Woodruff	Battelle Marine Sciences Laboratory
John Calambokidis	Cascadia Research
Tom Jagielo	Washington State Department of Fish and Wildlife
Farron Wallace	Washington State Department of Fish and Wildlife
Richard Stumpf	NOAA National Centers for Coastal Ocean Science
Mathew Kendall	NOAA National Centers for Coastal Ocean Science
Tracy Gill	NOAA National Centers for Coastal Ocean Science
Michelle Tomlinson	NOAA National Centers for Coastal Ocean Science
Tim Battista	NOAA National Centers for Coastal Ocean Science
Adam Zitello	NOAA National Centers for Coastal Ocean Science
Kevin McMahon	NOAA National Centers for Coastal Ocean Science
Kenneth Casey	NOAANESDISNational Oceanographic Data Center
Timothy Mavor	NOAANESDISCenter for Satellite Applications and Research
Ruth Yender	NOAA Office of Response and Restoration
Debra Simecek-Beatty	NOAA Office of Response and Restoration
Glen Watabayashi	NOAA Office of Response and Restoration
William Lehr	NOAA Office of Response and Restoration
Edward Bowlby	NOAA Olympic Coast National Marine Sanctuaries
John Barimo	NOAA Olympic Coast National Marine Sanctuaries
Nancy Wright	NOAA Olympic Coast National Marine Sanctuaries
Jennifer Hagen	Northwest Indian Fisheries Commission
Osa Odum	Northwest Indian Fisheries Commission
Bob Pavia	NOAA Office of National Marine Sanctuaries
Elizabeth Clarke	NOAA/NMFS Northwest Fisheries Science Center
Vera Trainer	NOAA/NMFS Northwest Fisheries Science Center
Gini Kennedy	NOAA NOS Communications and Education Division
Pam Rubin	NOAA NOS Communications and Education Division





U.S. Department of Commerce

Gary Locke, *Secretary*

National Oceanic and Atmospheric Administration

Dr. Jane Lubchenco, *Under Secretary for Oceans and Atmosphere*

National Ocean Service

John H. Dunnigan, *Assistant Administrator for Ocean Services and Coastal Zone Management*

